Biophysical Aspects of the BOLD Effect in Human Brain Mapping

By

Lin Tang

Dissertation

Submitted to the Faculty of the

Graduate School of Vanderbilt University

in partial fulfillment of the requirements

for the degree of

DOCTOR OF PHILOSOPHY

in

Physics

December, 2007

Nashville, Tennessee

Approved by

Professor John C. Gore

Professor Malcolm J. Avison

Professor Ronald R. Price

Professor Adam W. Anderson

Professor David J. Ernst

ACKNOWLEDGEMENTS

I have enjoyed my study and research journey through my graduate studies at Vanderbilt University. This work would not have been possible without the financial support of the National Institutes of Health, the Vanderbilt University Institute of Imaging Science, the Vanderbilt University Department of Physics or the Vanderbilt University Graduate School.

For this, I want to especially thank my advisor, Dr. John Gore, for offering me opportunities to gather extensive experience with major imaging facilities and approaches, for providing a stimulating work environment that allowed me to try out new ideas and to solve challenging problems with passion, and for his guidance, hospitality and support,

My thanks to Dr. Calum Avison for taking the time to examine my writings, and for his motivating discussions; to Dr. Ron Price, who is the first one who guided me into this field, and with whom I had a very pleasant introduction to research; to Dr. Adam Anderson, who taught my favorite class and was always of great guidance; to Dr. David Ernst for encouraging me to broaden my knowledge of science in an interdisciplinary field; and to Dr. Randolph Blake for inspiring discussions.

I am grateful to Frank Tong and his graduate students for helping me to perform retinotopic mappings. I would like to thank Silvina Horovitz for her gracious assistance in the design of my experiments, with whom I did my first ERP studies. Also I give thanks to Chris Cannistraci and Chris Gatenby for

enlightening discussions and fruitful collaboration. I am indebted to Nancy Hagans, who is always ready to help, and her efficient administrative assistance makes the work in the institute easier and smoother. I thank Robin Avison and Donna Butler for their technical expertise in MRI acquisition, Blake Niederhauser for his assistance in the NIRS acquisition, Jay Moore for very helpful discussions on perfusion MR imaging, and thanks to all the members at VUIIS; they have always been present with their knowledge, friendship and advice, that has made my graduate student life at Vanderbilt very enjoyable.

Finally, I would like express my deep gratitude to my beloved husband, Liguo Song, and my family, whose infinite love and support have helped me on this journey.

TABLE OF CONTENTS

ACKNOWLEDGEMENTS iii

LIST OF TABLES vii

LIST OF FIGURES viii

Chapter Page

I. INTRODUCTION 1

Physics of MRI and fMRI 2
Physics of MRI 2
Physics of fMRI 7
Brain activity and neuronal activity: physiology 8
Physiology of blood oxygen level dependent (BOLD) fMRI in neuroscience 11
Electroencephalography (EEG) and event-related potentials (ERPs) 16
Near infrared spectroscopy (NIRs) 18
Event-related design and integration of different modalities 19

II. NONLINEARITY OF HEMODYNAMIC RESPONSE TO TRANSIENT ACTIVATION AND DEACTIVATION 22

Introduction 22
Method 24
Subjects: 24
Stimulus Presentation 24
Data Acquisition 27
Data Analysis 27
Results 28
Conclusion 35

III. COMBINE NIRS AND FMRI TO INVESTIGATE HEMODYNAMIC RESPONSE TO TRANSIENT ACTIVATION AND DEACTIVATION 36

Introduction 36
Method 38
Subjects 38
Stimulus Presentation 38
Data Acquisition 40
Data Analysis 41
Results 42

Conclusion and Discussion 53

IV. MODELING BOLD RESPONSES 56

Introduction 57
Standard Balloon Model 58
Assumptions on the functional forms of blood flow 61
Fitting the Balloon Model 62
Fitting programs 63
Initial values 63
Fitting results 64
Developing the Balloon Model 66
Results 67
Conclusion & Discussion 70

V. DEACTIVATIONS IN PRIMARY VISUAL AREA WHICH CORRESPOND TO ACTIVATIONS IN EXTRASTRIATE VISUAL AREAS 74

Introduction 74
Method 76
Subjects 76
Stimulus Presentation 77
Data Acquisition 78
Data Analysis 78
Results 79
Discussion 84

VI. COMBINE ERP AND FMRI TO INVESTIGATE FEASIBILITY OF MAGNETIC-SOURCE MRI METHOD 90

Introduction 91
Method 94
Subjects 94
Stimulus Presentation 95
Data Acquisition 97
Data Analysis 98
Results 99
Conclusion and Discussion 102

VII. CONCLUSION AND FINAL DISCUSSION 104

EQUATIONS 109

REFERENCES 111

LIST OF TABLES

Table Page

Table II-1. List of the amplitudes of peak and the time to peak for fitted BOLD response to varying durations of stimulus interruption.....29

Table II-2. Amplitudes of peak (A_peak) and post undershoot/overshoot, time to peak (T_peak) and post undershoot/overshoot for BOLD response to stimulus-ON and OFF for 2sec or 4sec. There are significant differences in time to peak.....32

Table IV-1. List of the parameters which are used to describe functional forms of $f_{in}(t)$ in the Balloon Model. They were derived by least squares curve fitting of experimental data.....65

Table VI-1. Auditory oddball paradigm: the interval between oddballs varied to produce different oddball presentation frequencies.....95

LIST OF FIGURES

Figure Page

Figure I-1. The application of an external magnetic field results in the precession of the proton spin, and a short radiofrequency magnetic field results in the rotation of the magnetization to the transverse plane. 3

Figure I-2. Difference in magnetic susceptibility χ between blood and the surrounding extravascular space leads to microscopic magnetic field gradients in the vicinity of the blood vessels. 8

Figure I-3. a. Vasculature structure; b. Relationship between synaptic activity, neurotransmitter recycling and metabolic demand 9

Figure I-4. CBF, CBV, and $CMRO_2$ have different effects on Hb concentration. 10

Figure I-5. Change in CBF appears to be more than is necessary to support the small increase in O2 metabolism.(ΔCBF >> ΔCMRO2). 12

Figure I-6. Typical BOLD response to a brief stimulus. 13

Figure I-7. Some examples of functional mappings. 15

Figure II-1. Stimulus presentation in Paradigm III. 25

Figure II-2. Two reverse paradigms (I and II) of stimulus presentation. 26

Figure II-3. The average (n=5) event-related BOLD signal changes in the primary visual cortex in response to varying durations of stimulus interruption. a. Measured BOLD responses; b. Fitted BOLD responses using the gamma-variate function. 28

Figure II-4. Trend of the amplitudes of peak and the time to peak for fitted BOLD response to varying durations of stimulus interruption. 29

Figure II-5. Comparison between the measured (solid line) and predicted (dash line) BOLD response curves assuming linearity. The predictions using the response to shorter duration gaps are shown in the same row, and the measured responses to 2sec, 3sec, 4sec, 6sec, 8sec stimulus gaps plotted together with the corresponding predictions are shown in different columns. 30

Figure II-6. The normalized ratio of the area under the average BOLD responses curve to various durations of the stimulus-OFF. 31

Figure II-7. Compare BOLD responses to ON vs.OFF in V1 (average of 5 subjects): they are not mirror images, and different in magnitude and shape. 31

Figure II-8. BOLD responses in V1. a. Measured BOLD responses (average of 5 subjects); b. Fitted BOLD responses using the gamma-variate function. Deactivation responses are smaller and have longer latency but shorter time to peak, more narrow width and no significant post overshoot. 32

Figure II-9. Linearly convolve data from 2 s trials to estimate the 4 s duration stimulus. Red dash curves show the linear convolutions. Obviously, it tends to overestimate the response to functional activation, and underestimate the response to functional deactivation.....34

Figure III-1. Two reverse paradigms (I and II) of stimulus presentation. 39

Figure III-2. Arrangement of the transmission and detection fibers (matrix of 3x5). Pairs of adjacent incident (open circles) and detection (filled circles) fibers define optode (numbers) units.....41

Figure III-3. Compare BOLD responses to ON vs.OFF in V1 (average of 5 subjects): they are not mirror images, and different in magnitude and shape. 43

Figure III-4. Optical Topography (OT) maps in response to both 4sec stimulus-ON & OFF. 44

Figure III-5. Transient changes in both oxy-hemoglobin and deoxy-hemoglobin in V1 (subject BDN): a. NIR data in response to 4sec stimulus-ON. b. NIR data in response to 4sec stimulus-OFF. 46

Figure III-6. NIR response to 4sec activation vs. deactivation.....46

Figure III-7. Compare BOLD responses with NIR ([HbO_2], [Hb] and [HbT]) responses to 4sec stimulus-ON/OFF in V1. [HbO_2] and [HbT] showed similar relative magnitude and temporal properties for activation and deactivation with the correspondent BOLD signals. 47

Figure III-8. Compare BOLD responses with estimation from NIRS data to 4sec stimulus-ON/OFF in V1. They showed similar relative magnitude and temporal properties for activation and deactivation. Here constant w = 0.43 for stimulus-ON and w = 0.36 for stimulus-OFF. The left y-axis shows the %BOLD and the right y-axis is the ruler for NIR data. 51

Figure III-9. Compare NIR data obtain during different conditions: a, in response to 4sec stimulus-ON; b, in response to stimulus-OFF; data obtain during normal air breathing were showed in thicker lines, signal changes showed in thinner lines are obtained when subject inhales carbogen (95% O_2 + 5% CO_2). 53

Figure IV-1. Different simulated signal changes based on linear volume change of the power law: $v=f^{\alpha}$, and based on modified nonlinear volume changes for viscoelastic effects: $f_{out}(v) = v^{1/\alpha} + \tau \frac{dv}{dt}$ 60

Figure IV-2. Functional form of Flow-in based on the introduced parameters: *finMax*, *finDeR* (sec^{-1}), *finInR* (sec^{-1}), *finInDelay* (sec) and *finDeDelay* (sec). 61

Figure IV-3. Improved simulation by assumptions on nonlinear volume changes and dissymmetric flow changes. 62

Figure IV-4. Flow chart for MATLAB programs for data fitting.....64

Figure IV-5. BOLD responses to deactivations and their fits. The data can be well modeled by the modified Balloon Model. 65

Figure IV-6. BOLD responses obtained by Balloon Model using different patterns of Flow-in. 67

Figure IV-7. Compare Balloon Model simulated BOLD responses with the measured BOLD response to both stimulus on and off for various durations. 68

Figure IV-8. BOLD responses obtained by non-modified and modified Balloon model compared to experimental results. Red dash line showed linear convolution of HRF to 2sec. Modified Balloon model predicts the experimental data better and shows similar nonlinear properties of BOLD response to both activations and deactivations. 69

Figure IV-9. (a) Simulation of blood volume compared with functional form of blood flow, using the modified Balloon Model. (b) Simulated blood volume shows a smaller and slower decrease during the OFF period, and is consistent with the change patterns of total hemoglobin detected by NIRS. 70

Figure IV-10. Nonlinearity of Blood Flow induced by assumption of different flow-in time constants for stimulus onsets and offsets, and in turn better predicts the different nonlinear nature of BOLD responses to activations and deactivations. Red lines are linear summations from signals response to shorter durations.....71

Figure V-1. Connections between subsets of cortical visual areas (schematic diagram) [Tong 2003]. 75

Figure V-2. Three paradigms of typical event-related visual stimulus designs. 78

Figure V-3. fMRI identified extrastriate visual areas involved in responses to brief interruption of continuous stimulus, and showed interestingly different signal time courses compared to the expected deactivation in primary visual area. 80

Figure V-4. Different activation maps in response to different stimulus sensory. 81

Figure V-5. BOLD signal changes in response to various durations (1sec /2sec /3sec /4sec /6sec /8sec) of stimulus-OFF. 82

Figure V-6. Positive BOLD effect in extrastriate visual area in response to 1sec stimulus-OFF. 82

Figure V-7. Contrast maps between BOLD effect to stimulus-OFF vs. ON (upper row), or between BOLD effect to different durations of interruptions (lower row). 83

Figure V-8. Dual Source hyposthesis: a brief interruption was seen as 2 δ functions with different weight β1 and β2 (correspondent to the edges of stimulation switches.) 87

Figure VI-1. Auditory oddball paradigm 95

Figure VI-2. Face-presentation paradigm: black-car pictures were presented; red-0% noise added to the face picture; green-noisy image was created by adding gaussian noise with standard deviation of 20%; blue-noisy image was created by adding gaussian noise with standard deviation of 100%. 96

Figure VI-3. Magnetic source MRI (msMRI) images were acquired with offsets relative to stimulation onsets. 98

Figure VI-4. a P300 amplitude decreases as “oddball’ presentation frequency increases; b N170 amplitude decrease as noise added [Horovitz, 2004]. 100

Figure VI-5. left panel: BOLD activation map for the auditory oddball experiment; right panel: Activation map for face-sensitive experiment. P<0.001 101

Figure VI-6. Time courses of functional MRI signals in ROI(FFC) with different offsets relative to the stimulus (face) onset. These are no significant differences in the mean signal at 170, 180 or 400 ms post stimulus, and no differences from the prestimulus signal. 102

CHAPTER I

INTRODUCTION

The aims of the research described in this thesis were to study basic mechanisms of functional magnetic resonance imaging (fMRI) and to develop an improved understanding of the Blood Oxygen Level Dependent (BOLD) effect. To these ends, assessments of the nonlinear nature of brain activity during passive viewing of dynamic visuo-spatial imagery were conducted using event-related functional magnetic resonance imaging (er-fMRI), in vivo optical imaging and electrophysiology. In addition, several methodological issues and the neural and physiological bases of processing dynamic visuo-spatial imagery have been investigated.

The theoretical and background sections of this thesis consist of a selective overview of fMRI, Near-Infrared Spectroscopy (NIRS) and Event-related Potentials (ERPs), and a discussion of the advantages of their combination for functional neuroimaging. The methodological and experimental chapters describe (1) an investigation of how BOLD responses differ for transient activation and deactivation, and (2) an investigation of the feasibility of a method of MR imaging of brain activity based on detecting neuronal current induced magnetic field dephasing. The modeling section of the thesis involves: (1) the development of a Balloon Model that explicitly includes nonlinear physiological

variables in modeling the BOLD signal and (2) the use of insights gained from the model to better refine our understanding of the BOLD effect.

Physics of MRI and fMRI

Physics of MRI

Magnetic Resonance Imaging (MRI) has been used for medical diagnoses for around 30 years. It mainly records spatial maps of nuclear magnetic resonance (NMR) properties of water, since approximately 80 percent of human tissue is composed of water. In 1973, Lauterbur suggested NMR could be used to form images, and in 1977, the first clinical MRI scanner was patented. The high spatial resolution (≈ 0.1 - 1 mm in 3D) and excellent soft tissue contrast obtained with MRI make it a good non-invasive diagnostic tool, which can detect subtle tissue differences such as those produced by various pathologies such as tumor and stroke.

MRI produces images via manipulation of nuclear magnetic moments. As shown in Figure I-1, when a static magnetic field (B_0) is applied, multiple nuclear spins precess about the field direction, and this results in a net longitudinal equilibrium magnetization (M_0). The energy difference between the high (oriented with B_0) and low (oriented against B_0) energy protons is measurable and is expressed in the Larmor equation: $\omega_0 = \gamma B_0$ (where γ = 42.58 MHz/T for each hydrogen proton) and $\Delta E = h\omega_0$. Then when a small perpendicular oscillating magnetic field (B_1) is applied for a short time, if this oscillating frequency is tuned

to the Larmor frequency (~radiofrequency RF), the individual nuclei absorb energy and change state. In this resonance condition the tissue's magnetization (M) is tipped toward the transverse plane. It spirals down and the rotating transverse component induces a current signal in a coil wrapped around the sample. It is this set of fundamental principles that forms the physical basis of both nuclear magnetic resonance spectroscopy and imaging.

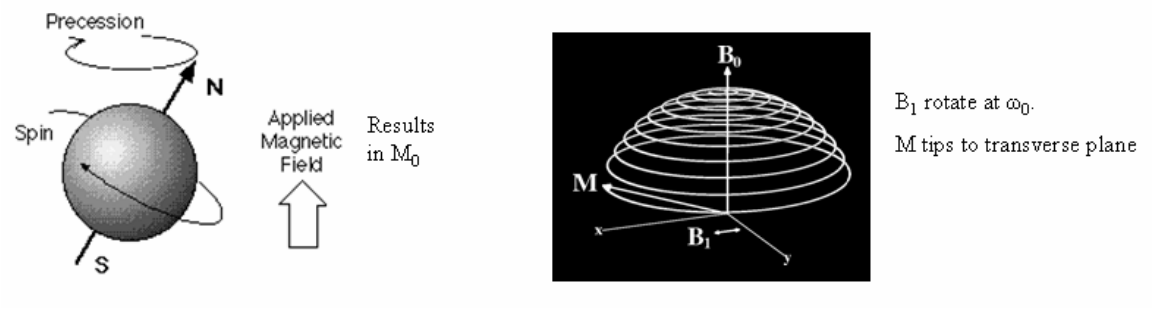

Figure I-1. The application of an external magnetic field results in the precession of the proton spin, and a short radiofrequency magnetic field results in the rotation of the magnetization to the transverse plane.

The time required for the protons to recover from their externally induced excited state to the state of magnetic equilibrium can be measured by T1, which is the *longitudinal relaxation* time. Each proton also induces a magnetic field around itself (a dipole field). Nearby molecules also have magnetic properties in the imaged tissue, so there is anthe intrinsic magnetic inhomogeneity which leads to different phases between the molecules over time. As the protons get out of phase, the transverse magnetization decays, and this is the so-called dephasing effect. T2 measures the *transverse relaxation*, which is the intrinsic

rate of decay of the MR signal after excitation. This decay occurs at different rates in different tissues. From the classical view, T2 is primarily due to the interaction between neighboring spins, or the dipolar interaction, which is proportional to $1/r^2$, where r is the distance between the spins' dipoles. Contrast in MRI is created because the ^1H atoms in different tissues have different relaxation rates, characterized by 1/T1 and 1/T2.

If the external field experienced by the spins is spatially non-uniform, then T2 is reduced to T2*. The field may be non-uniform because the tissue itself contains variations in bulk susceptibility. There are many physiological causes for such variations, such as tissue-air or tissue-bone interfaces. Also, the presence of blood hemoglobin in vessels and capillaries can affect T2* in the brain. Deoxyhemoglobin is paramagnetic and oxyhemoglobin is diamagnetic. Thus, T2* in brain tissue depends on the state of oxygenation of the blood as well as amount of blood within tissue.

Once the MR signal has been created, it is necessary to develop a means of spatially encoding the signal in order to form an image. We can utilize the fact that creating a spatially variant magnetic field will cause spatially variant signal frequency ($f(x)$).

$$f(x) = \gamma B(x) \qquad \text{[I-1]}$$

We take advantage of this by applying a constant gradient field (G_x) along one axis (x) during signal acquisition. The magnetic field, and therefore the MR frequency, is a linear function of position:

$$f(x) = \gamma(G_x x + B_0) \qquad \text{[I-2]}$$

where B_0 is a constant field onto which that gradient is imposed, G_x is the magnitude of a "gradient" field, and x is the position in space. When a gradient is applied, the strength of the MR signal at each frequency gives a measurement of the integrated signal strength at each position (x) along the frequency axis by means of a Fourier Transform.

$$S(x) = \int S(f(x)) \cdot e^{-2\pi i f(x)} df \qquad \text{[I-3]}$$

As time progresses the signal traces out a trajectory k_x in frequency-space proportional to the applied magnetic field gradient:

$$\int_0^t f(x,\tau) \cdot d\tau = \int_0^t \gamma G_x(\tau) x \cdot d\tau = (\int_0^t \gamma G_x(\tau) \cdot d\tau) \cdot x = k_x(t) \cdot x \qquad \text{[I-4]}$$

Similarly, the phase difference between adjacent spins in different positions along y-axis will change according to the duration a gradient G_y is left on along that direction. Hence, the gradient-duration product determines the ability to detect differences in position, this defined trajectory k_y. k_x and k_y define k-space.

From the basic k-space formula, it follows that we reconstruct an image $S(\mathrm{x,y})$ simply by taking the inverse 2D Fourier Transform of the sampled data $k_x(\mathrm{t})$ and $k_y(\mathrm{t})$:

$$S(x,y) = \iint S(k_x(t), k_y(t)) \cdot e^{-2\pi i (k_x(t)x + k_y(t)y)} \cdot dk_x dk_y \qquad \text{[I-5]}$$

In a standard spin echo or gradient echo scan, where the readout gradient (G_x) is constant, a single line along k_x axis of k-space is scanned every RF excitation. For a phase encoding gradient (G_y) in between the RF excitation and the commencement of the readout gradient (G_x), this line moves up or down in k-

space and we scan the line k_y=constant. Scanning acquisitions are repeated until k-space is sufficiently well covered. By applying magnetic field gradient (G_x and G_y) in different ways, we obtain different trajectory of k-space, e.g. sinusoidal, spiral or zig-zag trajectory of k-space.

With respect to the Fourier Transform and the Nyquist theorem (reconstruction of a signal from its samples is possible if the sampling frequency is greater than twice the signal bandwidth), we know that the step in k-space determines the field of view (FOV) of the image (i.e. FOV $\propto 1/\Delta k$) and the maximum value of k determines the resolution.

In addition, the TE value for the center of k-space determines the image's T2 contrast since the data at the center of k-space represent lower spatial frequencies than the data at the edges of k-space.

Magnetic Resonance Imaging (MRI) involves not only balancing spatial resolution and temporal resolution but also signal to noise ratio (SNR), contrast, scan time, field of view (FOV), and so forth. In conventional MRI, this challenge is addressed by sampling the signal repeatedly and gradually building up an image data set from these repeated samples. Alternately, Echo-planar imaging (EPI) is a fast image acquisition technique that forms a complete image following a single excitatory pulse. However, in EPI, the SNR is limited because of the extremely short sampling duration. For many functional MRI studies, multiple EPI images are acquired and compared.

Physics of fMRI

Functional MRI (fMRI) is a powerful noninvasive technique for investigating brain activity with high spatial resolution and good temporal resolution. It uses similar imaging techniques and the same equipment as conventional MRI and relies on detecting small changes in MRI signal associated with neuronal activity in the brain. It is providing unique information for neuroscience.

fMRI is an indirect method of measuring brain activity. It does not look at the electrical activity of neurons directly. Instead it measures the way in which the circulatory system responds to the increased energy demands of activated brain cells. Red blood cells (RBCs) go from an oxygenated to a deoxygenated state during functional activation, as oxyhemoglobin (HbO_2) converts to deoxyhemoglobin (Hb). During this process, the magnetic properties of RBCs change. Magnetic susceptibility χ refers to the magnetic response of a material when placed in a magnetic field and the generation of extra magnetic fields in materials that are immersed in an external field. Deoxyhemoglobin is paramagnetic ($\chi > 0$), and oxyhemoglobin is weakly diamagnetic ($\chi < 0$) — that is isomagnetic with respect to the surrounding tissue (Figure I-2). The relaxation rate of water molecules around paramagnetic ions (such as the those in deoxyhemoglobin) is enhanced (i.e.,T2* is shortened).

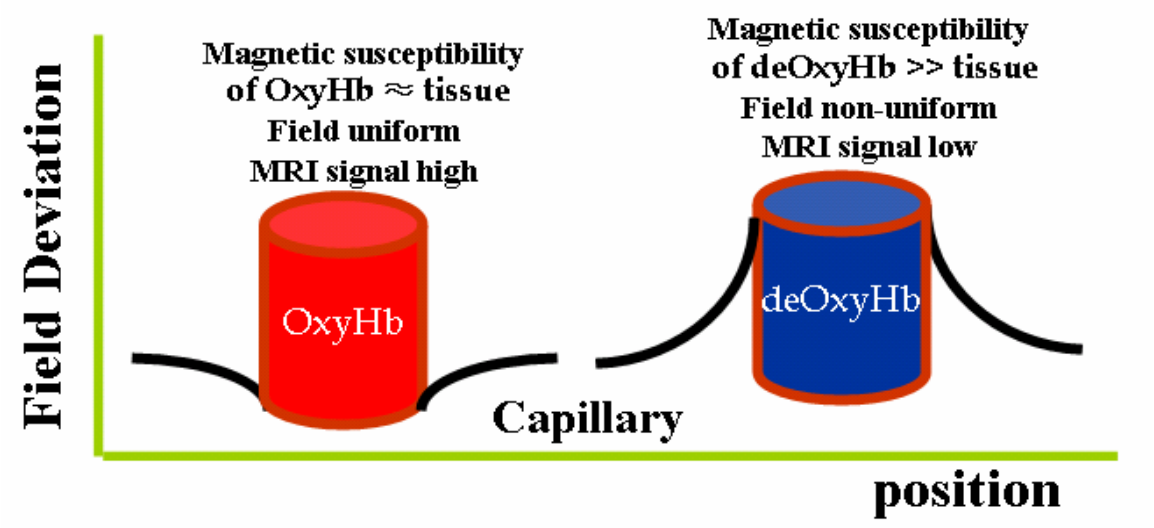

Figure I-2. Difference in magnetic susceptibility χ between blood and the surrounding extravascular space leads to microscopic magnetic field gradients in the vicinity of the blood vessels.

T2*-weighted images are acquired with pulse sequences sensitive to field variations and are performed to take advantage of the fact that deoxygenated hemoglobin is paramagnetic, whereas oxygenated hemoglobin is not. Because deoxyhemoglobin causes rapid dephasing, T2* is longer in regions much more oxygenated blood compared to those with less oxygenated blood. Thus, an area with more oxygenated blood will appear more intense on T2*-weighted images compared to an area with less oxygenated blood.

Brain activity and neuronal activity: physiology

Neuronal activity consumes most of the metabolic energy of the brain. Neuronal firing is responsible for most of the energy usage; only a small percentage of the energy is used for neurotransmitter recycling [Attwell, and

Laughlin, 2001]. The neurons rely on oxidative metabolism (Figure I-3b); therefore, the hemodynamic response is related to the need for oxygen, which in turn, is related to neuronal activity. Vasculature response in the brain is correlated with glucose and oxygen consumption and is slow relative to the underlying changes in neuronal activity. It is observed that cerebral blood flow increases following increased synaptic activity. This increase is proportional to glucose consumption [Fox et al., 1988] but does not correlate well with oxygen consumption. Though the blood flow delivers the required oxygen to neurons, it actually serves to deliver the level of glucose required by the astrocytes, regardless of blood oxygenation. Given that oxygen extraction from the blood vessels is less efficient at higher flow rates, there is a disproportionately large change in blood flow compared to oxygen metabolism [Fox et al., 1988; Buxton and Frank, 1997; Heegar and Ress, 2002].

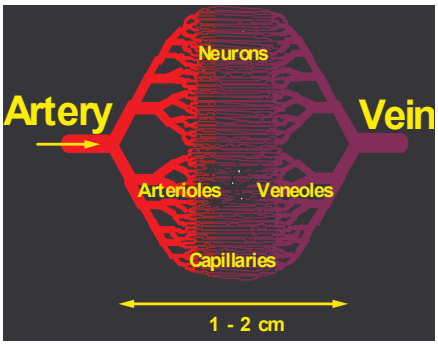

a

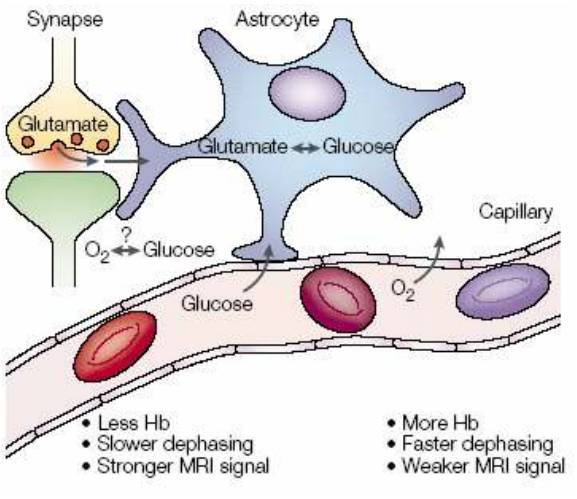

b

Figure I-3. a. Vasculature structure; b. Relationship between synaptic activity, neurotransmitter recycling and metabolic demand

The Cerebral Metabolic Rate of Oxygen ($CMRO_2$), the Cerebral Blood Flow (CBF), and the Cerebral Blood Volume (CBV) have different effects on oxyhemoglobin and deoxyhemoglobin concentrations (Figure I-4). The complicated mixture of these physiological adjustments in response to transient neuronal activity generates three phases of hemodynamic response.

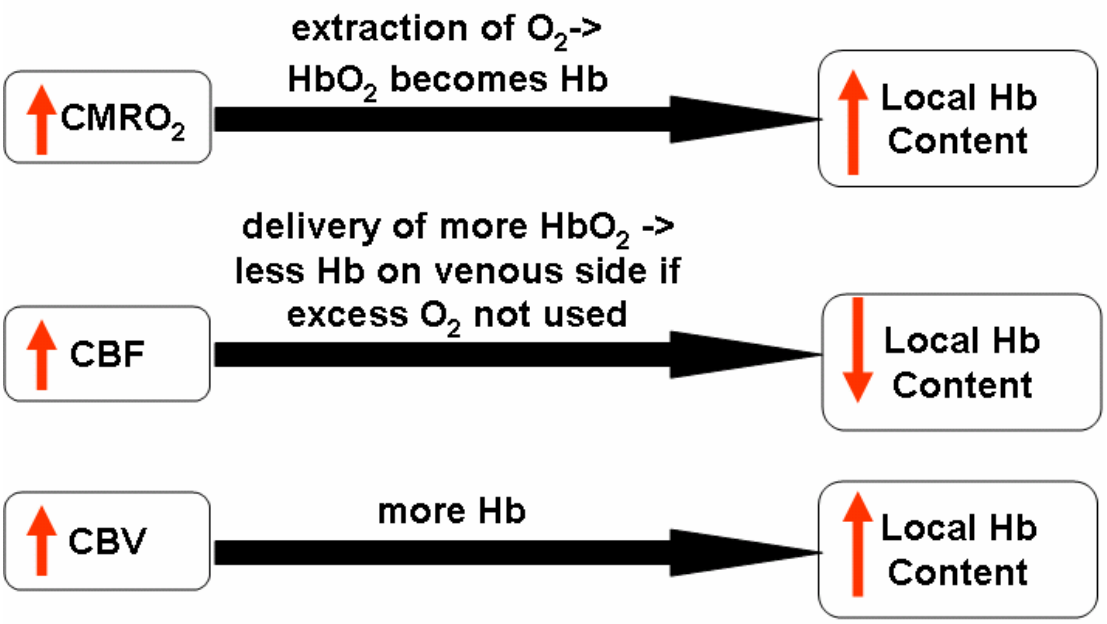

Figure I-4. CBF, CBV, and $CMRO_2$ have different effects on Hb concentration.

An external stimulus can induce neural activity, and in turn induce local physiological changes. The changes in the relationships among post-stimulus physiological variables generate different stages: The neural activity requires energy, and in the early phase, the cerebral metabolic rate of oxygen ($CMRO_2$) increases in tissue and demands an increase in the Oxygen Extraction Fraction (OEF). Blood becomes deoxygenated and then recruits more oxygen. The higher pressure of O_2 (pO_2) on the vascular wall increases the OEF that supports the

bioelectric work to sustain neuronal excitability, which, in turn, results in an increased concentration of Hb in blood vessels. A couple of seconds later, the cerebral blood flow (CBF) increases to supply more oxygen, but the change in CBF appears to be more than is necessary to support the small increase in O_2 metabolism., This mismatch results in higher HbO_2 concentration (as opposed to Hb concentration) on the venous side. The net result of this imbalance of ΔCBF (30%) to $\Delta CMRO_2$ (5%) [Fox and Raichle, 1986; Fox et al., 1988] is a decrease in the amount of deoxygenated blood within tissue. In this stage, the cerebral blood volume (CBV) also increases because of the requisite dilation of blood vessels, which is the mechanical response involved in the removal of waste while providing nutrients. Later on, the $CMRO_2$, CBF and CBV slowly return to normal levels; however, the return of CBV is slower than that of CBF.

Physiology of blood oxygen level dependent (BOLD) fMRI in neuroscience

The delivery of oxygen in the brain vascular network is a complicated process that involves several physiological factors associated with neuronal activity, such as CBF, CBV and $CMRO_2$. fMRI, which is based on the BOLD (blood oxygen level dependent) effect, records the magnetic resonance (MR) signal changes produced by the physiological adjustments in blood flow and volume that accompany the changes in oxygen metabolic demand [Ogawa, 1990]. Dephasing caused by deoxyhemoglobin is the main factor causing signal intensity variations in the BOLD-fMRI technique. The origins for main BOLD signal increases following a transient change in neural activity (T2* weighted) are that blood flow

increases greater than necessary to supply the oxygen in need by neuronal activation, which results in a decrease in amount of deoxygenated blood within tissue, so tissue becomes magnetically more uniform and MRI signal increases (Figure I-5).

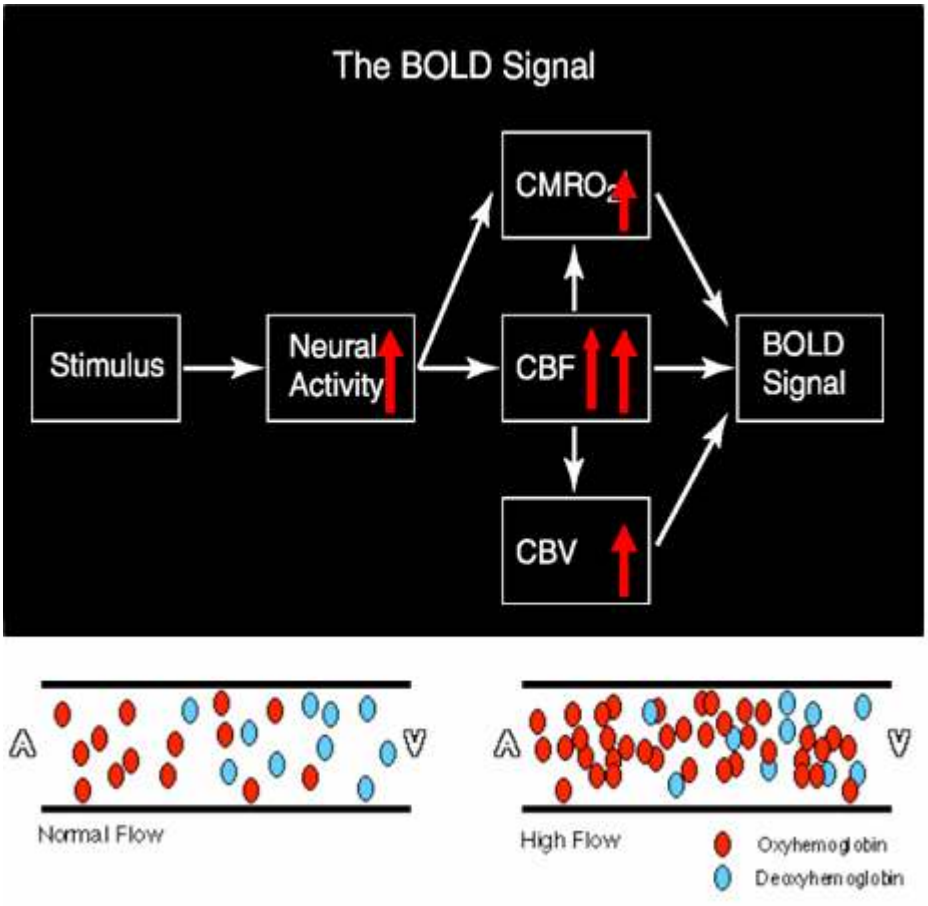

Figure I-5. Change in CBF appears to be more than is necessary to support the small increase in O2 metabolism.(ΔCBF >> ΔCMRO2).

The CBF, CBV, and $CMRO_2$ have different effects on oxyhemoglobin and deoxyhemoglobin concentrations, which affect the magnetic environment. There are complicated dynamic processes involved in response to transient neuronal

activity that generate three phases of BOLD response (Figure I-6): (1)an initial low amplitude negative response during 0.5 to 2 seconds following stimulation (the “pre-undershoot”) resulting from the increase of the Oxygen Extraction Fraction (OEF) prior to Cerebral Blood Flow (CBF); (2) a smooth rise to peak, typically over the interval 2 to 5 seconds, with a slower fall to baseline from 5 to 10 seconds because of the imbalance of ΔCBF and $\Delta CMRO_{2;}$ and (3) an even slower negative response that may last an additional 10 seconds or longer (the “post-undershoot”)because it takes longer for the blood volume to return to baseline after the oversupply of oxygenated blood has diminished.

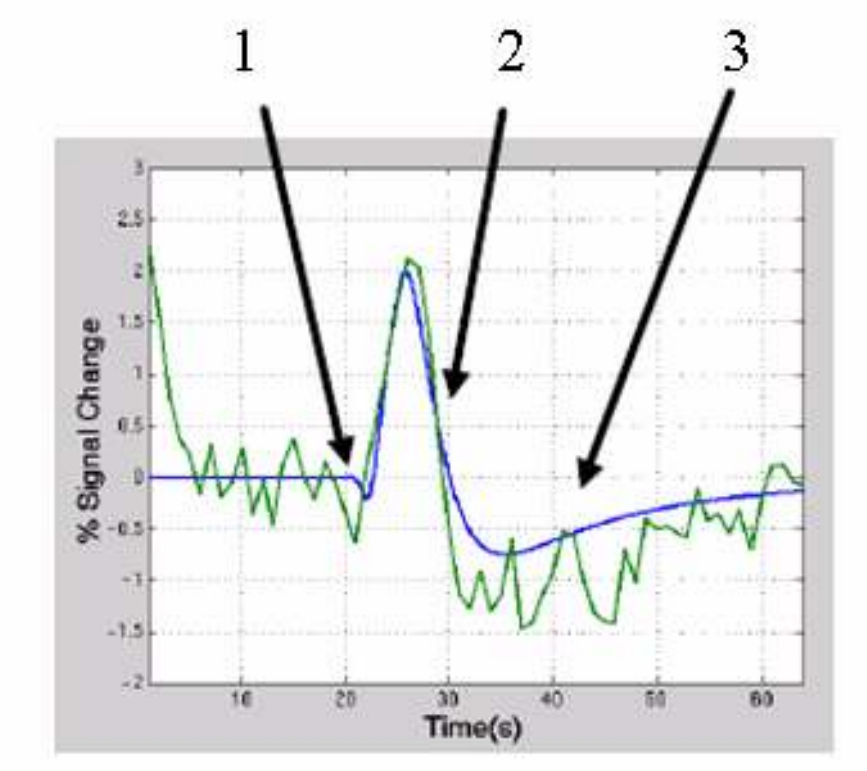

Figure I-6. Typical BOLD response to a brief stimulus.

The fMRI signal depends on the correlation between oxidative metabolism (cerebral metabolic rate of oxygen [$CMRO_2$]) and cerebral blood flow (CBF), which supports the bioelectric work to sustain neuronal excitability, as well as the requisite dilation of blood vessels (cerebral blood volume [CBV]), which is the mechanical response involved in removal of waste while providing nutrients. The signal change relative to these physiological factors can be expressed by the equation below (Hyder, 2004), where M and N are measurable physiological and magnetic constants:

$$\frac{\Delta S}{S} = M\left(\frac{\Delta CBF}{CBF} - \frac{\Delta CMRO_2}{CMRO_2}\right) - N\left(\frac{\Delta CBV}{CBV}\right) \qquad \text{[I-6]}$$

Usually, we obtain brain BOLD fMRI using a variety of experimental designs, either blocked (stimuli presented together in blocks) or event-related (stimuli presented separately). Then the time course of the MR signal must be analyzed. This signal time course varies by brain region since regions can respond differently to different stimulus conditions. Plus, MR signal intensities are arbitrary: they vary from magnet to magnet, coil to coil, within a coil (especially surface coil), day to day, even run to run; they may also vary from area to area in the brain (some areas may be more metabolically active). So we must always have a comparison condition within the same experiment to allow for baseline or control contrasts.

In order to achieve our goal, a proper statistical analysis is necessary. There are several software packages (e.g. SPM, BrainVoyager and Matlab) available for this task. Most use the general linear transform model (GLM) [Friston et al.

1995] approach, which assumes that the fMRI signal possesses linear characteristics with respect to the stimulus and that the temporal noise is white. Then activation maps (Figure I-7) are obtained at different response levels, as determined by the significance level and the established threshold for the number of continguous voxels that must be activated.

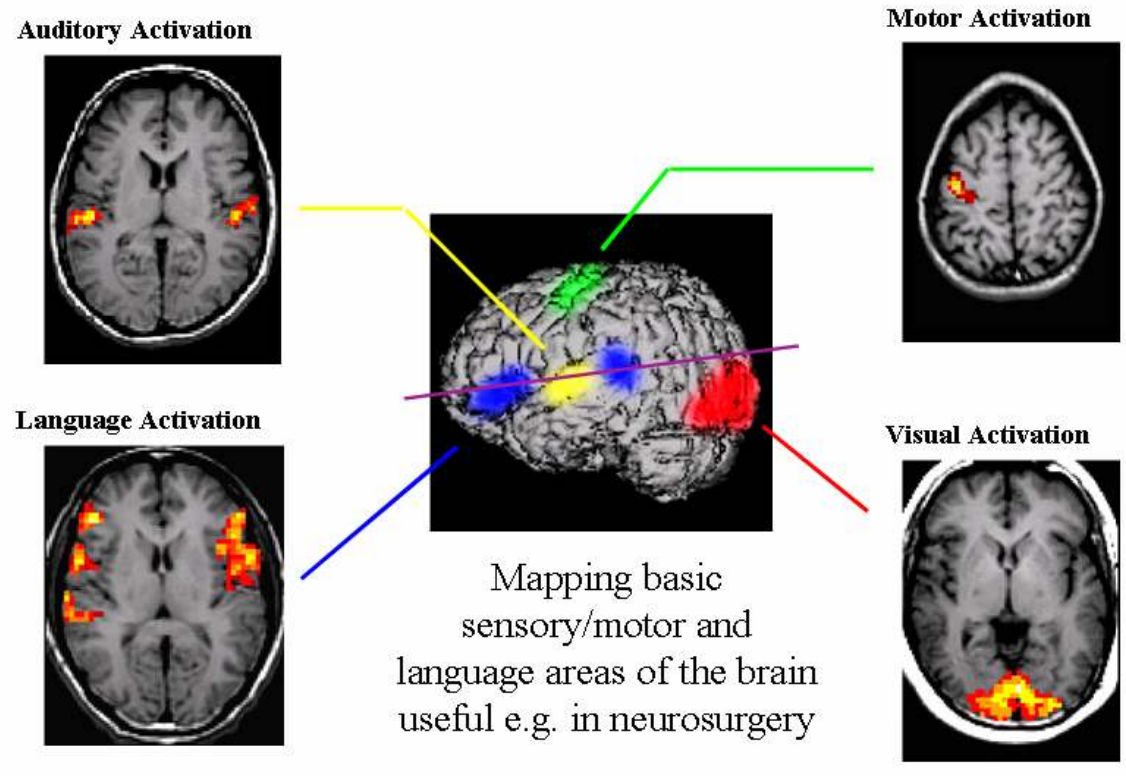

Figure I-7. Some examples of functional mappings.

We have discussed how the BOLD response is an indirect measure of neural activity, how its time course is long and has a related latency. There is not a simple relationship between amount of activity and MR signal intensity, and many questions remain about this relationship: How does the temporal shape of the fMRI response reflect activity? Can fMRI directly map neural activity? Is the

hemodynamic response function (HRF) linearly coupled to neural activity? How does hemodynamic response (HR) couple to mechanisms of activation? In addition to local activity, how do external factors affect BOLD signal? How are neural activity, physiological variables and BOLD signal related? What is the dominant source of BOLD signal in different brain areas? Can we find a good model that includes these underlying neuronal or physiological sources?

Electroencephalography (EEG) and event-related potentials (ERPs)

Compared to fMRI, electroencephalography (EEG) and the associated technique of event-related potentials (ERPs) have much higher temporal resolution (on the order of milliseconds), which allows them to measure changes in neural activity more directly.

Event-related potentials (ERPs) are brain electrophysiological responses time-locked to some "event". This event may be a sensory stimulus (such as sight, sound, or touch), a mental event (such as memory, imagination, or emotion), or the omission of a stimulus (such as an increased time gap between stimuli). ERP studies record small evoked potentials through electrodes that are placed on the scalp and other places on the head. ERPs that are recorded from the brain scalp originate from structures within the brain, and they are very low in voltage, on the order of microvolts. The signals picked up by electrodes can be amplified and displayed for interpretation.

The low frequency component of the electrophysiological signal reflects the superposition of synchronized neuronal currents, averaged over a larger volume

of tissue. This local field potential (LFP) is believed to reflect inputs and intra-cortical activity but is often (although not always) correlated with the output spiking activity in single- or multi-unit recordings. The multi-unit activity (MUA) is believed to reflect the spiking activity of neurons near the electrode tip (within ~200 μm).

ERPs can be subdivided into several components or component classes. These components are usually seen as a series of changes in polarity ("positives and negatives") of the averaged signal. Some ERP phase components are specifically related to a particular type of stimulus presentation. For example, P300 is a positive peak that can be detected around 300msec post task stimulus for oddball tasks. N170 is a negative evoked potential polarity that appears at around 170msec after each presentation of a face picture.

Neural activity involves the excitation of multiple neurons in complex patterns of firing and spiking. Cortical ERPs have been used extensively in research to map changes in neural activity related to an event with millisecond resolution. The topography of ERPs provides a window into understanding the brain processes in the cerebral cortex.

However, the main limitation of EEG/ERP is its comparably low spatial resolution. Though it can keep pace with the speed of neuronal processing in the cortex, it is hard to accurately locate the original generator of the surface potential in the brain.

Near infrared spectroscopy (NIRs)

It has long been known that light transmission and absorption in living tissue is sensitive to hemoglobin concentration and its oxygenation state (Milliken, 1933). The hemoglobin concentration and oxygenation state changes with response to local neural activity. Hence cortical function can be investigated by imaging reflected light. Modulation of the recorded intensity of reflected light by localized changes in the optical properties of brain vasculature is associated with neural activity. To capitalize on these changes, the low tissue absorption of near infrared light between approximately 650~950 nm is utilized. At this wavelength, light is differentially absorbed and scattered by oxyhemoglobin and deoxyhemoglobin. Transcranial near infrared spectroscopy (NIRS) detects this differentiation by using an array of optical fibers on the scalp to construct spatial maps of cortical activity. This noninvasive technique measures hemoglobin absorption and can provide spectroscopic information on chromophore concentration changes in oxyhemoglobin and deoxyhemoglobin (Hebden and Delpy, 1997). Measuring the light intensity modulated by the blood volume and hemoglobin oxygenation provides important information about the hemodynamic response to brain activation.

Many researchers have showed that NIRS results are consistent with other imaging techniques, such as fMRI and PET [Villringer 1997, Strangman 2002]. In addition, NIRS has been successfully used to monitor spatio-temporal blood volume and oxygenation changes in cortex during sensory or motor stimulation, cognitive function and hemodynamic fluctuations [Obrig 2000; Toronov 2000].

These have verified that NIRS is a reliable measure of brain function.

NIRS has good (~1mm) resolution, but its temporal resolution is similar to fMRI because of the duration of hemodynamic responses. The main limitation of NIRS is that absorption and scattering of NIR energy in the tissue makes it unsuitable for functional studies of deep structures. But at the cortical surface, NIRS is well suited for mapping functional cerebral hemodynamics, making it an effective method for studying the dynamics of physiological processes, particularly brain hemodynamics.

Event-related design and integration of different modalities

What is the briefest stimulus that fMRI can detect? This may vary according to brain region, and stimulus type. An event-related paradigm is designed to measure the brain's response after a transient stimulus presentation, and it allows for special types of experiments, such as those that require no adaptation to repeated stimuli, e.g. "oddball" studies. It also provides greater temporal control and allows for exploring changes in MRI signal over time. In addition, it is less affected by some confounds of noise and drift artifacts and makes randomization of stimuli (multiple trial types in one run) possible. The main drawback to event-related fMRI (ER-fMRI) is the statistical power lost compared to block designs. Increasing the number of the trials to obtain better statistical averaging is advantageous. ER-fMRI also requires more complex study design and analysis, especially regarding timing and baseline.

For the same event-related design, BOLD fMRI shows very good 3D spatial

resolution, but the temporal resolution of fMRI is limited. The reason is that the sluggishness of the hemodynamic response “blurs” the measured response to brain activation. Also fMRI is only an indirect measure of the neural activity. Techniques like EEG or ERP provide important information about the timing of neural responses but are limited in identifying the location from which the responses are generated. Compared to electrophysiological techniques of EEG and ERP, where source localization is very difficult, the spatial resolution of NIRS (~1mm) is quite good.

In this study, we aimed to understand how neuronal activity, hemodynamics and BOLD fMRI signals are related. There is a critical need to identify new strategies to enable the delineation of the spatial and temporal relation between behavior and brain function. The combination and co-registration of neuroimaging methods has been repeatedly recommended. ERP/EEG, NIR and fMRI show different and complementary advantages and disadvantages, so we seek to integrate these modalities to better investigate brain activation and its underlying neuronal and physiological mechanism.

The combination of fMRI, ERPs and NIRS would balance out the limited temporal resolution of fMRI and allow monitoring of fast changes in neuronal information processing by ERP. At the same time, fMRI provides measurements of event-related hemodynamic changes with millimeter spatial resolution and structural MR images of the brain can be co-registered to images from ERPs and NIRS to further improve source localizations.

Both physiological and neuronal mechanisms of BOLD fMRI signal remain to be fully understood. In the following chapters, two comparable event-related visual tasks were used to study the nonlinear nature of BOLD fMRI signals and their underlying origins. We found a strong correlation between BOLD effect hemodynamics as detected by fMRI and by NIRS. This, in combination with a theoretical model which explicitly includes nonlinear physiological variations, helps refine our understanding of the BOLD effect. Finally, the neuronal origins of the BOLD effect have been investigated and discussed in relation to the generation of ERPs.

CHAPTER II

NONLINEARITY OF HEMODYNAMIC RESPONSE TO TRANSIENT ACTIVATION AND DEACTIVATION

We report studies of the non-linear nature of blood oxygen level dependent (BOLD) responses to short transient deactivations in human visual cortex. Hemodynamic response functions (HRFs) associated with transient activation and deactivation in primary visual cortex acquired by functional magnetic resonance imaging (fMRI) have been compared and contrasted. We show that signal decreases for short duration deactivations are smaller than corresponding signal increases in activation studies. Moreover, the observed non-linear nature of deactivation is different from that of activation.

Introduction

Functional MRI based on the BOLD (blood oxygen level dependent) effect records the magneric resonance (MR) signal changes produced by alterations in tissue blood volume, flow and oxygenation. The time course of the BOLD signal change observed following a transient change in neural activity (the hemodynamic response function or HRF) reflects the physiological adjustments in blood flow and volume that accompany the changes in oxygen metabolic demand. These changes are not quantitatively matched to the changes in oxygen use and it is this mismatch that underlies the positive BOLD signal change. The MR signal increase following a transient excitation is believed to

arise because the flow and oxygenation increase are greater than are required to meet metabolic demand. Conversely, during a steady state of continuous activation, an equilibrium is established between flow and metabolism. When a transient decrease in activation occurs (e.g. by interrupting a stimulus) the oxygen demand is reduced. Experimentally the subsequent HRF for this "deactivation" corresponds to an MR signal decrease, suggesting that flow is reduced to a degree greater than that required to reestablish the same level of tissue oxygenation, or that oxygen demand remains high in the presence of decreased activity. The quantitative and temporal natures of the coupling of the physiological changes to decreases in neural activity are not well established. Furthermore, most analyses of event-related fMRI studies assume that the HRF for transient neural deactivation is simply the inverse of that for activation, which also has not been established.

The BOLD response to transient activations has been well studied previously, and for successive short duration stimuli the BOLD responses do not add linearly [Boynton 1996; Robson 1998; Liu 2000], but over-predict the effects of longer durations of a stimulus. A further characteristic of a linear system is that changes in response to both activation and deactivation should be reciprocal, but few studies have looked at deactivations. Birn et al. found the decrease in BOLD to removing a stimulus for short durations was smaller than predicted by a linear system. Hence, the BOLD response to both activation and deactivation are nonlinear and not reciprocal. BOLD effect reflects changes in neuronal activity, cerebral metabolic rate of oxygen, cerebral blood flow, and cerebral blood

volume, and precise nature of these are different for negative and positive BOLD signals.

We have investigated the hemodynamic response functions in visual cortex in response to both short activations (relative to a resting baseline) as well as to short interruptions of a steady state activating stimulus (deactivations). The extent to which positive and negative responses differ may shed light on models of BOLD responses and is important for the design and interpretation of experiments and for choosing appropriate methods of data analysis.

Method

Subjects

A total of 12 healthy volunteers (4 females, mean age 25.8, range 21-30 years) participated in the studies. All had normal or corrected to normal vision. Written informed consents were obtained from all volunteers prior to the examinations. All subjects were instructed to keep their eyes open and maintain constant attention throughout all experiments.

Stimulus Presentation

An 8Hz large-field contrast-reversing checkerboard pattern at 100% contrast served as a visual excitation stimulus (denoted as condition “ON”). A spatially uniform black screen served as a second condition (“OFF”). The scanner room lights were dim during all examinations. Combinations of these stimuli generated

by E-prime (Psychology Software Tools, Inc) were presented to the subjects in event-related manner (Figure II-1): Various durations of visual inactivity (stimulus "OFF" for 1sec, 2sec, 3sec, 4sec, 6sec, or 8sec) were interspersed during otherwise continuous visual stimulation ("ON") to assess the ability to detect transient deactivations and to test the signal linearity. A total of 8 scan runs were acquired, consisting of 2 repeated runs each of 1sec (18trials/run) and 2sec (14trials/run) duration of stimulus-OFF, and 1 run each of 3sec (16trials/run), 4sec (16trials/run), 6sec (8trials/run) and 8sec (8trials/run) duration of stimulus-OFF. Each run started with a flashing checkerboard ("ON") for 22s, followed by the variable durations of stimulus-OFF. The stimulus interval was 22sec for 1sec, 2sec, 3sec and 4sec stimulus-OFF and 26sec for the 6sec and 8sec OFF.

Stimulus-"ON"

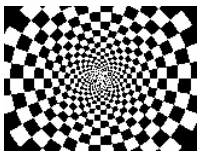

(flickering frequency = 8Hz)

Stimulus-"OFF":

OFF=1sec, ITI=22sec, 18trials/run x 2runs
OFF=2sec, ITI=22sec, 14trials/run x 2runs
OFF=3sec, ITI=22sec, 16trials/run x 1run
OFF=4sec, ITI=22sec, 16trials/run x 1run
OFF=6sec, ITI=26sec, 8trials/run x 1run
OFF=8sec, ITI=26sec, 8trials/run x 1run

Figure II-1. Stimulus presentation in Paradigm III.

We also investigated the hemodynamic response functions in visual cortex in response to transient activations as well as to transient deactivations. Two reverse event-related paradigms (Figure II-2) were generated using E-prime (Psychology Software Tools, Inc) and presented to the subjects: In the first, a transient activating stimulus (stimulus "ON" for 2 or 4 seconds) was presented within an otherwise continuous black screen ("OFF"). In the second, a transient deactivation was prduced (stimulus "OFF" for 2 or 4 seconds, interspersed during an otherwise continuous visual stimulation ("ON")). In total 80 trials were presented in 4 runs, and each condition (2 or 4sec of flickering checkerboard ON and 2 or 4sec of black screen OFF) was presented 20 times with a 20sec target to target interval. In addition, the pattern of baseline condition was always viewed for 20sec before the first target presentation to reach a steady-state.

ON = 2sec or 4sec; OFF = 2sec or 4sec

Figure II-2. Two reverse paradigms (I and II) of stimulus presentation.

To localize each subject's visual area, we performed a retinotopic mapping in which a traveling wedge of flickering checkerboard was presented before the actual functional runs.

Data Acquisition

MR images were acquired on a 3T Philips Achieva using an 8-channel SENSE head coil. Ten T1-weighted anatomic images were collected parallel to a line passing through the anterior-posterior commissures (AC-PC line) with 5mm slice thickness and 1mm gap and positioned to cover the visual areas. Then functional BOLD images were collected in the same planes, using a gradient echo EPI sequence (TR/TE=1sec/35msec, flip angle=70^{o}, FOV=22x22cm^2 and acquisition matrix size=80x80 reconstructed to 128x128).

Data Analysis

The hemoglobin concentration changes in different zones of visual cortex obtained using the NIR spectrometer and the BOLD signals obtained from the MR scanner were both analyzed using BrainVoyager QX and additional software running under MATLAB.

BOLD fMRI data were first motion corrected, realigned and coregistered with T1-weighted structural images collected using identical slice prescriptions, then registered to Talaraich coordinate brain. A general linear transform model (GLM) [Friston 1995], which assumes that the fMRI signal possesses linear characteristics with respect to the stimulus and that the temporal noise is white, was used to estimate the response. We first used a correlation template generated by convolving the box-car function of the stimulation paradigm with a canonical fMRI impulse response function described by Friston et al. [Friston 1994] to do the cross-correlation analysis [Bandettini 1993]. Cross-correlation

maps were thresholded (P < 0.001) to generate activation maps. After we performed an event-related general linear model (GLM) analysis to compute the activation maps, we then examined the time courses of the signals within the activated regions of interest (ROIs) for both transient activations and deactivations.

Results

Negative BOLD responses (or signal decreases) were found when the flickering checkerboard was interrupted. Figure II-3a shows the BOLD response curves following stimulus gaps ranging from 1 to 8 second duration, averaged across subjects.

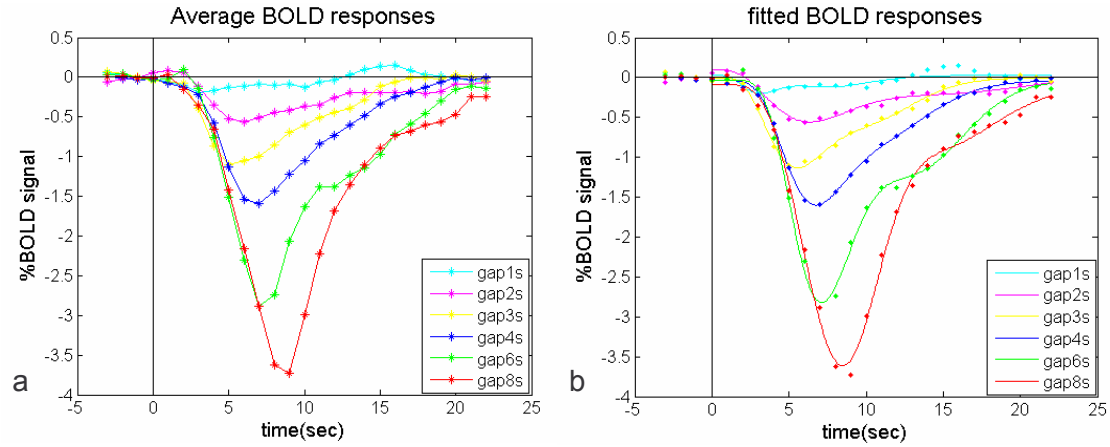

Figure II-3. The average (n=5) event-related BOLD signal changes in the primary visual cortex in response to varying durations of stimulus interruption. a. Measured BOLD responses; b. Fitted BOLD responses using the gamma-variate function.

We performed a least squares fit of the experimental signal-time curves with a double gamma-variate function of the form [Liao, et al., 2002]:

$$f(t) = (\frac{t}{d})^{a} e^{-(t-d)/b} - c(\frac{t}{d'})^{a'} e^{-(t-d')/b'} + E \qquad \text{[II-1]}$$

The fitted initial values for visual areas were selected as: a=7, b=0.9, d=6.3, a'=14, b'=0.9, d'=12.6, c=0.35, E=0.05.

Then we obtained the magnitude and temporal parameters of the fitted hemodynamic response functions (Figure II-3b) as shown in Table II-1 and Figure II-4. Comparing the fitted responses, we found that the deactivations to very short durations (<2sec) of stimulus OFF were barely detectable in area V1.

Table II-1. List of the amplitudes of peak and the time to peak for fitted BOLD response to varying durations of stimulus interruption.

Duration of Gaps	1sec	2sec	3sec	4sec	6sec	8sec
peak (%)	-0.20	-0.38	-1.13	-1.60	-2.82	-3.61
Time to peak (sec)	3.15	5.28	5.56	6.76	7.12	8.48

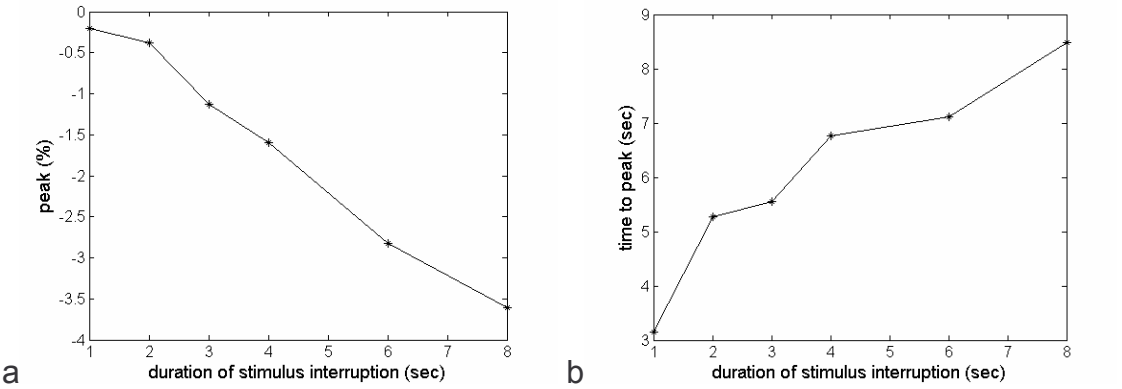

Figure II-4. Trend of the amplitudes of peak and the time to peak for fitted BOLD response to varying durations of stimulus interruption.

As shown in Figure II-5, we used the responses to shorter stimulus gaps to

predict the responses to longer gaps. Unlike the corresponding prediction of activation responses [Boynton 1996; Robson 1998; Liu 2000], the predicted curves of deactivation signals always tend to underestimate the experimental responses.

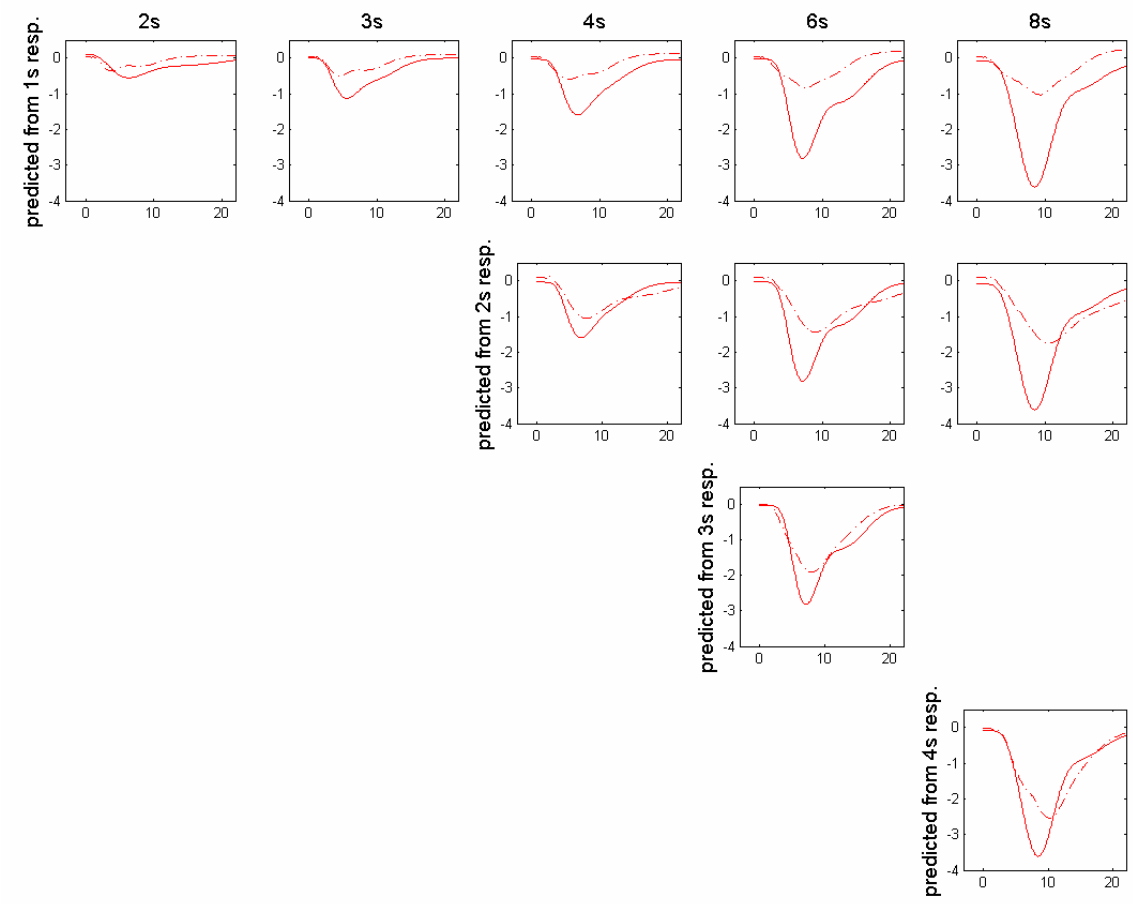

Figure II-5. Comparison between the measured (solid line) and predicted (dash line) BOLD response curves assuming linearity. The predictions using the response to shorter duration gaps are shown in the same row, and the measured responses to 2sec, 3sec, 4sec, 6sec, 8sec stimulus gaps plotted together with the corresponding predictions are shown in different columns.

The ratios of the areas under the experimental BOLD response curves to various durations of the stimulus-OFF were calculated, with the ratio at the

longest duration (8sec) normalized to 1, as shown in Figure II-6.

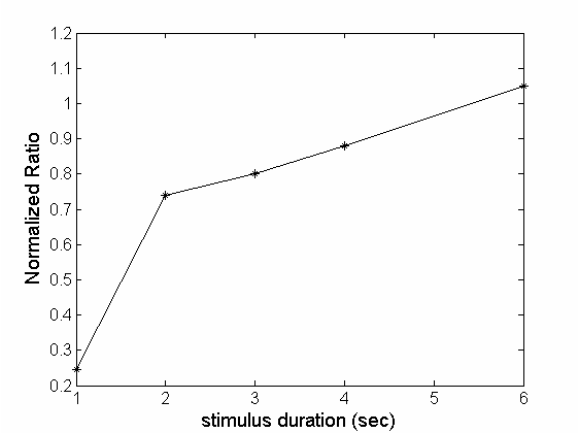

NR>1: overestimate the responses to longer duration of gap;

NR=1: perfect prediction (ideal linear system behavior).

NR<1: underestimate the responses to longer duration of gap.

Figure II-6. The normalized ratio of the area under the average BOLD responses curve to various durations of the stimulus-OFF.

The BOLD MR signal in primary visual area V1 showed different transient hemodynamic responses to the ON and OFF conditions as expected. A positive BOLD effect was found in V1 in response to the brief checkerboard stimuli, whereas a negative BOLD response (or signal decrease) was found when the checkerboard was interrupted (Figure II-7). fMRI signal time courses in response to 2 or 4 sec stimulus ON and OFF were also plot in one figure.

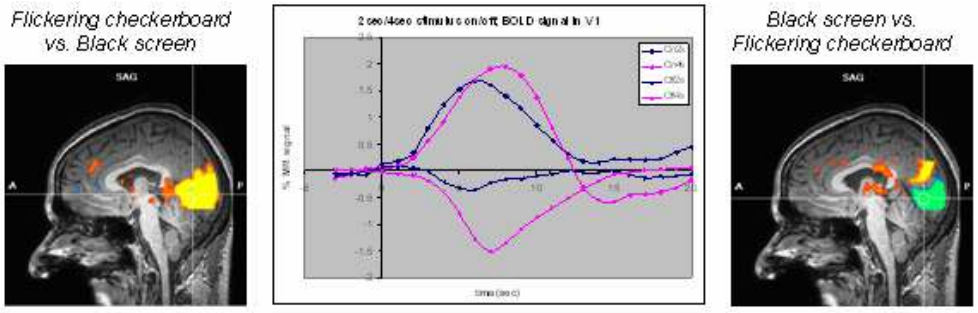

Figure II-7. Compare BOLD responses to ON vs.OFF in V1 (average of 5 subjects): they are not mirror images, and different in magnitude and shape.

Again, to compare the activation and deactivation responses, we fit the experimental signal-time curves with a gamma-variate function (equation [II-1]) of the form in the least-squares sense [Liao, et al., 2002]. Then we obtained the magnitude and temporal parameters of the fitted hemodynamic response functions (Figure II-8b) shown in Table II-2. Comparing the fitted responses, we found that the deactivation response to a 2sec stimulus OFF was very small in V1 compared to the positive signal increase recorded for a 2sec ON stimulus.

Table II-2. Amplitudes of peak (A_peak) and post undershoot/overshoot, time to peak (T_peak) and post undershoot/overshoot for BOLD response to stimulus-ON and OFF for 2sec or 4sec. There are significant differences in time to peak.

Parameters	T_peak(s)	A_peak(%)	T_undershot(sec)	A_undershot(%)
on2s	6.12	1.43	13.88	-0.08
on4s	7.53	1.93	15.37	-0.67
off2s	5.28	-0.38	/	/
off4s	6.76	-1.60	/	/

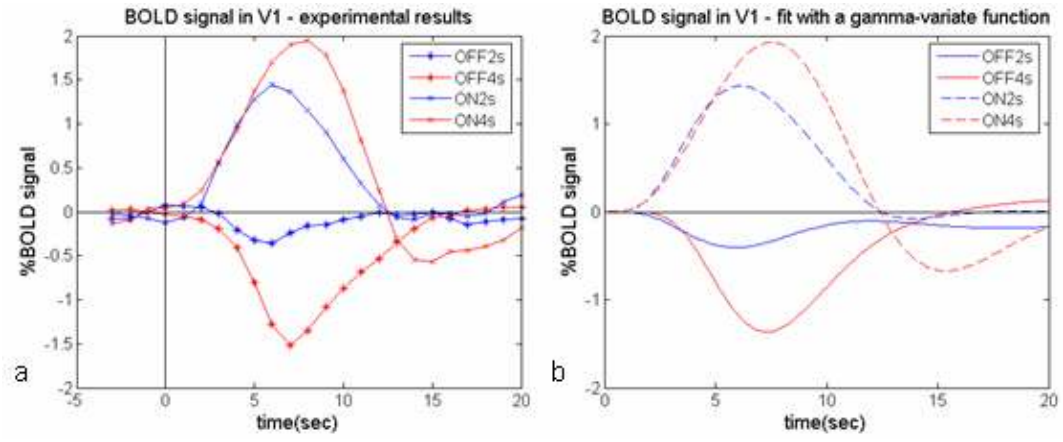

Figure II-8. BOLD responses in V1. a. Measured BOLD responses (average of 5 subjects); b. Fitted BOLD responses using the gamma-variate function. Deactivation responses are smaller and have longer latency but shorter time to peak, more narrow width and no significant post overshoot.

In addition, the ON responses for 2sec and 4sec were not related in linear fashion [Ogawa 1990, Boynton 1996],in agreement with previous reported investigations [Miller 2001] which verified that both the CBF and BOLD response nonlinearities showed an over-prediction of the ON response magnitude for long duration responses based on summing short duration responses in primary visual area. However, the OFF responses behaved quite differently: the negative BOLD changes did not behave linearly and the predictions using short duration data tend to underestimate the OFF responses to longer durations of deactivation (Figure II-9). These results are consistent with the previous report of Birn et al. [2005]. The deactivation responses were smaller and also had slightly longer latencies and shorter times to peak, and showed no significant post stimulus overshoots.

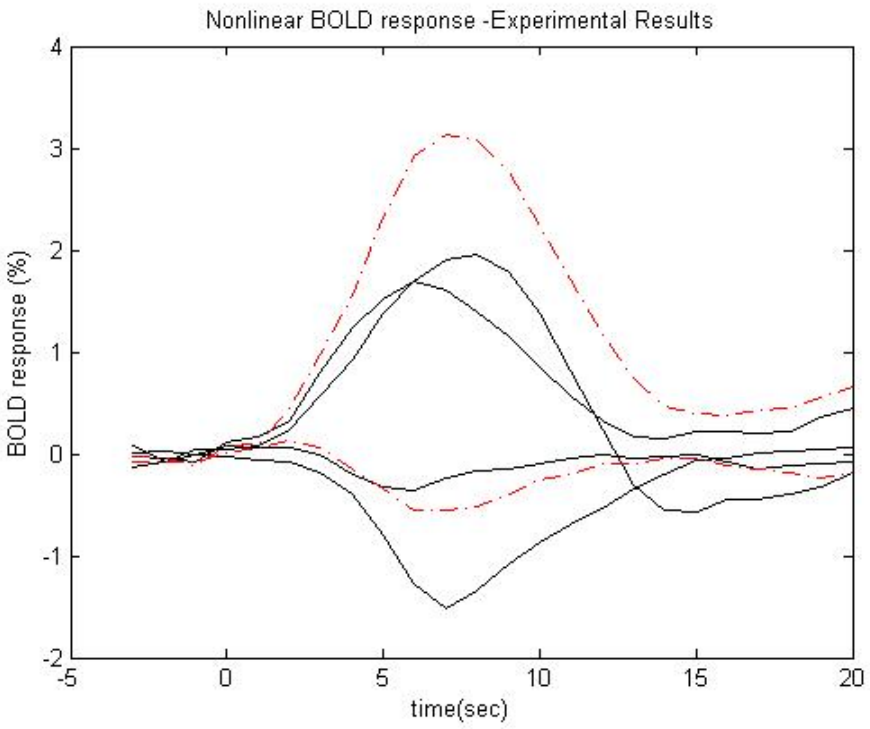

Figure II-9. Linearly convolve data from 2 s trials to estimate the 4 s duration stimulus. Red dash curves show the linear convolutions. Obviously, it tends to overestimate the response to functional activation, and underestimate the response to functional deactivation.

The fMRI data demonstrate the HRF to deactivation is smaller and has a different time course to the HRF for transient activation. Moreover, the HRF for deactivation exhibits a greater degree of nonlinearity. Our ability to detect short (<2sec) deactivations is therefore less than our ability to detect corresponding activations. During a steady state excitation equilibrium is achieved between blood flow, volume and oxygenation. When this is interrupted the sequence of physiological changes is different from those involved in the vaso-dilation that occurs in response to transient excitations, and the HRF presumably reflects those differences.

Conclusion

We have investigated the hemodynamic response functions (HRFs) in visual cortex in response to both short activations (relative to a resting baseline) as well as to short interruptions of a steady state activating stimulus (deactivations). Transient deactivation is not the mirror image of transient activation. The HRF for deactivation differs in magnitude and shape to that for increased activation. For short duration stimuli the HRFs do not add linearly and the magnitude of deactivation responses is smaller than for activation. The sensitivity to detect transient deactivation is therefore lower than for detecting activation. The extent to which these responses differ may shed light on models of BOLD responses and is important for the design and interpretation of experiments and methods of data analysis.

CHAPTER III

COMBINE NIRS AND FMRI TO INVESTIGATE HEMODYNAMIC RESPONSE TO TRANSIENT ACTIVATION AND DEACTIVATION

We used transcranial near-infrared spectroscopy (NIRS) and fMRI to investigate the positive and negative BOLD effects and recorded concentration changes in both oxy- and deoxy-hemoglobin in response to transient activations and deactivations, under normal conditions and after breathing carbogen.

Introduction

Near-infrared spectroscopy (NIRS) is a diffuse optical method that has been used to non-invasively monitor human brain function by relying on the fact that hemoglobin contains chromophores. Oxyhemoglobin (HbO_2) and deoxyhemoglobin (Hb) show different rates of selective light absorption. These useful optical properties make noninvasive spectroscopic measurement of oxy and deoxy-hemoglobin concentrations possible. These diffuse optical measurements can record physiological dynamics, such as changes in the concentrations of oxyhemoglobin [HbO_2], deoxyhemoglobin [Hb] and total hemoglobin [HbT] underlying the hemodynamic response to neuronal activity, and provide a useful window for qualitatively measuring changes in blood oxygenation and total blood volume.

While the optical topography (OT), in which NIRS is used for functional mapping of human cortex, is poor in spatial resolution and depth penetration.

fMRI based on the BOLD effect records the MR signal changes produced by alterations in tissue blood volume, flow and oxygenation. Combining the results from these two modalities has the potential to increase the information and obtainable by anyone of them to better understand the hemodynamic response to the neuronal activation, and the origin of the BOLD signal.

The gas, carbogen is a mixture of carbon dioxide (CO_2) and oxygen (O_2) gases. When carbogen is inhaled, the brain perceives an increase in CO_2 as a decrease in O_2, so the body reacts as if it was not receiving sufficient oxygen: breathing faster and deeper, increasing heart beating rate, and trying to remove carbonic acid from the bloodstream. It then significantly enhances blood flow rate. Hemoglobin is oxygen dependent, and is the predominant light absorber at NIR wavelength. The light transmission in response to carbogen inhalation is sensitive to the changes in hemoglobin saturation.

In this study, we used transcranial near-infrared spectroscopy (NIRS) [Kennan 2002] and fMRI at 3T to investigate both positive and negative BOLD effects. Using NIRS we recorded concentration changes in both oxy- and deoxy- as well as total hemoglobin levels by measuring changes of absorption at two different wavelengths in brain in response to both transient activations and deactivations. Similar experiments were also performed using fMRI.

We have investigated the hemodynamic response functions in visual cortex in response to both short activations (relative to a resting baseline) as well as to short interruptions of a steady state activating stimulus (deactivations). In addition to previous observed different nonlinearity of BOLD responses to

activation and deactivation, we also compared BOLD and NIRS measurements during various stimulation paradigms, and in the next chapter, we try to explain the mechanism of the observed BOLD by using a simulation model. The extent to which positive and negative responses differ may shed light on models of BOLD responses and is important for the design and interpretation of experiments and for choosing appropriate methods of data analysis.

Method

Subjects

A total of 7 healthy volunteers (2 females, mean age 25.8, range 22-29 years) participated in the studies. All had normal or corrected to normal vision. Written informed consents were obtained from all volunteers prior to the examinations. Five of the subjects participated in the NIR experiments and five of the subjects in fMRI experiments. Three of the subjects participated in both the NIR and fMRI experiments. Two of subjects participated in NIRS investigation on hemoglobin changes during normal breathing and carbogen breathing. All subjects were instructed to keep their eyes open and maintain constant attention throughout all experiments.

Stimulus Presentation

An 8Hz large-field contrast-reversing checkerboard pattern at 100% contrast served as a visual excitation stimulus (denoted as condition “ON”). A spatially

uniform black screen served as a second condition (“OFF”). The scanner room lights were dim during all examinations. In order to investigate the hemodynamic response functions in visual cortex in response to transient activations as well as to transient deactivations. Two reverse event-related paradigms (Figure III-1) were generated using E-prime (Psychology Software Tools, Inc) and presented to the subjects in event-related manner: paradigm I, a transient activating stimulus (stimulus “ON” for 2 or 4 seconds) was presented within an otherwise continuous black screen (“OFF”). Paradigm II, a transient deactivation was prduced (stimulus “OFF” for 2 or 4 seconds, interspersed during an otherwise continuous visual stimulation (“ON”)). In total 80 trials were presented in 4 runs, and each condition (2 or 4sec of flickering checkerboard ON and 2 or 4sec of black screen OFF) was presented 20 times with a 20sec target to target interval. In addition, the pattern of baseline condition was always viewed for 20sec before the first target presentation to reach a steady-state.

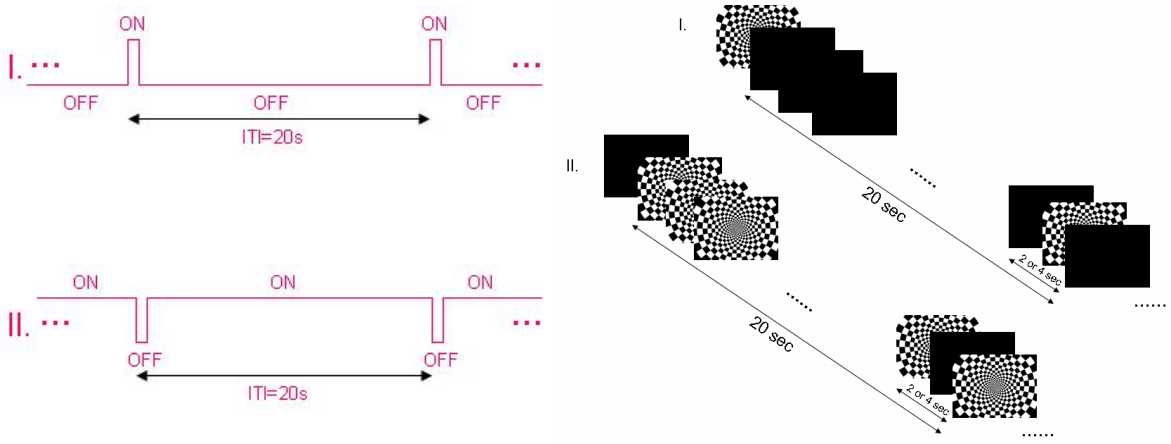

Figure III-1. Two reverse paradigms (I and II) of stimulus presentation.

To localize each subject’s visual area, we performed a retinotopic mapping in

which a traveling wedge of flickering checkerboard was presented before the actual functional runs.

Data Acquisition

MR images were acquired on a 3T Philips Achieva using an 8-channel SENSE head coil. Ten T1-weighted anatomic images were collected parallel to a line passing through the anterior-posterior commissures (AC-PC line) with 5mm slice thickness and 1mm gap and positioned to cover the visual areas. Then functional BOLD images were collected in the same planes, using a gradient echo EPI sequence (TR/TE=1sec/35msec, flip angle=70^{o}, FOV=22x22cm^2 and acquisition matrix size=80x80 reconstructed to 128x128).

NIR data were collected using a multi-channel near-infrared optical topography system (Hitachi topoETG4000) which employs laser diodes in the wavelength range of 700~900nm. The laser light is coupled to the subject via optical fibers on a pad laid out in matrix 3x5 (Figure III-2) so that the total hemoglobin changes were mapped over 9cm x 15cm area. Optodes were positioned on the surface of the skull to be able to sample signals from a central posterior region corresponding to primary visual cortex. Fibers are mounted on a plastic helmet which is fitted to the subject and held by adjustable straps. Optical signals representing [Hb], [HbO_2] and total blood volume changes were collected as described previously.

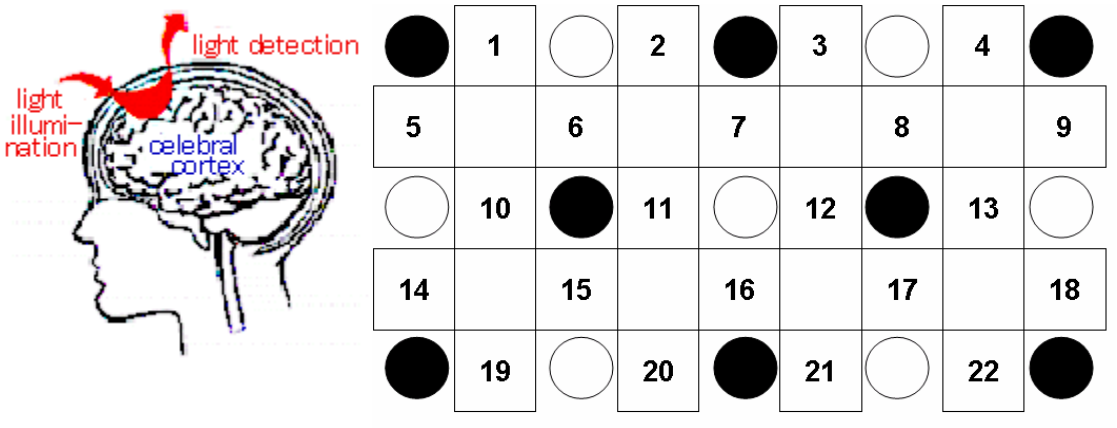

Figure III-2. Arrangement of the transmission and detection fibers (matrix of 3x5). Pairs of adjacent incident (open circles) and detection (filled circles) fibers define optode (numbers) units.

We also investigated the hemoglobin concentration changes during both stimulation ON and OFF in condition of inhaling carbogen gas mixture (95% O_2 + 5% CO_2). For normal breathing, the gas flow rate is around 6~15 l/min, and during carbogen inhaling, the flow rate increase to around 15~25 l/min = 32~53 $foot^3$/hr.

Data Analysis

The hemoglobin concentration changes in different zones of visual cortex obtained using the NIR spectrometer and the BOLD signals obtained from the MR scanner were both analyzed using BrainVoyager QX and additional software running under MATLAB.

fMRI data were first motion corrected, realigned and coregistered with T1-weighted structural images collected using identical slice prescriptions, then registered to Talaraich coordinates. We performed an event-related general linear model (GLM) analysis to compute the activation maps, and then examined

the time courses of the signals within the activated regions of interest (ROIs) for both transient activations and deactivations.

The hemodynamic parameters during stimulation were determined for each NIROT optode position to generate a two dimensional map. This map is then interpolated to produce the final optical image. NIRS data were down sampled from 10Hz to 1Hz, temporally filtered (using a linear trend filter) to avoid drift, then averaged in epochs for each stimulus period (2sec of signal in the pre stimulus period to account for the baseline) to obtain measurements of the event-related oxy- and deoxy-hemoglobin concentration changes for both ON and OFF stimuli.

Results

The BOLD MR signal in primary visual area V1 showed different transient hemodynamic responses to the ON and OFF conditions as expected. A positive BOLD effect was found in V1 in response to the brief checkerboard stimuli, whereas a negative BOLD response (or signal decrease) was found when the checkerboard was interrupted (Figure III-3). fMRI signal time courses in response to 2 or 4 sec stimulus ON and OFF were also plot in one figure. The BOLD response to deactivation is smaller, faster time to peak and shows no post over shoot.

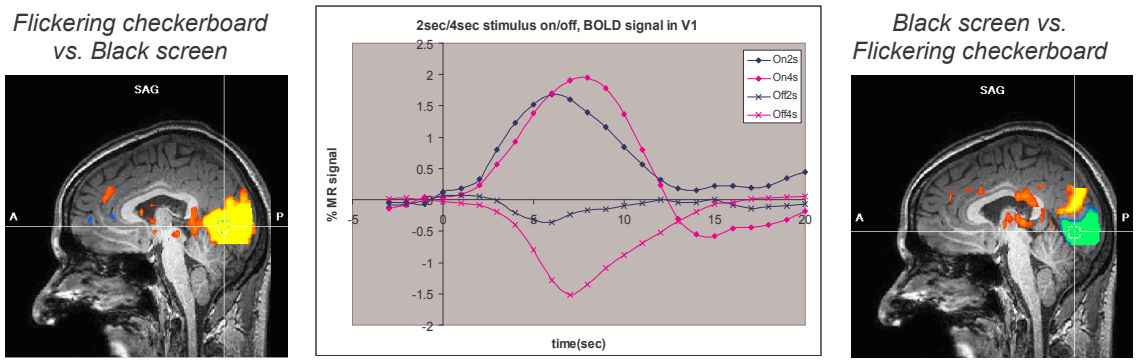

Figure III-3. Compare BOLD responses to ON vs.OFF in V1 (average of 5 subjects): they are not mirror images, and different in magnitude and shape.

The optical mapping obtained single subject OT maps (Figure III-4) and also showed event-related responses as a function of post stimulus time. The maps depict 9cm x 15cm areas of the central posterior region as described before. The areas of positive total hemoglobin activation are denoted by the hot color regions, and areas of negative activation are denoted by the blue regions.

a. NIROT to 4sec stimulus-ON

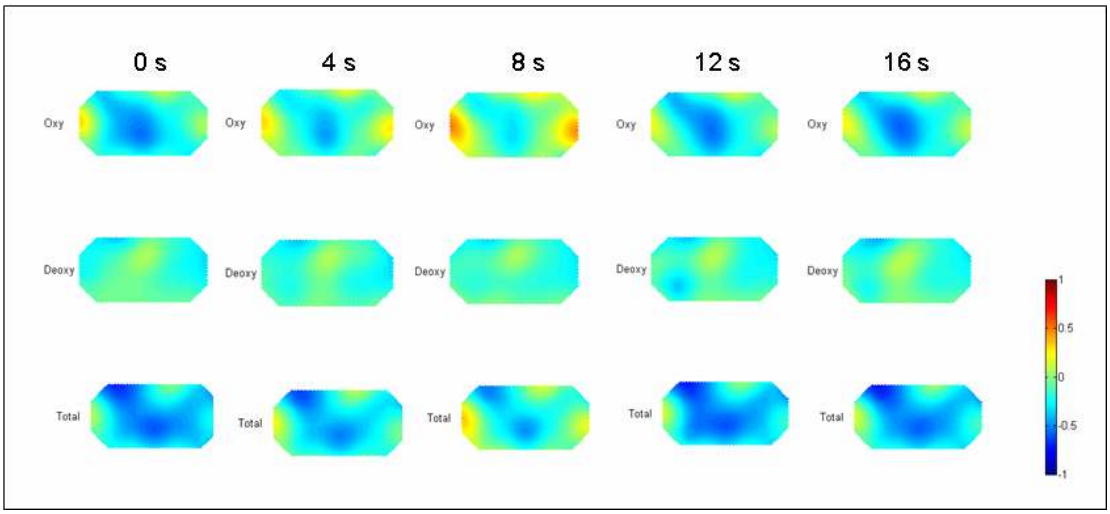

b. NIROT to 4sec stimulus-OFF

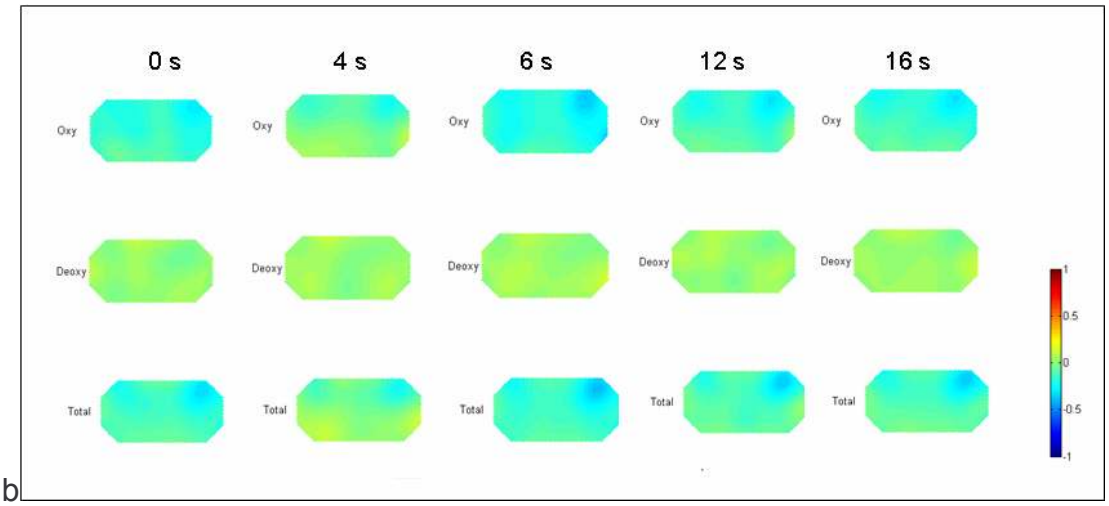

b

Figure III-4. Optical Topography (OT) maps in response to both 4sec stimulus-ON & OFF.

The magnitude of the hemoglobin responses during the stimulus ON and OFF were determined by integrating the time course centered at 0 s, 4 s, 8 s or 6 s, 12 s and 16 s post stimulus. Delayed and localized maximal positive response to the 4sec Stimulus-ON was seen in the map at 8s, and localized maximal negative response to 4sec stimulus-OFF were seen in the map at 6s. In general, [HbO_2]

and [HbT] changes are more significant than [Hb] changes, the signal changes in response to stimulus OFF are not as significant as in response to stimulus ON.

An increase in total hemoglobin in V1 in response to stimulus ON is consistent with an increase in blood volume and blood flow as observed during periods of enhanced neuronal activity.

The NIR data also showed transient changes in both oxy- and deoxy-hemoglobins (Figure III-5). In response to the transient deactivation (Fig III-5b), the total hemoglobin in the visual cortical area sampled by the NIR optodes decreased, and there was a corresponding increase in tissue deoxy-hemoglobin. The time course for vasoconstriction when regions deactivate does not appear significantly slower than that for vasodilation when areas activate. Our NIR studies found, as expected, that brief (4 sec) activation increased oxy- (HbO_2) and total hemoglobin (HbT) and decreased deoxyHb (Hb) (Figure III-5a), while transient deactivation decreased HbT and HbO_2, and increased Hb in V1 (Figure III-5b). The decrease in [HbO_2] is faster than the increase in [Hb] in response to transient deactivation. Also, the pre-undershoot/overshoot and post-undershoot/overshoot are more pronounced for NIR data in response to brief activation as compared to the response to brief deactivation.

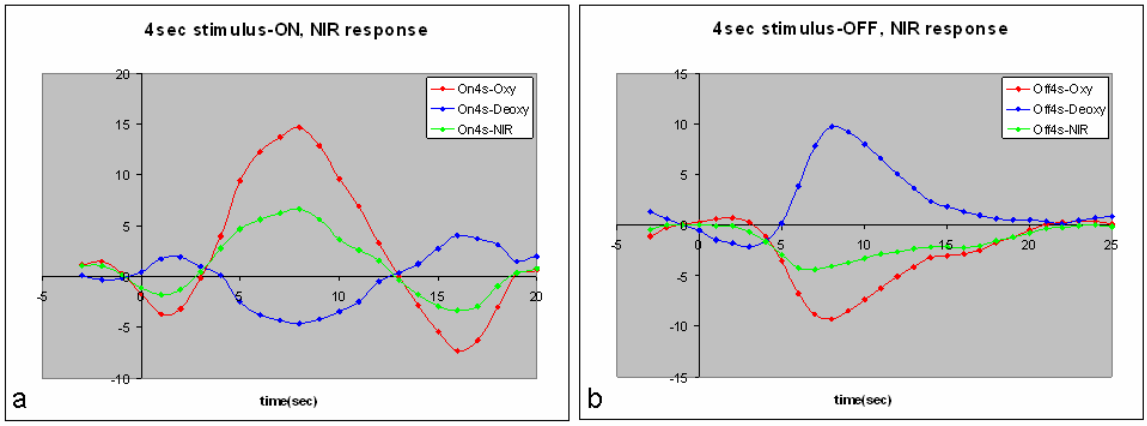

Figure III-5. Transient changes in both oxy-hemoglobin and deoxy-hemoglobin in V1 (subject BDN): a. NIR data in response to 4sec stimulus-ON. b. NIR data in response to 4sec stimulus-OFF.

Comparing the temporal paterns of HbO_2 concentration changes detected by NIRS in response to transient (4sec) activation versus deactivation (Figure III-6), we can see that the reduction in the hemodynamic response to deactivation is smaller, quicker and with narrower FWHM than it responses to activation. These results are consistent with the hemodynamic changes detected by fMRI.

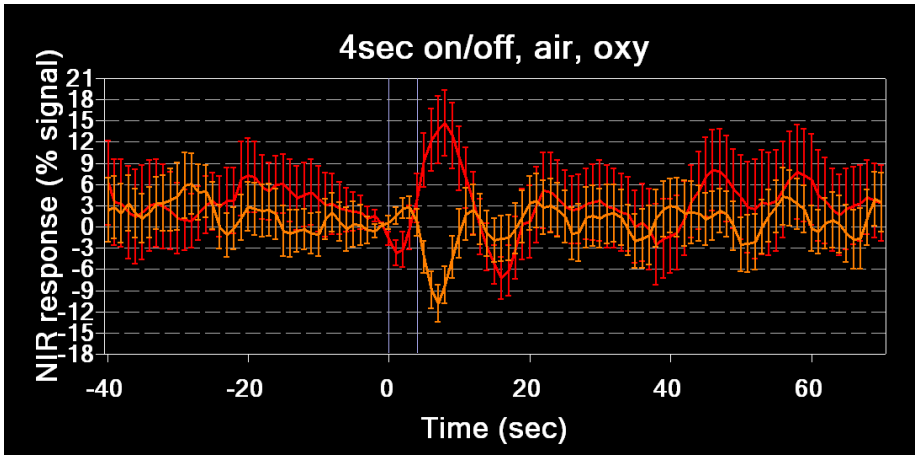

Figure III-6. NIR response to 4sec activation vs. deactivation.

These observations were qualitatively and quantitatively consistent with the observed fMRI time courses for a 4 sec activation/deactivation (Figure III-7). [HbO_2] and [HbT] in particular showed similar relative magnitude and temporal properties for activation and deactivation with the correspondent BOLD signals, verifying that NIRS can be used as an alternative method for measuring hemodynamic responses in event related studies of activation.

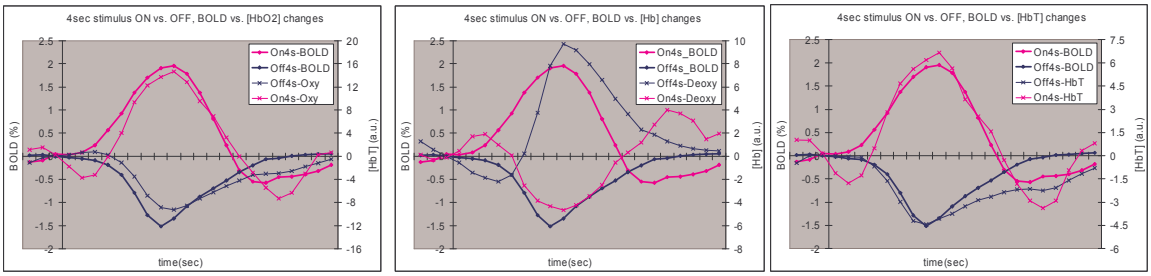

Figure III-7. Compare BOLD responses with NIR ([HbO_2], [Hb] and [HbT]) responses to 4sec stimulus-ON/OFF in V1. [HbO_2] and [HbT] showed similar relative magnitude and temporal properties for activation and deactivation with the correspondent BOLD signals.

The total hemoglobin, which reflects the change of blood volume, showed similar behavior to the BOLD response, but the blood volume change to stimulus onset was a little bit slower whereas the volume change to stimulus offset was slightly faster. We know that it is necessary for blood volume to increase faster than blood flow in response to stimulus onset and to decrease slower than blood flow in response to stimulus offset to explain the measured BOLD responses. Our results are consistent with this assumption in some degree. However the NIR response to 2 sec deactivation was again significantly blunted compared

with that for 2 sec activation, suggesting that the assumption of a universal HRF for all fMRI activations and deactivations needs closer scrutiny.

The BOLD fMRI and NIR results may be related. From some previous studies, we know that BOLD signal is a function of R_2* [Zhong, et al. 1998] in form of equation [III-1].

$$S = S_0 \exp(-\mathrm{TE}/\mathrm{T}_2^{*}) \qquad \text{[III-1]}$$

The BOLD signal changes upon simulation:

$$\frac{\Delta S}{S} = \frac{S - S_0}{S_0} = \exp(-TE \cdot \Delta R_2^{*}) - 1 \approx -TE \cdot \Delta R_2^{*} \qquad \text{[III-2]}$$

We assume that the gradient echo transverse relaxation rate due to magnetic susceptibility differences can be expressed in terms of the blood volume (V_{bl}) and the susceptibility (χ_{bl}) difference between the blood and surrounding tissue as [Kennan 1998]:

$$R_2^{*} = \kappa V_{bl} \chi_{bl} \qquad \text{[III-3]}$$

Where κ is a proportionality constant. The average venous T2 value for healthy subject at rest is about 100ms, i.e. R_2^{rest}=10sec^{-1}. The venous and capillary blood oxygenation increase after photic stimulation [Fox et al. 1986]. Corresponding changes in R_2^{*} are estimated to be about x%, i.e. R_2^{*act}=10 * (1-x%).

We further assume that to 1st order, the changes in tissue relaxation rate due to activation (ΔR_2^{*act}) are separable in terms of blood volume changes (ΔV_{bl}) and blood oxygenation dependent susceptibility changes in hemoglobin ($\Delta\chi_{bl}$)

$$\Delta \mathrm{R}_2^{act} = \Delta R_2^{v} + \Delta R_2^{Hb} = \kappa[\Delta V_{bl} \overline{\chi}_{bl} + V_{bl} \Delta \chi_{bl}] \qquad \text{[III-4]}$$

Here, the magnetic susceptibility of blood (χ_{bl}) depends on the blood oxygen saturation (Y) [Haacke 1997, Weisskoff 1992]:

$$\chi_{bl} = \chi_{oxy} + (1\text{-}Y)\,\delta\chi \qquad \text{[III-5]}$$

Where χ_{oxy} is magnetic susceptibility of completely oxygenated Red Blood Cell (RBC). (χ_{oxy}=-0.736ppm [Golay 2001, Spees 2001]); $\delta\chi$ is susceptibility difference between completely deoxygenated and completely oxygenated RBC. ($\delta\chi$=0.264ppm [Golay 2001, Spees 2001]); Y shows the fraction of hemoglobin that is present in the form of oxyHb. Then the BOLD signal changes dues to the stimulus induced local field perturbation can be expressed by equation [III-6]:

$$\Delta S/S_0 = -TE\,\Delta R_2^{*act}$$

$$= -TE\,\kappa[\Delta V_{bl}\,\bar{\chi}_{bl} + V_{bl}\Delta\chi_{bl}]$$

$$= -TE\,\kappa[\Delta V_{bl}\,\bar{\chi}_{bl} + V_{bl}\,\Delta(\chi_{oxy} + (1\text{-}Y)\,\delta\chi)]$$

$$\Delta S/S_0 = -TE\,\kappa[\Delta V_{bl}\,\bar{\chi}_{bl} + V_{bl}\,\Delta(1\text{-}Y)\,\delta\chi] \qquad \text{[III-6]}$$

Since the fractional concentration of deoxyhemoglobin (1-Y) can be detected by NIRS in term of concentration of deoxy-hemoglbin [Hb], and [HbT] changes detected by NIRS reflect percent volume changes, that is to say, $\Delta V_{bl} \approx V_{bl}\%HbT$; $\Delta(1\text{-}Y) \approx \%Hb$. Therefore we derived an equation for BOLD signal changes based on all these assumptions:

$$\Delta S/S_0 = -TE\,\kappa[(V_{bl} * \%HbT)\,\bar{\chi}_{bl} + V_{bl} * \%Hb * \delta\chi]$$

$$\Delta S/S_0 = -TE\,\kappa V_{bl}\,[\%HbT * \bar{\chi}_{bl} + \%Hb * \delta\chi] \qquad \text{[III-7]}$$

This equation [III-7] shows that the BOLD signal change is proportional to the weighted difference between the concentration changes of total hemoglobin Δ

[HbT] and deoxy-hemoglobin Δ [Hb]: %BOLD $\propto$ (%HbT-w*%Hb), the constant w is a weight constant (w = - $\delta\chi/\bar{\chi}_{bl}$).

The healthy subjects were found to have a mean oxygen saturation of 0.544±0.029 for venous blood [Haacke et al. 1997]. Assuming χ_{oxy}=-0.736ppm and $\delta\chi$=0.264ppm [Golay 2001, Spees 2001]), at this oxygen saturation, $\overline{Y^{rest}}$ =54.5%, the magnetic susceptibility of blood from equation [III-5] can be calculated: $\chi_{bl}^{rest}=\chi_{oxy}$ + (1-54.4%) $\delta\chi$= -0.616ppm. We assume $\bar{\chi}_{bl} \approx \chi_{bl}^{rest}$ for response to short transient activation, so that BOLD signal changes should be:

$$\Delta S/S_0|^{ON} = -TE\ \kappa[V_{bl} * \%HbT\ \bar{\chi}_{bl} + V_{bl} * \%Hb * \delta\chi]$$

$$= -TE\ \kappa V_{bl}\ [-0.616 * \%HbT + 0.264 * \%Hb]$$

$$\Delta S/S_0|^{ON} = 0.616*TE\ \kappa V_{bl}*(\%HbT - 0.43 * \%Hb) \qquad \text{[III-8]}$$

In addition, for response to short transient stimulus OFF during a continuous photic stimulation, the initial steady state is hyperoxygenated, so we simply assume that $\bar{\chi}_{bl} \approx \chi_{oxy}$ in this case. Then we obtain BOLD signal changes as:

$$\Delta S/S_0|^{OFF} = -TE\ \kappa[V_{bl}\Delta[HbT]\ \bar{\chi}_{bl} + V_{bl}\ \Delta[Hb]\ \delta\chi]$$

$$= -TE\ \kappa V_{bl}\ [-0.736* \%HbT + 0.264 * \%Hb]$$

$$\Delta S/S_0|^{OFF} = 0.736*TE\ \kappa V_{bl}*(\%HbT - 0.36 * \%Hb) \qquad \text{[III-9]}$$

Comparing the equations [III-8] and [III-9], we can see that Δ[Hb] is less weighted in response to transient stimulus OFF than to transient stimulus ON. It means blood volume change plays a more important role in BOLD response following the stimulus OFF. From figure III-7, decrease of [HbT] to transient stimulus OFF is smaller than its increase to stimulus ON. Also [Hb] increases

significantly in response to short transient stimulus-OFF. Considering their weighted role in generating BOLD signal from equation [III-8] and [III-9], we found the proportional magnitude changes to both stimulus onset and offset are consistent with the measured BOLD signal (Figure III-8).

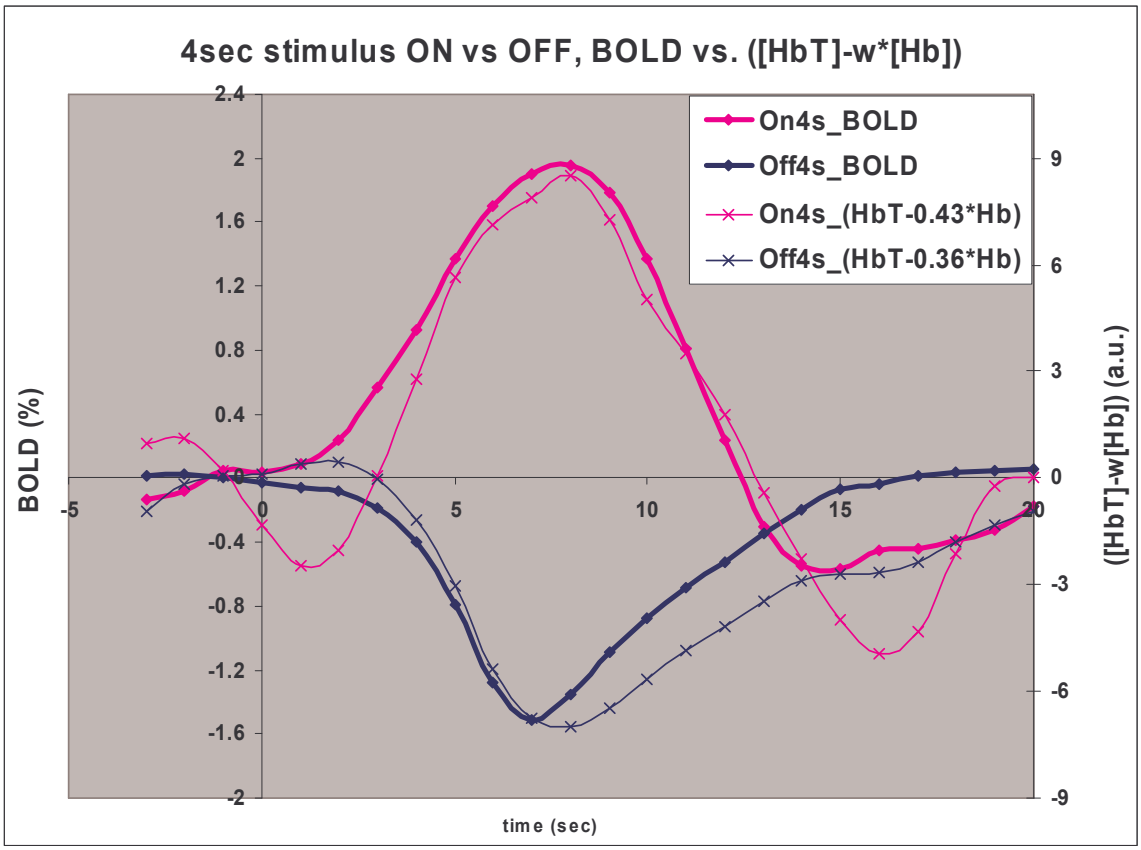

Figure III-8. Compare BOLD responses with estimation from NIRS data to 4sec stimulus-ON/OFF in V1. They showed similar relative magnitude and temporal properties for activation and deactivation. Here constant w = 0.43 for stimulus-ON and w = 0.36 for stimulus-OFF. The left y-axis shows the %BOLD and the right y-axis is the ruler for NIR data.

From the experimental data, we plot calculated ([HbT] – w*[Hb]) changes from the measured NIRS data and the experimental BOLD signal responses to 4sec stimulus OFF and OFF in one figure. They showed similar relative magnitude and temporal properties for signal increases and decreases. This

weighted differences between total hemoglobin concentration and deoxy-hemoglobin concentration, which reflects susceptibility induced signal changes, showed similar behavior to the BOLD response, but its change to stimulus onset shows more significant initial dip and post-stimulus undershoot in activation response. Besides the weighted difference to stimulus offset was a little bit larger than expected. During the estimation to responses to stimulus-OFF by susceptibility changes, the initial BOLD signal S_0 is not the signal at rest but an increased steady state signal. Furthermore, the average blood susceptibility $\overline{\chi}_{bl}$ during the responses to stimulus-ON and OFF periods should be more carefully selected, and it would influence the weight for changes of [HbT] and [Hb].

Compared with the NIR signal detected during normal breathing, the NIR signal changes while breathing carbogen show different natures (Figure III-9). In response to stimulus-ON, changes in [Hb] and [HbT] are not significantly different during normal or carbogen inhalation, whereas changes in [HbO_2] were significantly reduced by inhaling carbogen presumably because vasodilation already maximized. Meanwhile, the most significant reduction in concentration changes in response to stimulus-OFF during carbogen inhalation was found in the [Hb].

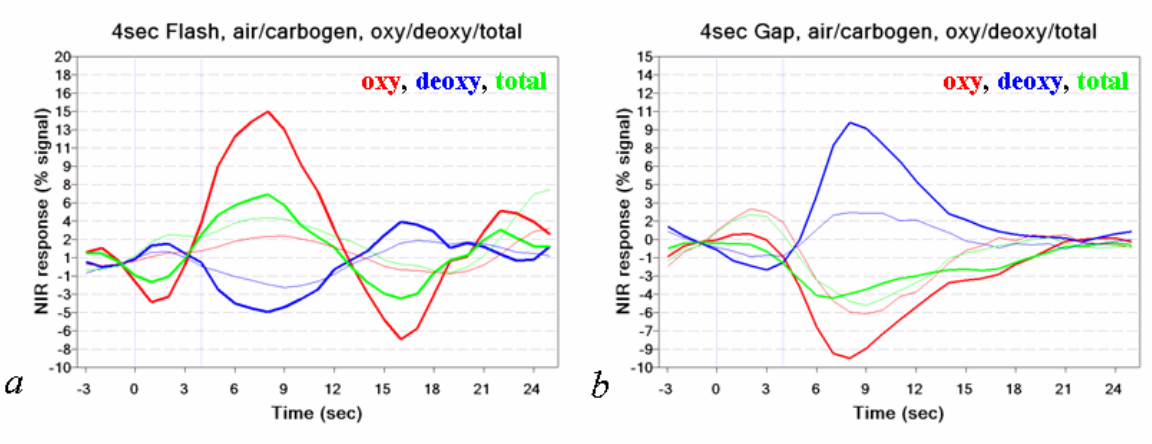

oxy, deoxy, total

Figure III-9. Compare NIR data obtain during different conditions: a, in response to 4sec stimulus-ON; b, in response to stimulus-OFF; data obtain during normal air breathing were showed in thicker lines, signal changes showed in thinner lines are obtained when subject inhales carbogen (95% O_2 + 5% CO_2).

Conclusion and Discussion

Both the fMRI and NIRS data demonstrate the HRF to deactivation is smaller and has a different time course to the HRF for transient activation. NIRS data are consistent with the fMRI data. A strong correlation between them is suggested from the physiological basis of BOLD signal changes due to neuronal stimulation by analyzing the contribution of blood volume and magnetic susceptibility. Moreover, the HRF for deactivation exhibits a greater degree of nonlinearity. Our ability to detect short (<2sec) deactivations is therefore less than our ability to detect corresponding activations. During a steady state excitation equilibrium is achieved between blood flow, volume and oxygenation. When this is interrupted the sequence of physiological changes is different from those involved in the

vasodilation that occurs in response to transient excitations, and the HRF presumably reflects those differences.

The carbogen inhalation saturates the blood oxygenation and blood flow rate. There are only small differences in total hemoglobin changes, which reflect the blood volume changes, in response to stimulus-ON which implies that under carbogen inhalation blood flow is maximized. Hence the signal changes more directly reflect the oxygen consumption changes associated with neuronal activity during carbogen inhalation, reducing the influence from blood flow.

Furthermore, from the physiological basis for BOLD signal changes due to neuronal stimulation by separating the blood volume and magnetic susceptibility coontribution, the mean fraction of oxygen saturation in the resting state ($\overline{Y^{rest}}$) would be higher during carbogen inhalation, so the $\overline{\chi}_{bl}$ for response to both short transient activation and deactivation during carbogen inhalation will be similar. From figure III-9 and equation [III-7], we can predict that the magnitude of BOLD signal changes to both short transient activation and deactivation during carbogen inhalation will also be similar, which means positive and negative BOLD might be more reciprocal. Thus, during the carbogen inhalation, the relationships of physiological dynamics tend to be more linear and the BOLD responses are more linearly related to the neuronal activity. Again, this prediction verified our previous assumption that BOLD signals are more directly related to the neuronal activity during carbogen inhalation.

Based on these studies, we propose that the nonlinear nature of BOLD responses to activations and deactivations are mainly driven by the nonlinear

relationships of physiological dynamics than by the neuronal dynamics itself. To account for this, we developed a simulation model which explicitly includes the nonlinear relationships of physiological variables in the next chapter and further discuss this hypothesis. The NIRS data will be utilized to constrain and justify the model.

CHAPTER IV

MODELING BOLD RESPONSES

We have investigated the hemodynamic response functions (HRF) in visual cortex in response to both short activations (relative to a resting baseline) as well as to short interruptions of a steady state activating stimulus (deactivations). We have previously observed nonlinearities of blood oxygenation dependent (BOLD) responses associated with transient activation and deactivation in primary visual area, and compared and contrasted hemodynamic response functions (HRFs) in BOLD and near infrared spectroscopy (NIRS) during various functional magnetic resonance imaging (fMRI) paradigm. In this chapter we try to explain the mechanism of the observed BOLD responses by using a computer simulation model. The extent to which these various responses differ may aid the evaluation of models of BOLD responses and is important for the design and interpretation of experiments and for choosing appropriate methods of data analysis.

Standard models of the BOLD effect have been described previously by others, but as shown below, these do not adequately account for the experimental findings. However, the standard balloon model of BOLD effects may be modified to account for the observed non-linear nature of deactivations by appropriate changes to simple hemodynamic parameters without recourse to new assumptions about the nature of the coupling between activity and oxygen use.

Introduction

Functional MRI detects the BOLD response which is a hemodynamic response to neuronal activity induced by a stimulus. Hence the degree of nonlinearity of measured BOLD responses must be the result of either nonlinear neuronal dynamics or nonlinear hemodynamic relationships to underlying physiological factors, e.g. cerebral blood flow (CBF), cerebral blood volume (CBV), cerebral metabolic rate of oxygen ($CMRO_2$) and so forth.

It has been demonstrated that neuronal responses to visual stimuli are nonlinear using direct electrical recordings in animals [Logothetis et al., 2001; Muller et al., 1999], so nonlinear neuronal responses are expected in human visual cortex. Furthermore, these studies shown that the amplitude of the neuronal response to a visual stimulus reflects the behavior of those neuronal populations contributing, but the increased latency is difficult to explain using only neuronal mechanisms. In addition, it has also been demonstrated in simulations that the linearity can be affected by various hemodynamic parameters. Some simultaneous CBF and BOLD studies [Miller et al. 2001; Obata et al. 2004] suggest a hemodynamic rather than a neural origin for the nonlinear nature of transient BOLD responses. Thus the contributions of neuronal or hemodynamic factors to the nonlinearity are still poorly known, but our following modeling studies look at the nonlinearity of BOLD responses to both ON and OFF stimuli in order to give more to explain these phenomena.

As described in previous chapters, a nonlinear model based on an impulse function e.g. gamma variation function in equation 2-1, helps predict the interaction between rapid ER-fMRI, and is helpful for fitting data, but it does not reflect a biologically plausible origin for the non-linear natures of BOLD. Thus it is necessary to develop a model that explicitly includes (nonlinear) properties of the vasculature, neurons and other physiological phenomena, and to use insights from such modeling to explain and refine the HRF.

To account for our findings, we adapted the standard Balloon Model [Buxton 1998; 2004] in which flow is regulated in a manner that leads to over and under swings in blood oxygenation relative to the levels required to maintain metabolic demands.

Standard Balloon Model

The key physiological variables incorporated in the model are the total deoxyhemoglobin (q) and the blood volume (v), both normalized to their values at rest. In this model, the fractional BOLD signal change is written as [Buxton 1998]:

$$\frac{\Delta S}{S} = V_0 \left[k_1(1-q) + k_2(1-\frac{q}{v}) + k_3(1-v) \right] \qquad \text{[IV-1]}$$

where k_1, k_2, k_3 are dimensionless parameters and depend on several experimental and physiological parameters; and V_0 is the resting venous blood volume fraction.

The central idea of the model is that the venous compartment is treated as a distensible balloon. The inflow to the balloon f_{in} is the cerebral blood flow, while the outflow from the balloon f_{out} is an increasing function of the balloon volume.

The two dynamical variables are the total deoxyhemoglobin $q(t)$ and the volume of the balloon $v(t)$. Equations may then be developed assuming conservation of mass for blood and deoxyhemoglobin as they pass through the venous balloon [Buxton 1998]:

$$\frac{dq}{dt} = \frac{1}{\tau_0}\left[f_{in}(t)\frac{E(t)}{E_0} - f_{out}(v)\frac{q(t)}{v(t)} \right] \qquad \text{[IV-2]}$$

$$\frac{dv}{dt} = \frac{1}{\tau_0}\left[f_{in}(t) - f_{out}(v) \right] \qquad \text{[IV-3]}$$

where τ_0 is mean transit time through the balloon at rest, $E(t)$ is the oxygen extraction fraction, and E_0 is the resting oxygen extraction fraction.

In our simulations, the outflow (equation [IV-6]) was modeled as a pure function of blood volume *v*. Experimental studies of altered flow states [Grubb, 1974] have indicated that the steady-state relationship between cerebral blood volume (CBV) and flow (CBF) can often be described by an empirical power law: $v=f^{\alpha}$. However the prevailing conditions during the transition between steady-state levels may be different. For calculation purposes, Buxton proposed a simple model for such viscoelastic effects in which f_{out} is treated as a function both of the balloon volume and the rate of change of that volume. [Buxton 1998; 2004].

$$E(f_{in}(t)) = 1 - (1 - E_0)^{1/f_{in}(t)} \qquad \text{[IV-4]}$$

$$f_{out}(v) = v^{1/\alpha} + \tau\frac{dv}{dt} \qquad \text{[IV-5]}$$

where α is the stiffness exponent coefficient and τ controls how long this transient adjustment requires.

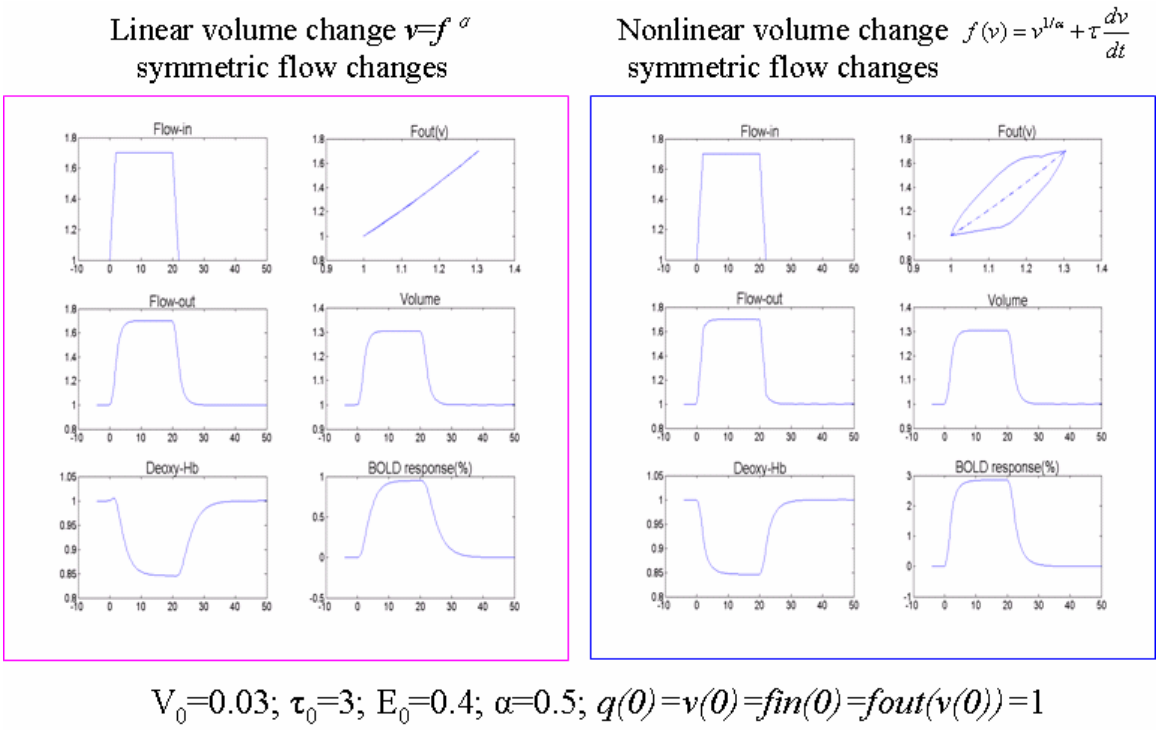

Figure IV-1. Different simulated signal changes based on linear volume change of the power law: $v=f^{\alpha}$, and based on modified nonlinear volume changes for viscoelastic effects: $f_{out}(v) = v^{1/\alpha} + \tau \frac{dv}{dt}$.

From given initial conditions and using careful selections of the model parameters k_i, V_0, E_0, α and τ_0 (which may be estimated from early numerical and experimental measurements: $k_1=7E_0$ [Ogawa 1993], $k_2=2$, $k_3=2E_0-0.2$ [Boxerman 1995]) different temporal patterns of response may be created for different functional forms of $f_{in}(t)$.

In our case we chose $V_0=0.03$, $E_0=0.4$, $\alpha=0.5$ and $\tau_0=4$ for the initial values for responses to visual Stimulus-ON, these are typical resting values. However this baseline condition is changed after viewing continuous visual stimulation ("ON"), so $V_0=0.04$, $E_0=0.26$, $\alpha=0.5$ and $\tau_0=4$ are the initial values for transient

responses to Stimulus-OFF, these values are steady-state values which were generated from the resting values.

Assumptions on the functional forms of blood flow

To obtain the value of $f_{in}(t)$ at any specified time, we assume it is =1 at rest, and introduce some new parameters: maximal inflow, denoted as *finMax*; inflow decrease rate $\left|\frac{df_{in}}{dt}\right|_{\text{activation}}$, denoted as *finDeR*; inflow increase rate $\left|\frac{df_{in}}{dt}\right|_{\text{deactivation}}$, denoted as *finInR*; delay of inflow increase with response to stimulus-ON, denoted as *finInDelay*, and delay of inflow decrease with response to stimulus-OFF, denoted as *finDeDelay*. (Figure IV-2)

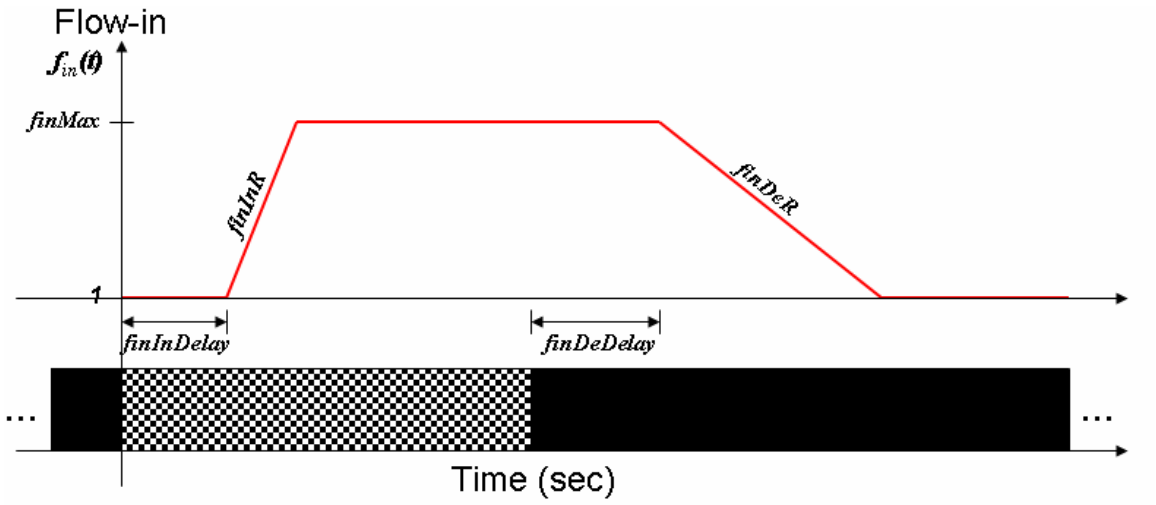

Figure IV-2. Functional form of Flow-in based on the introduced parameters: *finMax*, *finDeR* (sec^{-1}), *finInR* (sec^{-1}), *finInDelay* (sec) and *finDeDelay* (sec).

From figure IV-3, you can see improved simulations on all physiological variables, such as blood volume changes and blood deoxy-Hb changes, as well

as on BOLD signal changes by the assumption of the asymmetric flow changes. Here we show simulations for the response to 20sec activation. The initial values are V_0=0.03, E_0=0.4, α =0.5 and τ_0=4; and we assume the latency for flow change in response to stimulus onset is 2sec; and it takes 1sec for the blood flow increases from resting state (*finRest* =1) to maximum (*finMax* =1.6); but needs 4sec for the blood flow returns to resting state. Based on these assumptions, the BOLD signal shows more features than previous simulations as in Figure IV-1.

V_0=0.03; τ_0=3; E_0=0.4; α=0.5;

$q(0)=v(0)=f_{in}(0)=f_{out}(v(0))=1$;

Delay=2sec

finMax=1.7

1→Max: 1sec

Max→1: 4sec

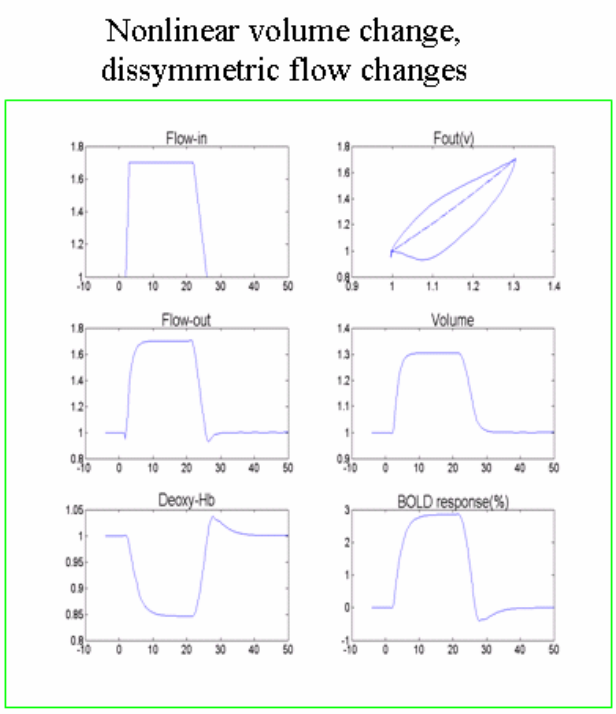

Figure IV-3. Improved simulation by assumptions on nonlinear volume changes and dissymmetric flow changes.

Fitting the Balloon Model

The choice of waveforms for the various flows as a function of time clearly affects the nature of the response. The assumption that it takes less time for

blood inflow to increase to meet the demands in reaction to stimulus onset than to decrease in response to offset can be justified, as shown below. The optimal selection of these parameters may be derived by considering the physiological conditions nd experimental data.

Fitting programs

To address questions about the selection of the flow parameters, we developed a fitting program in which the BOLD signal predicted by the Balloon Model based on equations [IV-1], [IV-2] and [IV-3] was fit to the measured BOLD response in a least squares sense. In this Matlab program, the Balloon model fitting performed a least squares curve fitting function of *lsqcurvefit*(*@sfcn, p0,t,Sexp*); the function calls BOLD signal function *sfcn*(*p,t*) (equation [IV-1]) and fit the signal function to the measured BOLD signal. Meanwhile, the signal function *sfcn*(*p,t*) solves the ordinary differential equations *ode45*(*@vqfcn,t,[v0,q0],p*) for the balloon volume and total deoxyhemoglobin *vqfcn*(*p,t*) (equation [IV-2] and [IV-3]).

Initial values

To perform the nonlinear data fitting, the initial values for those parameters were selected empirically as *finMax*=1.6, *finDeR*=1.2sec^{-1}, *finInR*=0.3sec^{-1}, *finDeDelay*=2sec, and *finInDelay*=1.5sec, then the best fitting parameters can be derived by the fitting programs described above. MATLAB codes were written to realize the fitting, the flow chart for the software to obtain the best fitting parameters as mentioned above is given in Figure IV-4.

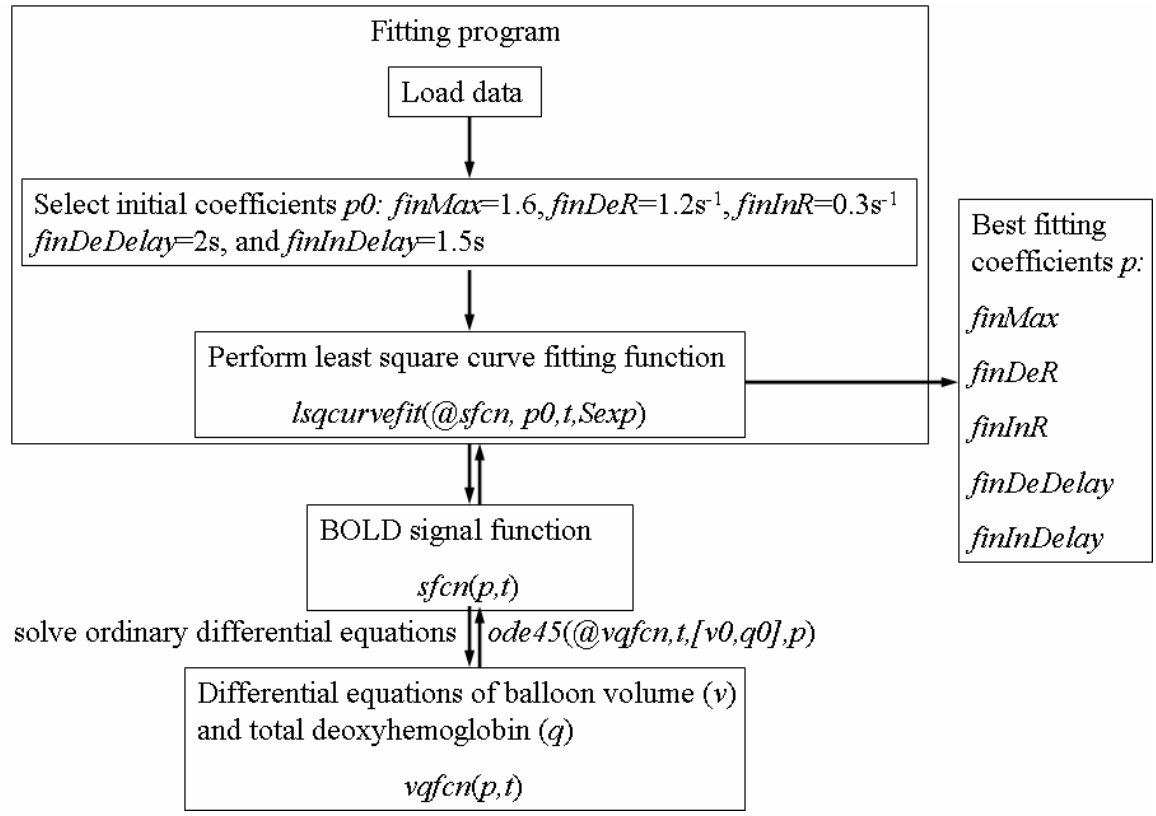

Figure IV-4. Flow chart for MATLAB programs for data fitting.

Fitting results

The fitted BOLD responses to deactivations by the modified Balloon model are shown in Figure IV-5. As shown in Figure IV-5, the modified Balloon Model fits the BOLD responses to deactivations quite well, and similar temporal information was obtained. Then the best fitting parameters derived by the least squares curve fitting programs for each data set are shown in Table IV-1.

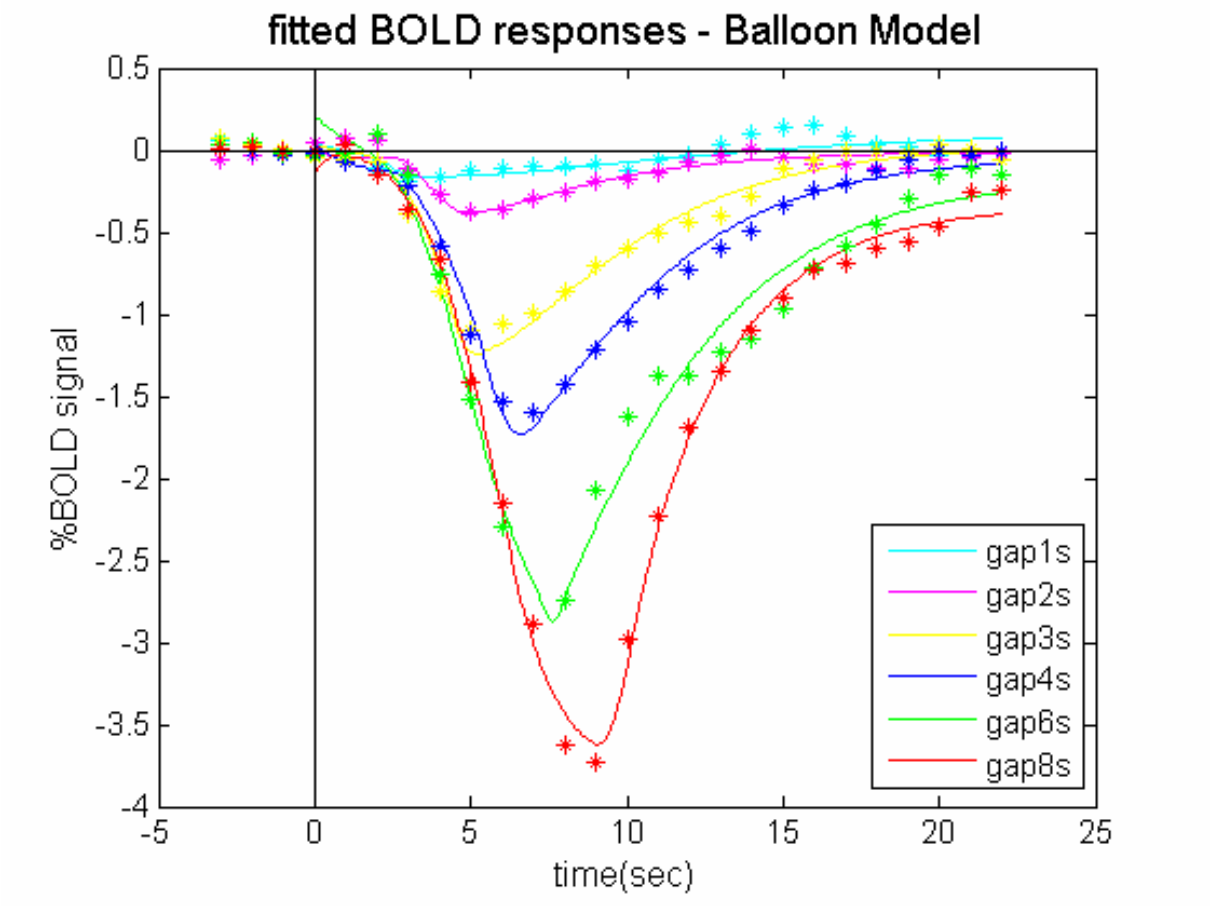

Figure IV-5. BOLD responses to deactivations and their fits. The data can be well modeled by the modified Balloon Model.

Table IV-1. List of the parameters which are used to describe functional forms of $f_{in}(t)$ in the Balloon Model. They were derived by least squares curve fitting of experimental data.

	finMax	*finDeR* (sec^{-1})	*finInR* (sec^{-1})	*finDeDelay* (sec)	*finInDelay* (sec)
OFF_1s	1.61	0.22	0.20	1.95	1.26
OFF_2s	1.59	0.12	0.52	2.00	1.43
OFF_3s	1.56	0.15	0.89	1.55	2.05
OFF_4s	1.51	0.12	0.62	2.27	2.27
OFF_6s	1.51	0.14	1.53	2.00	1.49
OFF_8s	1.59	0.13	0.86	1.89	1.04
Average	1.56	0.15	0.77	1.94	1.59

Table IV-1 suggests that it takes longer for the blood inflow to change in response to stimulus OFF than to ON. These are consistent with the experimental results that BOLD response to deactivation has longer latency as seen in Figure II-7. It also shows that the increase in the rate of blood inflow to activation is usually larger than the rate of decrease when deactivating. That is to say faster flow increases from a low flow state than flow decreases from a high flow state.

Developing the Balloon Model

Based on these fitting results, we optimized the parameters so that non-linear responses can be obtained from the model by assuming different time courses for flow decreases compared to flow increases. For example, if we assume the Flow-in at rest is 1, and maximal Flow-in is 1.6, we can then also postulate that the increase of Flow-in during balloon inflation occurs more rapidly than the decrease of Flow-in during deflation. If we set the time for Flow-in to reach its maximum to be 1sec, but the time for it to go back to the rest level as 4sec, then we obtain significant differences in Flow-in patterns in response to the ON or OFF conditions for different stimulus durations, as shown in the left column in Figure IV-5. Here the delay of Flow-in changes in response to both the ON and OFF conditions is set to 2sec. We select the time $\tau_{\pm}$ in equation [IV-5] as the time of Flow-in to increase or decrease representatively. Then τ_{+} should be always shorter than τ_{-}. In this way we are able to obtain different patterns of BOLD responses to Stimulus-ON/OFF, as shown in the right column in Figure IV-6.

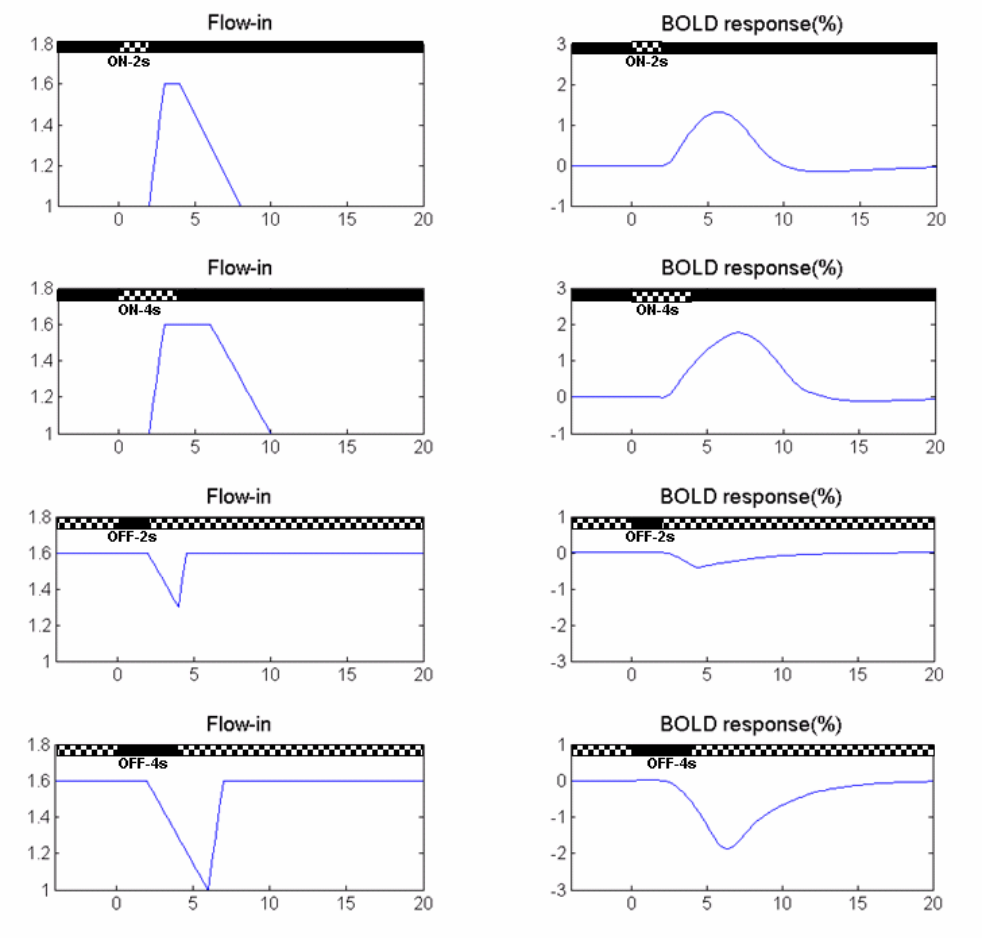

Figure IV-6. BOLD responses obtained by Balloon Model using different patterns of Flow-in.

Results

With these small but significant modifications, the shapes and nonlinearities of the BOLD responses to both activations and deactivations obtained by the Balloon Model agree well with our experimental results (Figure IV-7 and IV-8).

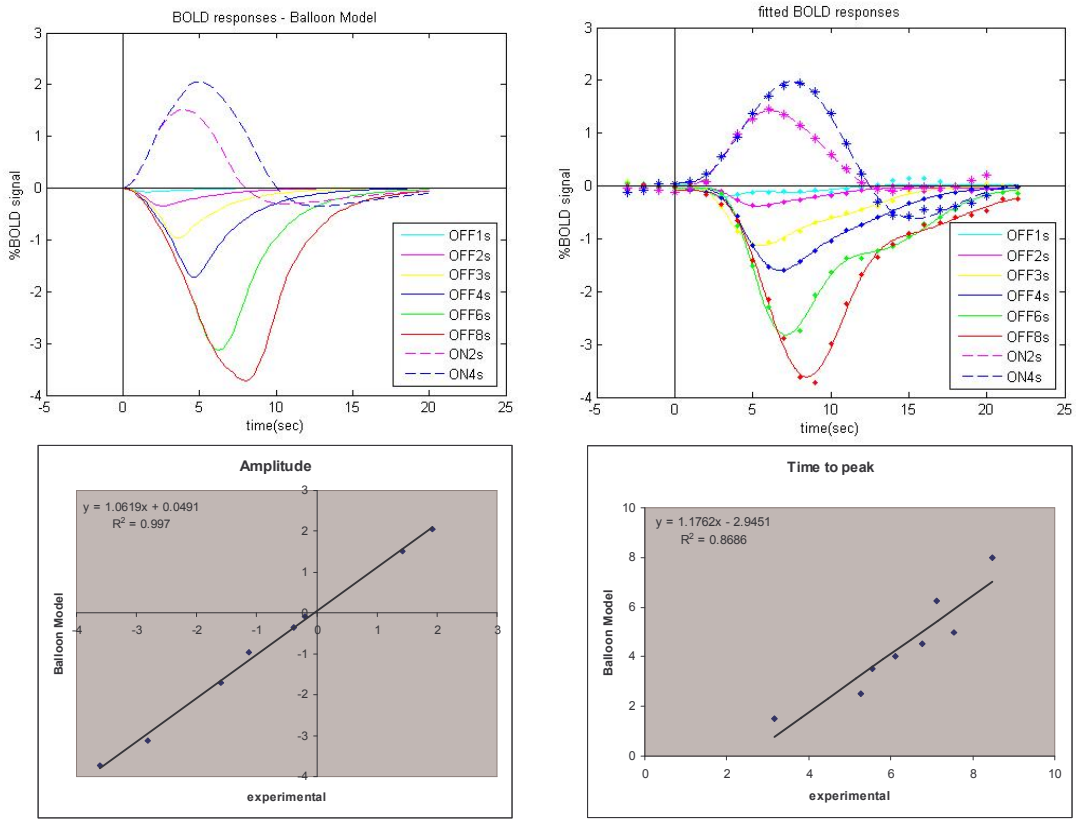

Figure IV-7. Compare Balloon Model simulated BOLD responses with the measured BOLD response to both stimulus on and off for various durations.

For example the absence of a post-stimulus overshoot for BOLD responses to transient stimulus-off and the magnitudes of the BOLD responses to short OFF stimuli were well modeled. Faster flow increases from a low flow state result in a larger oxygen extraction, hence a larger BOLD signal in response to brief ON stimuli. Unlike the case of the BOLD response to activation, linear convolution of HRFs from short duration interruptions tends to underestimate BOLD responses for deactivations. The standard Balloon Model predicts non-linear superposition of HRFs but it predicts reciprocal behavior for transient activations and deactivations. As shown in Figure IV-7 and IV-8, the modified Balloon Model

models the BOLD responses to both activation and deactivations well and does not predict reciprocal HRFs.

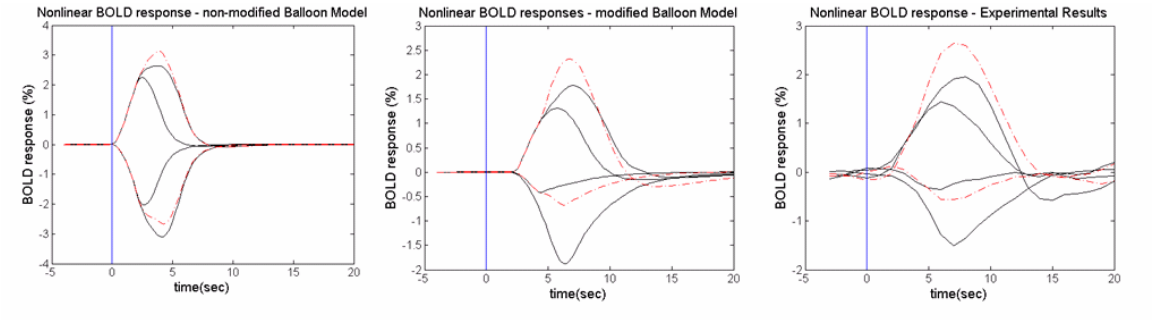

Figure IV-8. BOLD responses obtained by non-modified and modified Balloon model compared to experimental results. Red dash line showed linear convolution of HRF to 2sec. Modified Balloon model predicts the experimental data better and shows similar nonlinear properties of BOLD response to both activations and deactivations.

The simulations in this modified Balloon Model study not only show beautiful estimations of observed BOLD dynamics, but also show reasonable nonlinear hemodynamic relationships of underlying physiological variables. Figure IV-9a shows that blood volume dynamics are always slower than flow changes during both stimulus onset and cession period. These time constants have been used to explain the post-stimulus undershoot that is often observed for activation. NIRS experiments also verified this. As shown in Figure IV-9b, concentration changes of total hemoglobin, which is associated with blood volume changes, indicate a smaller and slower decrease during the OFF period, which is consistent with the modeled blood volume changes by this modified Balloon Model. The difference is that the actual [HbT] increase much more slowly than expected, especially following a brief cession of stimulus. The delayed return of [HbT], which reflects

blood volume change, needs to be more carefully considered and can be utilized to constrain and justify the model.

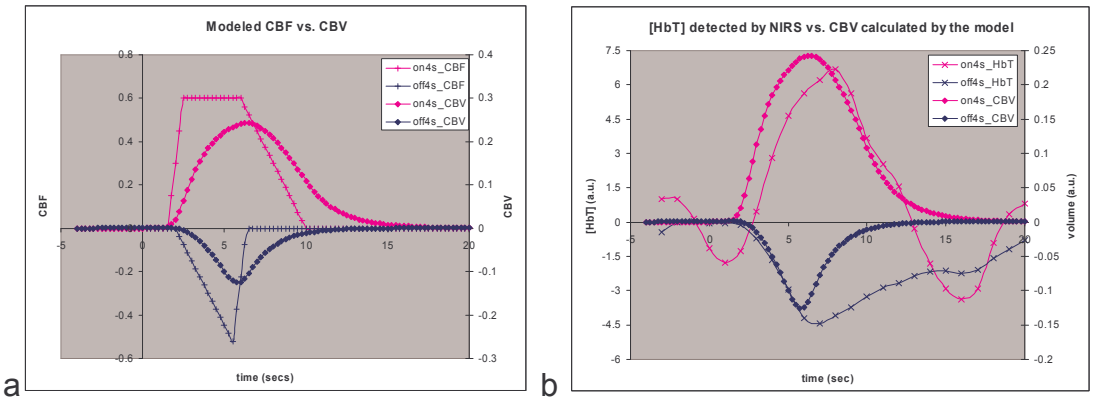

a b

Figure IV-9. (a) Simulation of blood volume compared with functional form of blood flow, using the modified Balloon Model. (b) Simulated blood volume shows a smaller and slower decrease during the OFF period, and is consistent with the change patterns of total hemoglobin detected by NIRS.

We can provide a better explanation without losing consistency with experimental observations by carefully selection of the viso-elastic time constant for inflation and deflation. As optimized in our modified Balloon Model, the constant for inflation τ_+ was selected shorter than the constant for deflation τ_-. Then the latent blood volume dynamics drive the BOLD signal to a reasonable decrease during brief OFF periods.

Conclusion & Discussion

We modified the Balloon model by assuming that the increase of Flow-in during inflation occurs more rapidly than the decrease of Flow-in during deflation. By this means the experimental responses can be well modeled, and the different nonlinear properties for both activation and deactivation were also

predicted (Figure IV-10). The nonlinearity responses can be explained by different flow-in time constants for stimulus onsets and offsets suggesting that hemodynamic effects alone can explain the causes of the nonlinear BOLD fMRI responses.

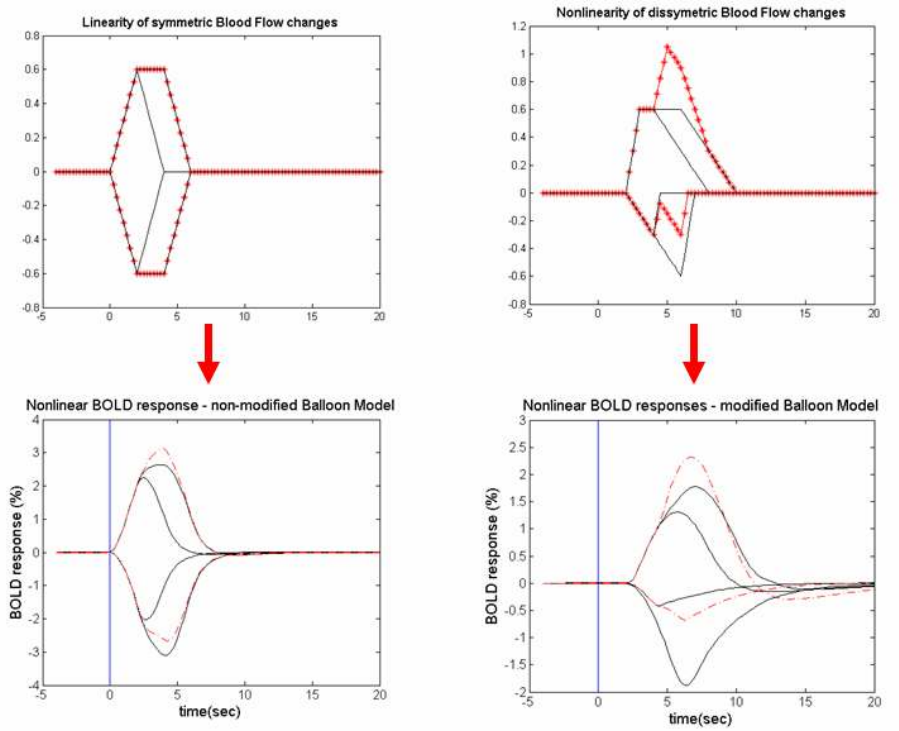

Figure IV-10. Nonlinearity of Blood Flow induced by assumption of different flow-in time constants for stimulus onsets and offsets, and in turn better predicts the different nonlinear nature of BOLD responses to activations and deactivations. Red lines are linear summations from signals response to shorter durations.

The nonlinear responses can be explained by different flow-in time constants to stimulus onsets and offsets suggesting that it is not neuronal dynamics but hemodynamic effects alone that cause the nonlinear BOLD fMRI responses. BOLD fMRI closely reflects the underlying nonlinear relationships of physiological factors and asymmetric flow-in increases compare to decreases.

Our studies showed that more accurate simulations of BOLD signals can be obtained if nonlinear properties of physiological variables (e.g. CBF, CBV, OEF, etc) and asymmetric flow-in increases compared to decreases are included in the Balloon Model. The different nonlinear natures of BOLD responses in primary visual area to transient activations and deactivations are mainly driven by nonlinear physiological dynamics, as proposed in the previous chapter, and the model simulation again verified this hypothesis.

Furthermore, we know that changes in deoxy-Hb concentration and changes in blood volume can be detected by NIRS. The BOLD signal predicted by the Balloon Model is also a function of deoxyhemoglobin (q) and the blood volume (v) as showed in equation [IV-1]:

$$\frac{\Delta S}{S} = V_0\left[k_1(1-q) + k_2(1-\frac{q}{v}) + k_3(1-v)\right] \qquad \text{[IV-1]}$$

Where k_1=7E_0 [Ogawa 1993], k_2=2, k_3=2E_0-0.2 [Boxerman 1995]). We have discussed the different initial values for response to stimulus onset and offset:

V_0=0.03, E_0=0.4 (ON) → k_1=2.8, k_2=2; k_3=0.6;

V_0=0.04, E_0=0.26 (OFF) → k_1=1.82, k_2=2, k_3=0.32;

Since in the Balloon Model, both q and v are normalized to their values at rest:

$(q\text{-}1) \sim$ %Hb;

$(v\text{-}1) \sim$ %HbT*n (here n is a proportionality constant)

Then the BOLD signal changes in the Balloon Model can be rewritten as:

$\Delta S/S = V_0[k_1*(1\text{-}q)*v + 2*(v\text{-}q) + k_3*(1\text{-}v)*v]$

$\approx V_0[-k_1*\%\text{Hb}*\bar{v} + 2(\%\text{HbT}*\text{n} - \%\text{Hb}) - k_3*\%\text{HbT}*\text{n}*\bar{v}]$

$= V_0[\%\text{HbT}*(2\text{-}k_3*\bar{v})*\text{n} - \%\text{Hb}*(k_1*\bar{v} + 2)]$

$$\Delta S/S = V_0*(2-k_3*\bar{v})*n\ [\%HbT-\%Hb*(k_1*\bar{v}+2)/[(2-k_3*\bar{v})*n]] \quad [IV-6]$$

Hence the BOLD signal changes are proportional to the weighted difference between the concentration changes of total hemoglobin Δ [HbT] and deoxy-hemoglobin Δ [Hb]: %BOLD $\propto$ (%HbT-w*%Hb), where the weight constant w= (k_1*$\bar{v}$+2)/[(2-k_3*$\bar{v}$)*n]. Because v changes between 1~1.3 from simulation results of the Balloon Model, then to simplify, we chose $\bar{v}$=1 for response to stimulus ON; and $\bar{v}$=1.3 for response to stimulus OFF. Therefore:

$$w^{ON} = (2.8*1+2)/[(2-0.6*1)*n] \approx 3.43/n \quad [IV-7]$$

$$w^{OFF} = (1.82*1.3+2)/[(2-0.32*1.3)*n] \approx 2.76/n \quad [IV-8]$$

We found that if n=7.9, then the weight constant for response to stimulus ON and OFF would be 0.43 and 0.35 which are consistent with the weight constant s we calculated from the method of separation of blood volume and magnetic susceptibility effect in the previous chapter as shown in equation [III-8] and [III-9]. The strong consistency between the susceptibility method and the Balloon Model again verify that physiological variables detected by NIRS data have strong linear correlation with the BOLD signals, and combining these two modalities can provide insight into the functional activity of the brain and the underlying physiological basis of the HRFs.

Finally, it must be emphasized that the relationship between neuronal activity and the BOLD response is still not fully understood, and the question of whether fMRI can accurately characterize neuronal dynamics or map relative neuronal populations is an open question and needs further consideration.

CHAPTER V

DEACTIVATIONS IN PRIMARY VISUAL AREA WHICH CORRESPOND TO ACTIVATIONS IN EXTRASTRIATE VISUAL AREAS

We investigated the spatial and temporal patterns of the transient hemodynamic responses in both primary visual cortex V1 and extrastriate visual cortex for both positive and negative BOLD effects induced by turning visual stimuli either ON or OFF (activation *or* deactivation). The expected responses in primary visual area V1 may depend on simple sensory attributes of the stimulus, but the responses of higher order visual areas do not necessarily follow the trends of the responses in V1 and may reflect other aspects of visual processing.

Introduction

Functional MRI signal might reflect not only the stimulus-induced firing rates of the local neuronal population, but also sub-threshold activity, simultaneous excitation and inhibition, or feed back from distant, higher level areas. How neuronal activity, hemodynamics and fMRI signals are related is still unclear. Many factors can influence the relationship among them. In different brain functional areas, these interactions among neuronal activity, hemodynamic and fMRI may also be different.

The primary visual cortex (V1) provides many feature analyses of the visual scene at a fine scale. Extrastriate visual cortex is a belt of visually responsive areas of cortex surrounding the primary visual cortex, and various posterior

extrastriate regions perform some other aspects of information processing, e.g. early neurophysiological and neuroimaging studies found that visual awareness was best correlated with neural activity in extrastriate visual areas [Tong 2003], and specific neural regions or circuits are important for awareness because of their functional properties, connectivity or functional role in the network. Connections between these subsets of cortical visual areas are shown in Figure V-1.

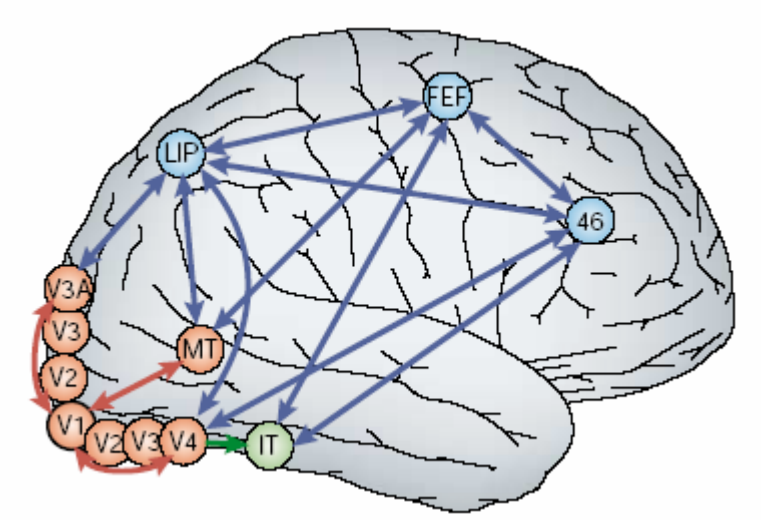

Figure V-1. Connections between subsets of cortical visual areas (schematic diagram) [Tong 2003].

Some hierarchical models propose that although V1 provides necessary input, only higher order extrastriate areas that project to frontal-parietal attentional areas are directly involved in awareness [Rees 2002, Crick 1995]. Interactive models propose that dynamic recurrent circuits between V1 and higher areas are necessary to maintain a visual representation in awareness [Pollen 1999, Lamme 2000, Bullier 2001]. These models yield different predictions about whether

awareness will be impaired by V1 disruption if extrastriate activity remains intact. Further investigation of V1 and its interactions with higher areas might provide important insights into the neural basis of visual awareness.

We have investigated the hemodynamic response functions (HRFs) in primary visual cortex (V1) in response to both short activations (relative to a resting baseline) as well as to short interruptions of a steady state activating stimulus (deactivations). The extent to which these responses differ may shed light on models of BOLD responses and is important for the design and interpretation of experiments and methods of data analysis. Moreover, whereas the expected responses in V1 may depend on simple sensory attributes of the stimulus, the responses of higher-level posterior extrastriate visual areas such as V2, V3 may reflect other aspects of visual processing and may not follow the trends of the responses in V1. We therefore investigated the spatial and temporal patterns of the transient hemodynamic responses in both V1 and extrastriate visual cortex for both positive and negative BOLD effects induced by turning visual stimuli either on or off.

Method

Subjects

A total of 5 healthy volunteers participated in fMRI experiments for comparisons of BOLD responses to activations with deactivations. All had normal or corrected to normal vision. Written informed consents were obtained from all

volunteers prior to the examinations. All subjects were instructed to keep their eyes open and maintain constant attention throughout all experiments.

Stimulus Presentation

An 8Hz large-field contrast-reversing checkerboard pattern at 100% contrast served as a visual stimulus (denoted as condition “ON”). In our baseline condition subjects viewed a spatially homogeneous black screen (denoted as condition “OFF”). In our comparison condition subjects viewed a spatially homogeneous bright screen (denoted as condition “BRIGHT”). Three event-related paradigms generated by E-prime (Psychology Software Tools, Inc) were presented to healthy subjects (Figure V-2): I. Brief stimulus-ON (2sec or 4sec) during otherwise continuous stimulus-OFF; II. Various durations of visual inactivity (stimulus-OFF for 1sec, 2sec, 3sec, 4sec, 6sec, or 8sec) interspersed during otherwise continuous visual stimulation-ON; III. Brief stimulus-BRIGHT (2sec or 4sec) interspersed with otherwise continuous stimulus-ON. The target to target interval was 22sec for 1sec, 2sec, 3sec and 4sec stimuli and 26sec for the 6sec and 8sec stimuli. Each type of stimulus (2sec/4sec of flickering checkerboard ON and 1sec/2sec/3sec/4sec/6sec/8sec of black screen OFF or 2sec/4sec of bright screen BRIGHT) was presented multiple (≈ 20) times.

A run of retinotopic mapping was performed in which a traveling wedge of flickering checkerboard was presented to localize each subject’s subsets of visual area before each scan.

Paradigm I.

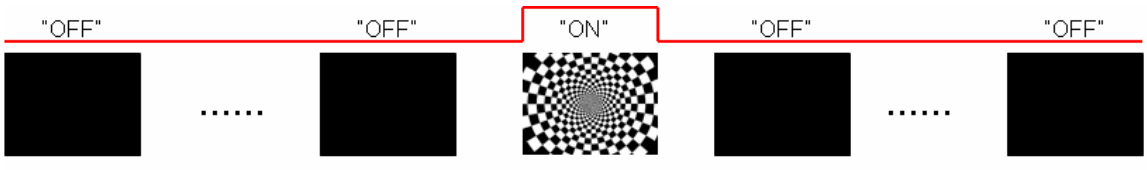

Paradigm II.

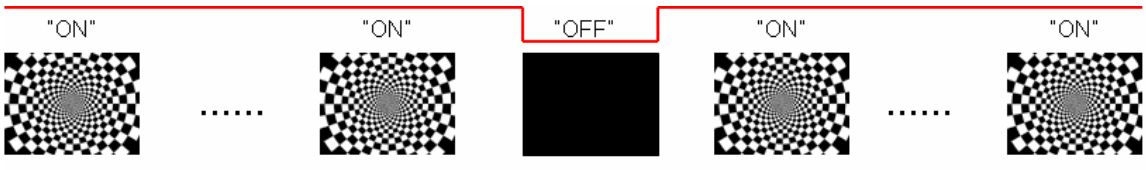

Paradigm III.

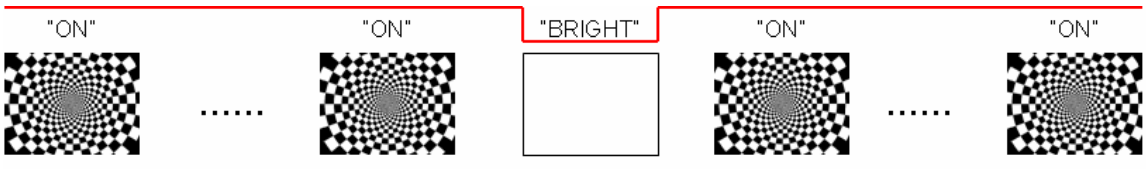

Figure V-2. Three paradigms of typical event-related visual stimulus designs.

Data Acquisition

MR images were acquired on a 3T Philips Achieva scanner. Ten T1-weighted anatomic images were collected parallel to AC-PC line with 5mm slice thickness and 1mm gap and positioned to cover the visual areas. Then functional images were collected in the same planes, using a gradient echo EPI sequence (TR/TE=1s/35ms, flip angle=70^{o}, FOV=22x22cm^{2} and acquisition matrix size=80x80 reconstructed to 128x128).

Data Analysis

The BOLD signals obtained from the MR scanner were analyzed using

BrainVoyager and custom analysis software running under MATLAB.

fMRI data were first motion corrected, realigned and coregistered with T1-weighted structural images collected using identical slice prescriptions, then registered to Talaraich coordinates. We performed an event-related general linear model (GLM) analysis to compute the activation maps, and then examined the time courses of the signals within the activated regions of interest (ROIs) for both transient activations and deactivations.

Results

By briefly turning stimulus on after continuous black screen, as well as turning stimulus off after continuous flashing checkerboard, we detected the fMRI signal changes in response to both stimulus-ON and OFF, correspond to activation and deactivation. As we can see from Figure V-3, positive vs. negative BOLD effect correspondent to luminance increment or decrement were shown in primary visual area as expected. The shapes of the BOLD responses are nonlinearly different with different durations of stimulus-OFF. On the other hand, the BOLD MR signal in extrastriate visual area showed positive hemodynamic response to both transient stimulus-ON and OFF, i.e. the extrastriate visual area showed the same positive BOLD response even when the sensory strength of the stimulus was reduced.

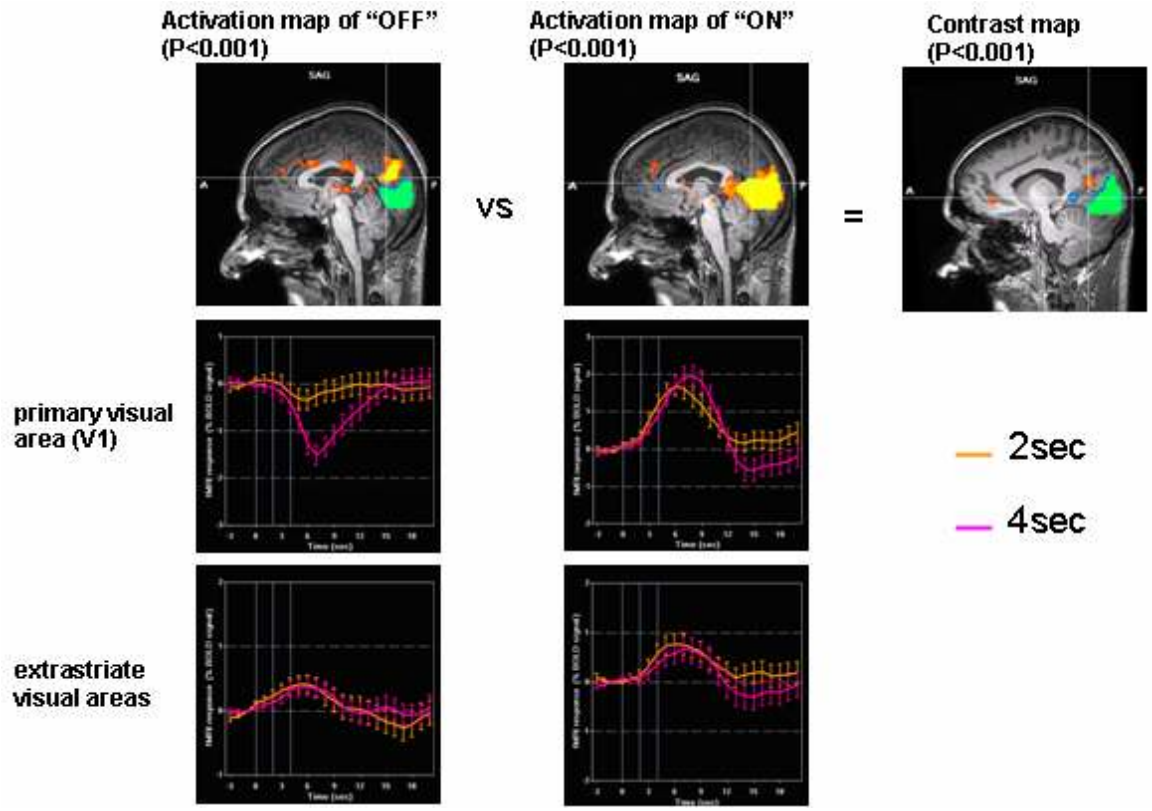

Figure V-3. fMRI identified extrastriate visual areas involved in responses to brief interruption of continuous stimulus, and showed interestingly different signal time courses compared to the expected deactivation in primary visual area.

Moreover, when the black screen was replaced by a bright screen (BRIGHT) as interruption during continuous flickering checkerboard, there was no corresponding positive BOLD response or significant hemodynamic transient changes in extrastriate visual areas were detected (Figure V-4). These phenomena showed that response in extrastriate visual area does not depend on simple sensory attributes of the stimulus.

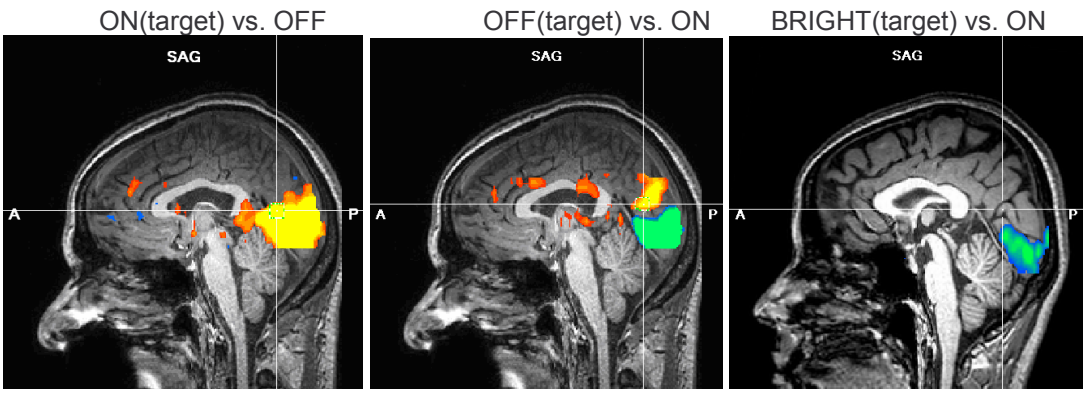

Figure V-4. Different activation maps in response to different stimulus sensory.

BOLD responses in V1 showed different amplitude and temporal attributes corresponding to different durations of stimulus-OFF and ON. But similar increases of fMRI signal in response to different durations of either activations or deactivations were found in extrastriate visual areas (Figure V-3).

We further studied the BOLD effect to different durations of interruption, and the results indicate that time courses of BOLD signal showed totally different patterns in primary and extrastriate visual areas (Figure V-5). Unlike the significant different fMRI signals in primary visual area as shown in the left panel, similar time courses of fMRI BOLD signal in response to different durations of interruption were found in extrastriate visual areas, as seen in the right panel. That is to say that the positive BOLD responses in extrastriate visual areas showed no direct relation with the duration of stimulus cession. Consider the response to 1sec Stimulus-OFF for example (Figure V-6); though deactivation is not easy to be seen in V1, a significant signal increase can still be clearly seen in extrastriate visual area.

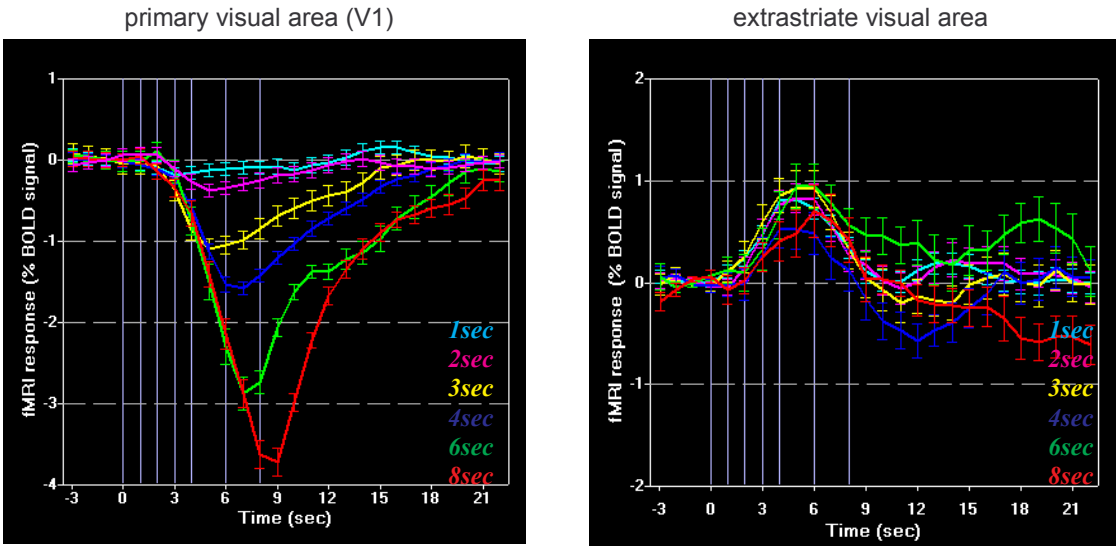

Figure V-5. BOLD signal changes in response to various durations (1sec /2sec /3sec /4sec /6sec /8sec) of stimulus-OFF.

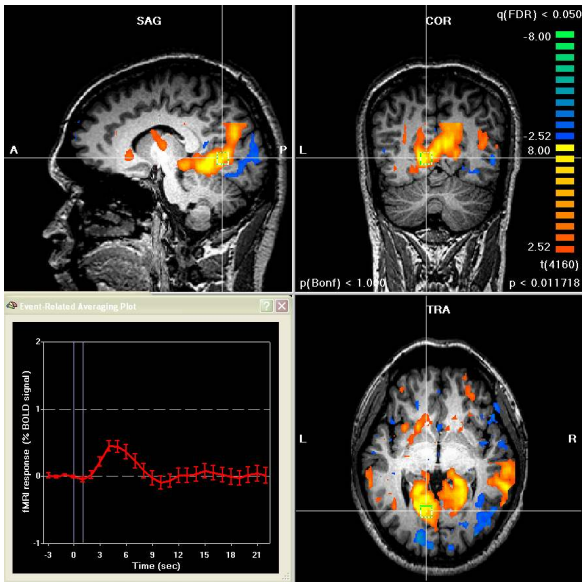

Figure V-6. Positive BOLD effect in extrastriate visual area in response to 1sec stimulus-OFF.

In addition, the BOLD signal increases in extrastriate visual cortex showed no significant delay and faster time to peak. These immediate increases in BOLD signal in the extrastriate visual areas suggest that the latent change of regional

CBF is not the key physiological factor that generates these positive BOLD signals. Other potential physiological correlates might provide the variability in behavior. The changes in oxygenation which are more immediately related to neuronal activity are possible causes. Hence the intrinsic neuronal activity in the extrastriate visual cortex might play a more direct role in generating the fMRI signal.

Again, from the contrast maps between BOLD effect to stimulus-OFF vs. ON, or between BOLD effect to different durations of interruptions shown in Figure V-7, we notice that some extrastriate visual areas were eliminated by this contrast, thus they are independent of either sign or durations of the stimulation.

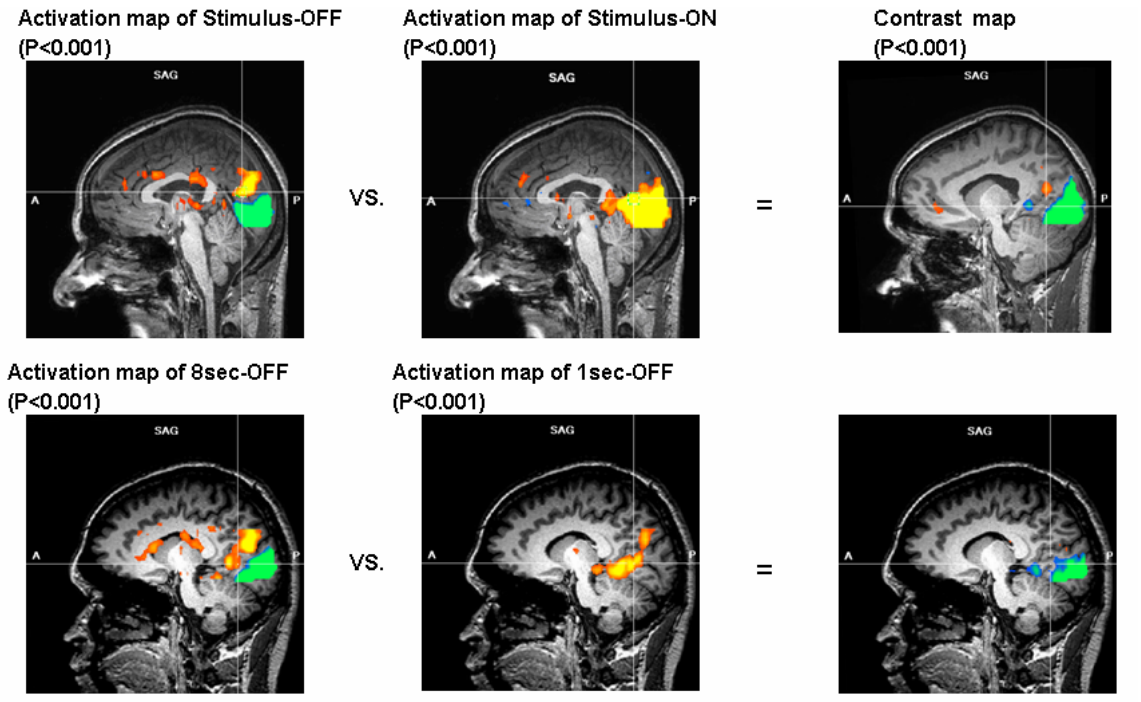

Figure V-7. Contrast maps between BOLD effect to stimulus-OFF vs. ON (upper row), or between BOLD effect to different durations of interruptions (lower row).

Discussion

The event-related responses to ON and OFF in primary visual area V1 presumably reflect the effects of a transient onset of activation (in which case blood flow must increase to meet demands) or a transient reduction of activation (in which case blood flow decreases) and thus they may be expected to have different temporal forms reflecting the physiological conditions. Based on recent results that a luminance increment produces similar activation of V1 and extrastriate visual area, whereas a luminance decrement produces activation in extrastriate visual areas but relative suppression in V1, we expect the V1 response to be specific to the luminance change and to be different in response to stimulus-ON, OFF or BRIGHT. It is also likely that feedback from the extrastriate visual areas (V2 or higher) plays a role, since they have direct reciprocal connections (Figure V-1).

BOLD signals increase with no significant delay in extrastriate cortex, and are independent of duration of stimulus-OFF. There is similarly significant activation in extrastriate cortex in response to different duration of stimulus-OFF: extrastriate areas are significantly activated even for duration of stimulus-OFF as short as 1sec. It is a challenge to interpret this new interesting phenomenon.

We postulate two potential mechanisms underlying the activations in extrastriate visual cortex even when sensory strength of the stimulus is reduced. Mechanism 1 assumes that positive BOLD response adjacent to the striate visual cortex is a compensatory response to optimize task performance. Mechanism 2

assumes that positive BOLD response adjacent to striate visual cortex is a direct result of increased local neuronal activity.

If mechanism 1 is the case then decreased rCBF in deactivated area (e.g. V1) might produce an increased rCBF in surrounding areas. Consequently, we should be able to detect reversely synchronous hemodynamics in these two areas. And the hemodynamic responses should be task load dependent (stimulus correlated). These seem to be inconsistent with what we have observed. We detected not only similar positive BOLD responses in extrastriate visual cortex in response to both brief stimulus-ON and OFF, but also similar time courses of fMRI signal in response to various durations of tasks. In addition, unlike the different latencies in response to different durations of stimulus changes, immediate changes in fMRI signal onset in the extrastriate visual areas give us a hint that the blood flow is not the key physiological factor that causes this signal increase.

Global blood flow is task dependent. We performed a preliminary ASL experiment to obtain CBF information using the same event-related paradigms. The ASL perfusion maps show that in V1, CBF matches the BOLD signal changes. But there were no blood flow changes parallel to the BOLD changes in extrastriate regions. In extrastriate visual areas, though the demand for oxygenation level decreases in response to decrement of luminance, the signal increases since the blood flow remains at a high level. This again verified that blood flow is not a main driving factor, but oxygenation which is independent and uncoupled with blood flow here could be. So, unlike the BOLD effect in V1 which

is mainly driven by the changes in CBF we have verified in previous chapters, the positive BOLD effect in extrastriate visual areas should have other origins. And it is possible that stimuli switching itself may change the coupling between neuronal activity and regional hemodynamic factors, e.g. CBF, CBV and OEF.

Mechanism 2 assumes that the positive BOLD response adjacent to the striate visual cortex is neuronal origin. And this neuronal activity can be partitioned into components: intrinsic neuronal activity or transient task-evoked activity. The intrinsic neuronal firing is a spontaneous activity that continues during resting state and is used to support ongoing neuronal signaling [Raichle 2006]. The transient task-evoked activity that generates the positive BOLD responses here could be associated with the need for focused attention. It reacts to the switch of stimulation luminance.

There is also the possibility that neurons within extrastriate areas respond mainly to changes in luminance independent of the sign of the change. Thus transient changes between ON and OFF represent two identical sources of stimulation.

A Dual-Source HRF can be obtained by convolution of a conventional two-gamma HRF with two separated δ functions with different weight β1 and β2. We can then fit these with experimental hemodynamic changes to get the parameters β1 and β2 as shown in voxel beta plots (Figure V-8). Then we can see that primary visual area was activated in response to activation and deactivated by deactivation, but extrastriate visual area was activated irrespective of sign and to both edges of stimulation luminance changes. These

results suggest that BOLD effect in the area is less dependent on flow changes and independent of the sign of stimulation. The neuronal response to changes in stimulation luminance is more directly related to the positive BOLD response in the extrastriate visual cortex.

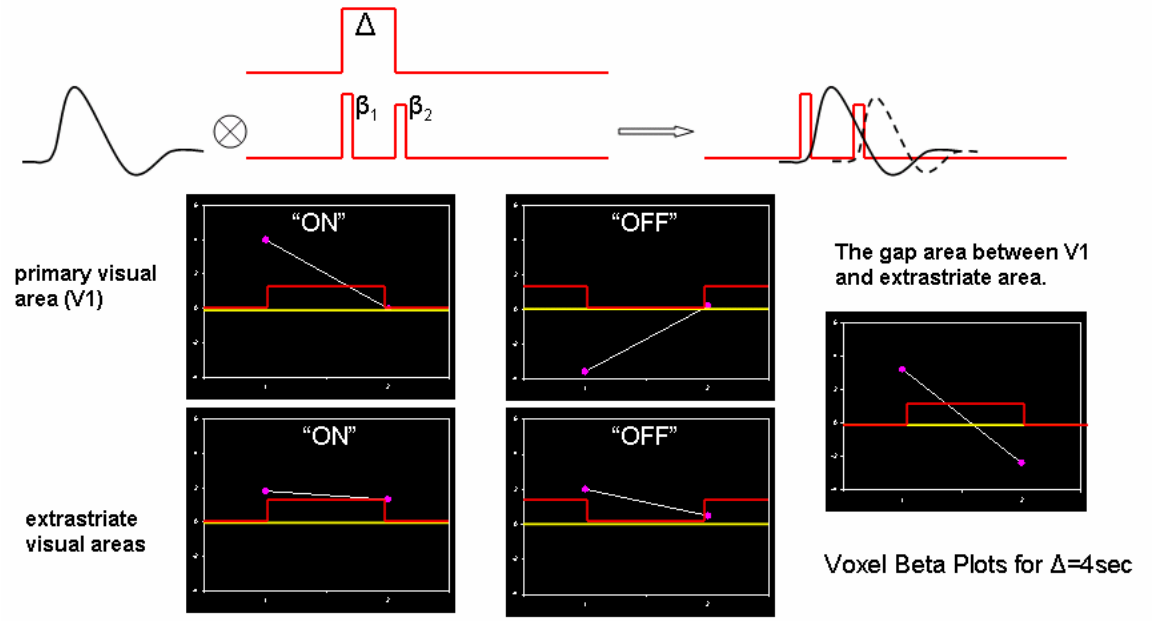

Figure V-8. Dual Source hyposthesis: a brief interruption was seen as 2 δ functions with different weight β1 and β2 (correspondent to the edges of stimulation switches.)

Recent neuroimaging studies of patients with unilateral V1 damage indicate that visual information can still reach extrastriate areas after V1 has been lesioned or inactivated [Goebel 2001]. Although their firing rates are reduced, a substantial proportion of neurons in some extrastriate areas remain responsive to visual stimuli. The BOLD responses in extrastriate visual cortex might therefore be dominated by changes in baseline firing rates, which have been found to

increase with attention. Though these small changes in baseline firing rates might appear negligible compared with the changes induced by attention on responsive neurons, with a rapid spread of activity through visual processing streams, if a relatively large proportion of neurons change their baseline firing rates then a positive BOLD effect may still be detectable.

This baseline firing is a spontaneous neuronal activity which is believed to be the origin of the spontaneous fluctuations in the BOLD signal [Fox and Raichle, 2007]. These spontaneous BOLD fluctuations can be of equal magnitude to the brain response observed in response to tasks or stimuli, and it continues during both resting state conditions and task performance [Fox 2006, Nir 2006]. The findings that the coherent spontaneous fluctuations account for variability in event-related BOLD responses highlight the importance of spontaneous BOLD activity and suggest that measured neuronal responses represent an approximately linear superposition of task-evoked neuronal activity and ongoing spontaneous activity. The majority of spontaneous BOLD fluctuations are below 0.1Hz, and our BOLD signals are in this frequency range. Thus it is possible that this intrinsic activity is responsible for the positive BOLD effect in higher-level extrastriate visual areas.

In summary, there are several findings in this study: the event-related responses to ON and OFF in primary visual area V1 behaved as expected, a luminance increment produces similar positive activation of V1 and extrastriate visual areas; A luminance decrement produces signal decreases in V1 but positive activation in extrastriate visual areas!

The hemodynamic responses in V1 presumably reflect the effects of a transient onset of activation in which case blood flow must increase to meet demands; or a transient reduction of activation in which case blood flow decreases. That is to say, the rCBF matches the BOLD signal changes in V1.

While the primary sensory area V1 behaves as expected, the hemodynamic responses for extrastriate visual areas are not easily explained in terms of simple responses to sensory stimuli. Possible explanations include: [1] Neurons in extrastriate regions respond to changes in stimulation, irrespective of sign and [2] BOLD changes in extrastriate regions are less dependent on flow changes and more dependent on changes in oxygenation, which is directly related to neural activities. In addition, BOLD signal in extrastriate visual areas may be mainly driven by neural origins than by hemodynamics. Further studies are required to elucidate the mechanism by which the BOLD response is sometimes positive and sometimes neutral in extrastriate visual areas for similar changes in sensory strength in V1.

CHAPTER VI

COMBINE ERP AND FMRI TO INVESTIGATE FEASIBILITY OF MAGNETIC-SOURCE MRI METHOD

fMRI has become the method of choice for mapping brain activity in human subjects and detects changes in regional blood oxygenation and volume associated with local changes in neuronal activity. While imaging based on blood oxygenation level dependent (BOLD) contrast has good spatial resolution and sensitivity, the hemodynamic signal develops relatively slowly and is only indirectly related to neuronal activity. The previous studies investigated the physiology of BOLD activity in various visual areas using similar stimulation paradigms by different modalities (NIRS and fMRI) and developed a model to explain these. Alternatively, it has been proposed that the BOLD response may be related more closely to the local field potentials (synaptic activity) than to spiking neuronal activity. Thus, in this chapter, an alternative approach termed magnetic source MRI (msMRI) is studied. MsMRI is based on the premise that neural activity may be mapped by MRI with greater temporal resolution by detecting the local magnetic field perturbations associated with local neuronal electric currents. We used a hybrid ms/BOLD MRI method to investigate whether msMRI could detect signal changes that occur simultaneously at the time of the production of well defined event related potentials, the P300 and N170, in regions that previously have been identified as generators of these electrical signals. Robust BOLD activations occurred after some seconds, but we were

unable to detect any significant changes in the T2*-weighted signal in these locations that correlated temporally with the timings of the ERPs.

Introduction

There is continuing interest in the development of improved methods for mapping brain function and organization. Functional MRI (fMRI) is one of the most important and useful of current techniques and is based on the sensitivity of MRI to changes in blood oxygenation, flow, and volume that accompany with changes in brain activation [Ogawa, 1990]. The spatial and temporal resolutions of this technique are limited by the nature of the coupling between neuronal electrical activity and the corresponding hemodynamic response. Spatial resolutions on the order of 1 mm and temporal resolutions on the order of 1 sec are readily achieved. There is considerable interest in developing methods to map neural events with greater temporal resolution.

Signal transfer along an axon is based on the ability of the membrane to alter its permeability to Na+ and K+ ions. These changes are caused by the opening of voltage-sensitive channels as a result of an approaching action potential. The action potential can be approximated by two oppositely oriented current dipoles whose separation depends on the conduction velocity. The magnitude of each dipole is about 100fAm. Although the precise natures of neural currents are complex, they generate weak magnetic fields within tissue that in principle may affect NMR signals [Cohen, 1984; Nunez, 2001; Bandettini, 2005]. One approach to detecting these fields is to try to measure the spatial displacement induced by

neuronal electrical currents by the Lorentz effect [Song, 2001; Truong, 2006]. In addition, several groups have suggested that neural activity may be detected by MRI by measuring the signal losses and/or phase shifts produced by the local magnetic field perturbations associated with the local electric currents [Bodurka, 2002; Xiong, 2003]. This general approach has been termed magnetic source MRI (msMRI). Calculations predicting the magnitudes of these effects support the possibility that msMRI may be able to map neuronal activity in the human brain at high temporal and spatial resolution.

MR signals decrease when R2* (1/T2*) increases, which may arise whenever the nuclei within a voxel experience different magnetic fields for significant time intervals so that their NMR signals become dephased. In principle the local currents caused by neuronal activity could cause such effects. The msMRI protocol reported by Xiong et al (2003) measured the integrated activation within a short time frame (on the order of msec) [Xiong, 2003]. They showed that msMRI signals were measurable and equal to 1.12%±0.54% of the background MRI signal. They also tested the relationship between the msMRI signal strength and the echo time (TE). A nonlinear relationship between TE and msMRI magnitude was observed as predicted by a theoretical model. The data fit well with a quadratic current-dipole model of the magnetic fields induced by neuronal firing [Hobbie, 1997].

Unlike Bodurka's methods [Bodurka, 1999; 2002], which were based on measuring net signal phase changes, the method of Xiong et al. was based on measuring changes in signal magnitude in standard fMRI techniques. Xiong et al.

postulated that both positive and negative phases of MRI signals could destructively add, so that no net phase is detectable. On the other hand, the magnitude of the MRI signal may significantly change due to neuro-magnetic fields. Nuclear spins experiencing local field inhomogeneities produced by neural currents may lose phase coherence, resulting in a decrease of MRI signal magnitude. They proposed that magnitude measurements could be more sensitive for measuring in vivo neuronal activity than phase measurements. Experimentally, Chow et al. showed evidence of phase cancellation in the optic nerve and visual cortex, and demonstrated that only amplitude changes would be expected [Chow, 2004].

Neural activity involves the excitation of multiple neurons in complex patterns of firing and spiking. However, event-related electrophysiological studies have been explored for many years and several experimental paradigms in common use produce a relatively large amplitude, well defined surface potential at a specific time after a particular type of stimulus is presented. These so-called ERPs are often the results of a few discrete regions generating relatively large amounts of activity at specific times. We postulated that within a focal generator of an ERP, there should be significant neuronal currents that could induce MR signal dephasing at or around the time of the appearance of the surface ERP. We therefore looked for MR signal changes at the time of well known ERPs in those regions believed to be active in their production.

In the present study, we adapted the method of Xiong et al. [Xiong, 2003] to investigate whether we could detect an msMRI signal correlated in time and

amplitude with two well defined event related potentials (ERPs), in locations previously identified as putative generators of the ERPs. The two ERPs investigated were the P300 produced by auditory oddballs, whose amplitude increases with decreasing frequency of the oddball event [Horovitz, 2002], and the face-sensitive N170, whose amplitude decreases with increasing noise level in the face presentation [Horovitz, 2004].

Method

The study was designed to identify regions of msMRI signal change associated with a well characterized brain activation paradigm, and to confirm that any signal changes observed are due to currents produced by neural activity. Our strategy was to use a paradigm in which the level of neural activity within a region could be modulated in a predictable manner, as measured by the electrical evoked response potential (ERP), and by subsequent event-related BOLD fMRI signal changes. We selected the auditory “oddball” paradigm and a face-sensitive paradigm, because it has been shown that the amplitude of the P300 and N170 responses can be modulated in a predictable manner.

Subjects

A total of 12 healthy volunteers (5 females, mean age 25.6, range 20-32 years) participated in the Auditory Oddball studies. Five of the subjects participated in the ERP experiments, five of the subjects in the BOLD-fMRI experiments, eight of the subjects in msMRI experiments and three of them

participated in all experiments. Among these volunteers who participated in the Auditory Oddball studies, 4 healthy volunteers including 2 females with age range from 21 to 29 (mean age=25.5) also participated in the Face-Sensitive MRI studies.

All subjects had normal hearing and normal or corrected-to-normal vision. A written informed consent was obtained from all volunteers prior to the examinations. All subjects were instructed to maintain constant attention throughout all experiments.

Stimulus Presentation

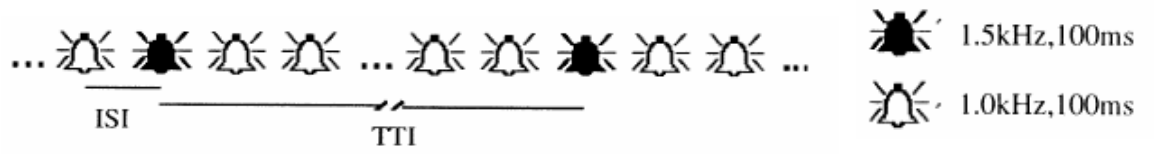

Figure VI-1. Auditory oddball paradigm

Table VI-1. Auditory oddball paradigm: the interval between oddballs varied to produce different oddball presentation frequencies.

Tones between targets	TTI (seconds)	Probability (%)	#target/run
12-13	15±0.6	8	10
16-17	19.8±0.6	6	10
24-25	29.4±0.6	4	10

Auditory oddball - Auditory stimuli generated by E-prime (Psychology Software Tools, Inc) were presented to healthy subjects every 1.2s. The frequent stimuli were 1kHz tones of 100ms duration, while rare stimuli -“oddballs”- were 1.5kHz tones of the same 100ms duration (Figure VI-1). The interval between

oddballs was varied within runs to produce oddball presentation frequencies of 4%, 6% and 8% (Table VI-1). The different probabilities of oddballs were presented randomly. In total 50 oddballs for each presentation frequency were presented in 5 runs.

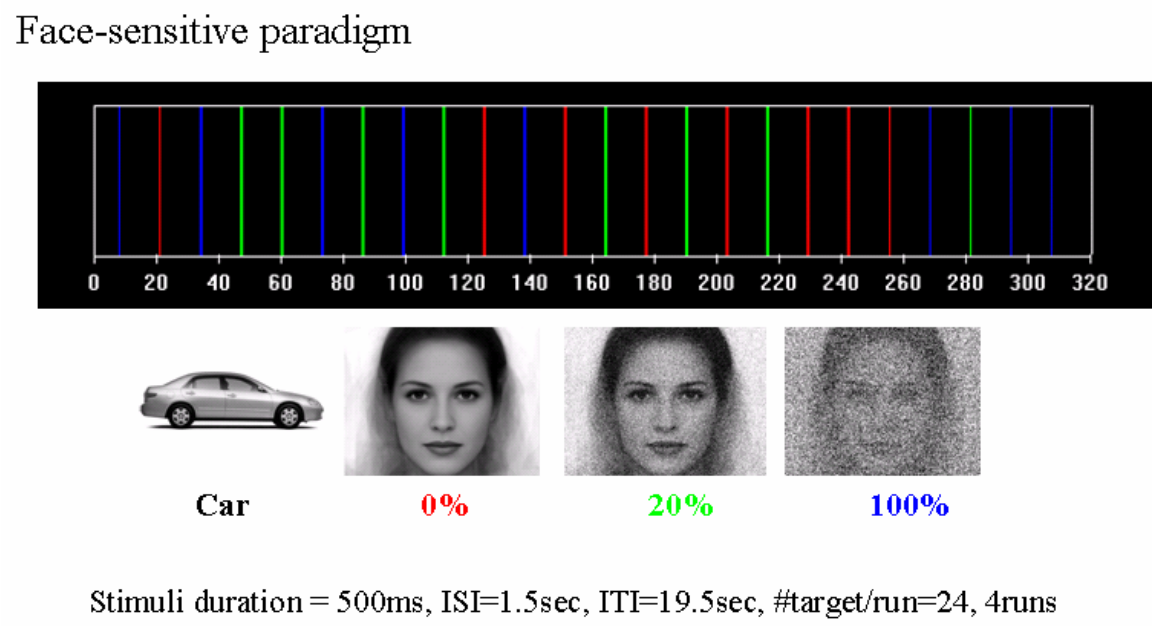

Figure VI-2. Face-presentation paradigm: black-car pictures were presented; red-0% noise added to the face picture; green-noisy image was created by adding gaussian noise with standard deviation of 20%; blue-noisy image was created by adding gaussian noise with standard deviation of 100%.

Face processing - Visual stimuli generated by E-prime (Psychology Software Tools, Inc) were presented to healthy subjects for a period of 500 ms every 1.5s. In order to localize the area, before the event-related experiments, a block-design Face-Presentation experiment in which randomly intermixed block of 30s different faces presentation plus 20s fixations with block of 30s objects presentations plus 20s fixations were presented to obtain a sustained

hemodynamic responses. The frequent stimuli were pictures of cars, while pictures of faces with different noise levels of 0%, 20% and 100% were presented every 19.5s (Figure VI-2) in event-related fashion. 24 face pictures were presented to the subject in one run.

Data Acquisition

ERPs were collected from electrode Pz using a single scalp electro-cap with earlobe reference and recorded on a computer running Scan4.2 and controlling SynAmp amplifiers (Neuroscan, Inc). The temporal resolution was set to be 2msec, band pass filter 0.05–100 Hz and Gain is 500.

BOLD functional images were acquired on a 3T Philips Achieva (with a 6-channel head coil, SENSE factor = 2) using a gradient echo EPI sequence; slice thickness=5mm, gap=1mm, TE=35ms, flip angle=70^{o}, FOV=22x22cm^{2} and acquisition matrix size=80x80 reconstructed to 128x128. 16 axial slices with TR=1.2s were acquired for the Auditory Oddball experiments, and 10 coronal slices with TR=1.5s for the block-design Face-Presentation experiments. A tool on the PHILIPS scanner console called iViewBold can describe simple block design paradigms and perform analysis while scanning and display correlation/activation maps in real-time. These real time activation maps are helpful for picking up the slice containing the region of interest.

For magnetic source MRI (msMRI) studies, the imaging parameters were the same except that only 1slice containing an ROI of interest was obtained. MR images of the slice including the supramarginal gyri were acquired at 325 or 425

or 525msec after presentation of the “oddball” in the P300 study. MR images of slices including the fusiform gyri were acquired with either 170msec or 180msec or 400msec delay relative to face stimulation onset in different runs. These delays were chosen in order to be able to study the time course of the T2*-weighted MR signal before and after the mean time of the maximum P300 or N170 ERP amplitudes (Figure VI-3).

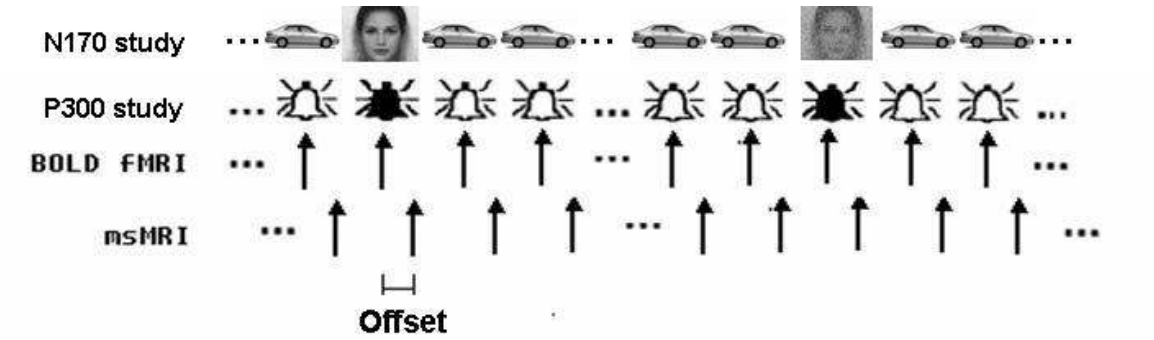

N170 study: Offset = 170msec or 180msec or 400msec; TR=ITI=1.5sec.

P300 study: Offset = 325msec or 425msec or 525msec; TR=ITI=1.2sec.

Figure VI-3. Magnetic source MRI (msMRI) images were acquired with offsets relative to stimulation onsets.

Data Analysis

Scan4.2, SPM2, BrainVoyage QX and custom analysis package running under MATLAB were used for data analysis. ERP data were analyzed using Scan4.2. Signals were DC offset correction and averaged in epochs (200~800 msec) and individually baseline corrected. Band pass filters was set to 0.05 ~ 100Hz respectively, while a notch filter was set to 30Hz. Hemodynamic response signals obtained from MR scanner were then analyzed using SPM2, BrainVoyager QX and custom analysis software running under MATLAB. BOLD

fMRI data were first motion corrected, realigned and coregistered with T1-weighted structural images collected using identical slice prescriptions, then registered to Talaraich coordinate brain. A general linear transform model (GLM) [Friston 1995], which assumes that the fMRI signal possesses linear characteristics with respect to the stimulus and that the temporal noise is white, was used to estimate the response. We first used a correlation template generated by convolving the box-car function of the stimulation paradigm with a canonical fMRI impulse response function described by Friston et al. [Friston 1994] to do the cross-correlation analysis [Bandettini 1993]. Cross-correlation maps were thresholded ($P < 0.001$) to generate activation maps. Then a 1x3 voxel ROI was identified from the activated voxels. Within the ROI, a resting baseline was calculated for each "oddball" / face-presentation cycle by averaging 2 images obtained right before stimulus onset, then the percentage average intensity changes through time were calculated and showed as a time course.

Results

It was previously established that the N170 amplitude monotonically decreases as Gaussian noise is added to the picture of a face [Horovitz 2004]. We have also previously confirmed the inverse relationship between P300 amplitude and "oddball" frequency. The P300 amplitude decreases as "oddball' presentation frequency increases. Our studies confirmed the same behaviors (Figure VI-4).

a 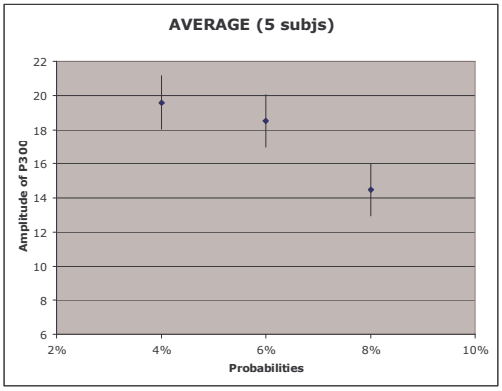

b 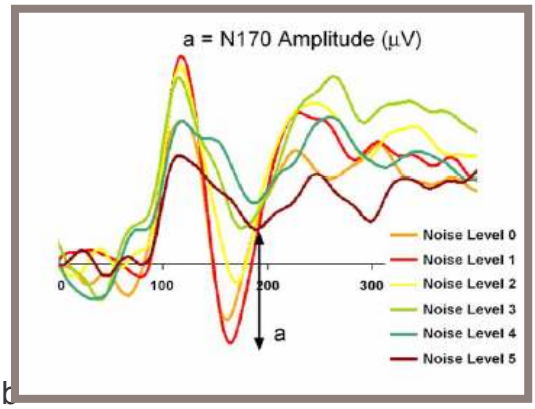

Figure VI-4. a P300 amplitude decreases as “oddball’ presentation frequency increases; b N170 amplitude decrease as noise added [Horovitz, 2004].

Conventional event-related BOLD-fMRI analyses by cross-correlation analysis identified the same regions that showed covariations of BOLD signals and ERP amplitudes as previously described (Figure VI-5). For example the BOLD signals in the supramarginal gyrus (SMG) and anterior cingulate (ACG) [Tarkka, 1995 & 1998; Mulert 2004] and the P300 amplitude at Pz showed significant inverse correlations with the “oddball” frequency [Horovitz, 2003]. In addition, the BOLD signals in face fusiform gyrus (FFA) and the N170 amplitude showed inverse correlations with noise level [Horovitz, 2004].

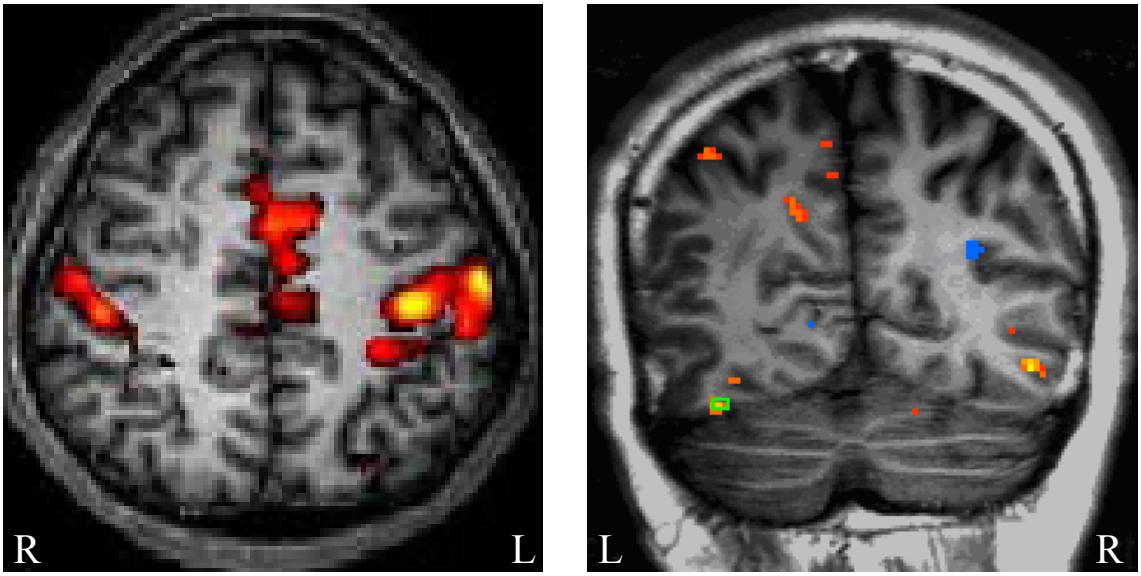

Figure VI-5. left panel: BOLD activation map for the auditory oddball experiment; right panel: Activation map for face-sensitive experiment. P<0.001

Despite these robust BOLD activations which peaked several seconds after ERP, we have so far been unable to identify reliable msMRI signal amplitude changes at or near the timing of the ERPs that correlate with the corresponding ERP or BOLD data. Spatio-temporal activation maps (t-test) from a hybrid ms/BOLD fMRI study showed no significant signal loss (P<0.1) in SMG and ACG in auditory “oddball” studies for all 3 different offsets at 300~500ms after the oddballs. Early fMRI signal changes in FFA at different times after onset of face-presentation also showed no difference. Figure VI-6 shows the T2*-weighted signal time courses for N170 runs where images were synchronized to 170, 180 or 400 ms post stimulus, and shows no difference in the mean signal at any of those times, and no difference from the prestimulus signal. Similarly, no significant signal changes were seen at times corresponding to the P300 ERP in the auditory oddball condition.

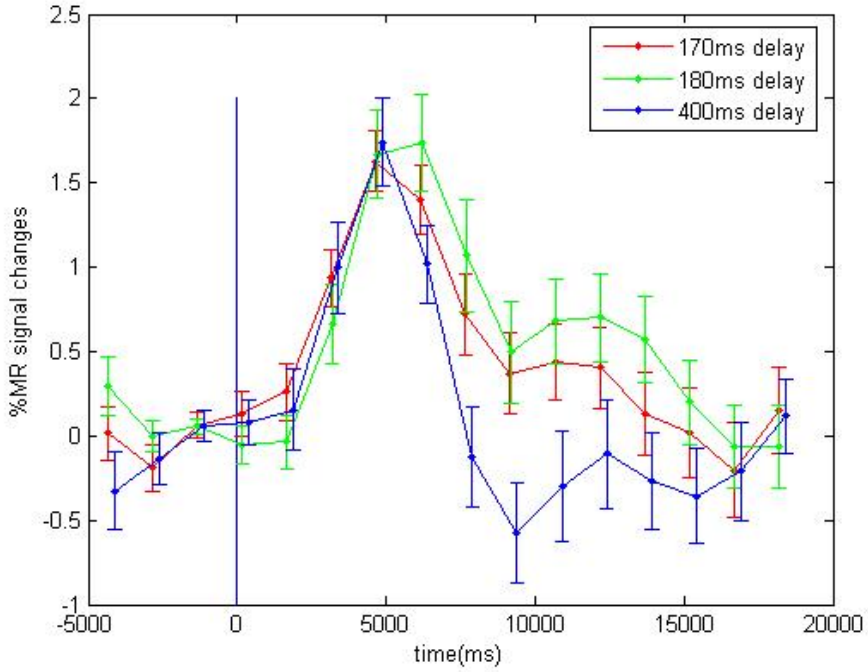

Figure VI-6. Time courses of functional MRI signals in ROI(FFC) with different offsets relative to the stimulus (face) onset. These are no significant differences in the mean signal at 170, 180 or 400 ms post stimulus, and no differences from the prestimulus signal.

Conclusion and Discussion

These experiments used an event-related design to probe the response of the T2*-weighted MRI signal at the time and in the locations of well-characterized ERP generators. We found no reliable evidence of changes in the MRI signal occurring at those times and locations when maximal neural activity (as judged by the surface ERP) is expected. These results suggest that the effects of neural dipole currents on the T2*-weighted signal which have been proposed as a direct measure of neural activity, lie below the level of detection at 3T using the

paradigm investigated here, or that the maxima in these ERPs do not correspond to times of significant current-induced dephasing.

We aimed to establish whether msMRI is a reliable method that greatly increases the temporal resolution of MRI for detecting changes of neuronal activity with no compromise of spatial resolution. We were unable to identify reliable signal changes due to these stimuli at times other than when the BOLD hemodynamic effect has developed some seconds after the causal event.

While transient magnetic field effects have shown promise in studies performed in vitro [Bodurka, 2002; Konn, 2003; Park, 2004; Petridou, 2006], they have not been reliably validated in vivo. Various methods have been used to increase the detectability of magnetic fields. For example, others [Chu, 2004; Bianciardi, 2004; Parkes, 2007] introduced methods that can separate neuromagnetic field effects from BOLD effects, and they did not see significant effects related to magnetic field changes associated with human neuronal activity. Thus our study supports these other findings. The sensitivity of MRI for detecting amplitude changes produced by neuronal currents is too low to be practically useful.

CHAPTER VII

CONCLUSION AND FINAL DISCUSSION

In our studies, the hemodynamic response functions (HRFs) associated with transient activation and deactivation in both primary visual cortex (V1) and higher-level extrastriate visual cortex (V2 and higher) acquired by functional magnetic resonance imaging (fMRI) have been compared and contrasted. We also used transcranial near-infrared spectroscopy (NIRS) and fMRI to investigate the relationship between the positive / negative blood oxygen level dependent (BOLD) effects and recorded concentration changes in both oxy- and deoxy-hemoglobin in response to transient activations and deactivations.

We reported the non-reciprocal non-linear nature of BOLD responses to short transient stimulus offsets compared to that of BOLD responses to short transient stimulus offsets in human primary visual cortex V1. We showed that signal decreases for short duration offsets were smaller than corresponding signal increases in activation studies, and also had slightly longer latencies and shorter times to peak, and showed no significant post stimulus overshoots. Moreover, the linear summation of BOLD signal decrease tends to underestimate the observed BOLD signal changes.

The studies described also demonstrated the good consistency between fMRI and NIRS data: the HRF to deactivation is smaller, quicker, narrower, and has a different time course to the HRF for transient activation. The strong correlation

between them was proven by reference to a method that considers the changes in blood susceptibility. Hence combining the results from these two modalities has the potential to provide greater nformation and to overcome the limitations of each.

Based on these studies, we proposed a hypothesis that different nonlinear natures of BOLD responses to activations and deactivations are mainly driven by the nonlinear relationships of physiological dynamics.

To account for these findings and hypothesis, we developed a physiological simulation model termed the modified Balloon Model which explicitly includes the nonlinear relationships of physiological variables, such as CBF, CBV, and OEF. By assuming that the increase of Flow-in during inflation occurs more rapidly than the decrease of Flow-in during deflation, the experimental responses can be well modeled, and the different nonlinear properties for both activation and deactivation were also predicted. These results suggest that hemodynamic effects alone can explain the causes of the nonlinear BOLD fMRI responses in primary visual cortex V1.

The strong correlation between NIRS data and BOLD fMRI data was proven again by using the Balloon Model. Hence NIRS complements fMRI by providing more insights into the underlying physiological basis of the BOLD signals, aids the evaluation and justification of the Balloon Model, and raised some interesting questions for future work.

In addition, we investigated the different spatial and temporal patterns of the transient hemodynamic responses in both primary visual cortex V1 and

extrastriate visual cortex for both positive and negative BOLD effects induced by turning visual stimuli either ON or OFF (activation *or* deactivation). The expected responses in primary visual area V1 may depend on simple sensory attributes of the stimulus, but the responses of higher order visual areas do not follow the trends of the responses in V1 and may reflect other aspects of visual processing. We have considered some potential explanations and believe that increases in BOLD responses adjacent to the striate visual cortex is neuronal in origin. Whether it results from intrinsic spontaneous activity or transient task-evoked activity, further work may help to clarify this issue.

The timing and location of putative generators (synaptic activity induced local field currents) of some well defined ERPs have been identified and localized in the brain. Theoretically, the local neuronal currents induce local magnetic field perturbations, and in turn they cause spin dephasing which may be mapped by MRI. An approach termed magnetic source MRI (msMRI) is based on the premise that neural activity may be mapped by MRI with greater temporal resolution by detecting the local magnetic field perturbations associated with local neuronal electric currents. We used a hybrid ms/BOLD MRI method to investigate whether msMRI could detect signal changes that occur simultaneously at the time of the production of well defined event related potentials, the P300 and N170, in regions that previously have been identified as generators of these electrical signals. We found no reliable evidence of changes in the MRI signal occurring at the times and in the locations of well-characterized ERP generators. These results suggest that the effects of dipole currents

generated by local synaptic activity on the T2*-weighted signal lie below the level of detection at 3T using the stimulation paradigms investigated here, or that the maximal neural activity (as judged by the surface ERP) do not correspond to times of significant current-induced magnetic field dephasing. The sensitivity of MRI for detecting amplitude changes produced by neuronal currents is too low to be practically useful.

The studies we have performed focus on the origins of BOLD activity in human brain using different modalities and modeling methods. The BOLD signal is not a direct measure of neuronal activity, but reflects local variations in hemoglobin concentration changes that are determined by a combination of physiological variables, such as blood flow, blood volume and oxygen metabolism. We now know much about the physiological basis of BOLD activity. Although much is known about the physiological basis, the neuronal basis of the BOLD activity is an important but an unanswered question. Though the sensitivity of MRI for detecting amplitude of magnetic field dephasing produced by neuronal currents is too low to be practically useful, the fact that extrastriate visual cortex is more related to neuronal activity might open a new door to study the neuronal basis of the BOLD response. More has yet to be discovered. Although much is know about the physiology underlying task-evoked BOLD responses, the physiology underlying spontaneous BOLD fluctuations might not be the same. How do BOLD activities as well as spontaneous BOLD fluctuations relate to electrical measures of neuronal activity and how do physiological factors couple with neuronal activity remain unknown. In many cases, gas mixture inhalation

blocks stimulus related blood flow changes and in turn reduce event-related BOLD activity, but spontaneous fluctuations can remain unchanged, and local field potential induced by synaptic activity appears to be distinct from. This would be a direction for future investigation. NIRS studies would be still helpful in understanding the coupling of physiology and neuronal activity.

EQUATIONS

$f(x) = \gamma B(x)$ [I-1] 4

$f(x) = \gamma(G_x x + B_0)$ [I-2] 4

$$S(x) = \int S(f(x)) \cdot e^{-2\pi i f(x)} df$$ [I-3] 5

$$\int_0^t f(x,\tau) \cdot d\tau = \int_0^t \gamma G_x(\tau) x \cdot d\tau = (\int_0^t \gamma G_x(\tau) \cdot d\tau) \cdot x = k_x(t) \cdot x$$ [I-4] 5

$$S(x,y) = \iint S(k_x(t), k_y(t)) \cdot e^{-2\pi i (k_x(t)x + k_y(t)y)} \cdot dk_x dk_y$$ [I-5] 5

$$\frac{\Delta S}{S} = M\left(\frac{\Delta CBF}{CBF} - \frac{\Delta CMRO_2}{CMRO_2}\right) - N\left(\frac{\Delta CBV}{CBV}\right)$$ [I-6] 14

$$f(t) = (\frac{t}{d})^a e^{-(t-d)/b} - c(\frac{t}{d'})^{a'} e^{-(t-d')/b'} + E$$ [II-1] 29

$S = S_0 \exp(-TE/T_2^*)$ [III-1] 48

$$\frac{\Delta S}{S} = \frac{S - S_0}{S_0} = \exp(-TE \cdot \Delta R_2^*) - 1 \approx -TE \cdot \Delta R_2^*$$ [III-2] 48

$R_2^* = \kappa V_{bl} \chi_{bl}$ [III-3] 48

$$\Delta R_2^{act} = \Delta R_2^v + \Delta R_2^{Hb} = \kappa[\Delta V_{bl} \bar{\chi}_{bl} + V_{bl} \Delta \chi_{bl}]$$ [III-4] 48

$\chi_{bl} = \chi_{oxy} + (1\text{-}Y)\ \delta\chi$ [III-5] 49

$\Delta S/S_0 = -TE\ \kappa[\Delta V_{bl}\ \bar{\chi}_{bl+} V_{bl}\ \Delta(1\text{-}Y)\ \delta\chi]$ [III-6] 49

$\Delta S/S_0 = -TE\ \kappa V_{bl}\ [\%HbT * \bar{\chi}_{bl+} \%Hb * \delta\chi]$ [III-7] 49

$\Delta S/S_0|^{ON} = 0.616 * TE\ \kappa V_{bl} * (\%HbT - 0.43 * \%Hb)$ [III-8] 50

$\Delta S/S_0|^{OFF} = 0.736 * TE\ \kappa V_{bl} * (\%HbT - 0.36 * \%Hb)$ [III-9] 50

$$\frac{\Delta S}{S} = V_0\left[k_1(1-q) + k_2(1-\frac{q}{v}) + k_3(1-v)\right]$$ [IV-1] 58

$$\frac{dq}{dt} = \frac{1}{\tau_0}\left[f_{in}(t)\frac{E(t)}{E_0} - f_{out}(v)\frac{q(t)}{v(t)} \right] \quad \text{[IV-2]} \quad \text{.....59}$$

$$\frac{dv}{dt} = \frac{1}{\tau_0}\left[f_{in}(t) - f_{out}(v) \right] \quad \text{[IV-3]} \quad \text{.....59}$$

$$E(f_{in}(t)) = 1 - (1 - E_0)^{1/f_{in}(t)} \quad \text{[IV-4]} \quad \text{.....59}$$

$$f_{out}(v) = v^{1/\alpha} + \tau\frac{dv}{dt} \quad \text{[IV-5]} \quad \text{.....59}$$

$\Delta S/S = V_0$*(2-k_3*$\bar{v}$)*n [%HbT-%Hb*(k_1*$\bar{v}$+2)/[(2-k_3*$\bar{v}$)*n]] [IV-6] 73

w^{ON}=n*(2.8*1+2)/(2-0.6*1) ≈ n*3.43 [IV-7].....73

w^{OFF}=n*(1.82*1.3+2)/(2-0.32*1.3) ≈ n*2.76 [IV-8] 73

REFERENCES

1. Ames, A.I. CNS energy metabolism as related to function. Brain Res. Rev. 2000; 34: 42–68.

2. Attwell, D. and Laughlin, S.B. An energy budget for signaling in the grey matter of the brain. J. Cereb. Blood Flow Metab. 2001; 21: 1133–1145.

3. Bandettini, P.A., Jesmanowicz, A., Wong, E.C. and Hyde, J.S. Processing strategies for time-course data sets in functional MRI of the human brain. Magn Reson Med 1993; 30:161–173.

4. Bandettini, P.A., Petridou, N., Bodurka, J. Direct detection of neuronal activity with MRI: Fantasy, possibility, or reality? Applied Magnetic Resonance 2005; 29 (1): 65-88.

5. Bianciardi, M., Di Russo, F., Aprile, T., Maraviglia, B. and Hagberg, G.E. Combination of BOLD-fMRI and VEP recordings for spin-echo MRI detection of primary magnetic effects caused by neuronal currents. Magn Reson Imaging. 2004; 22(10):1429-40

6. Birn R.M. and Bandettini, P.A. The effect of stimulus duty cycle and ‘‘off’’ duration on BOLD response linearity. NeuroImage 2005; 27: 70 – 82.

7. Bodurka, J. and Bandettini, P.A. Toward Direct Mapping of neuronal Activity: MRI Detection of Ultraweak, Transient Magnetic Field Changes. Magnetic Resonance in Medicine 2002; 47:1052-1058.

8. Bodurka, J., Jesmanowicz, A., Hyde, J.S., Xu, H., Estkowski, L. and Li, S.J. Current-induced magnetic resonance phase imaging. J Magn Reson 1999; 137: 265-271.

9. Bodurka, J., Zhao, X., and Li, S.J. Analysis of physical mechanisms of respiration-induced fMRI signal changes. In: Proc 8th Annual Meeting ISMRM, Denver, 2000; p 1006.

10. Boxerman, J.L., Bandettini, P.A., Kwong, K.K., Baker, J.R., Davis, T.L., Rosen, B.R., and Weisskoff, R.M. The Intravascular Contribution to fMRI Signal Change: Mote Carlo Modeling and Diffusion-Weighted Studies in Vivo. Magn. Reson. Med. 1995; 34: 4-10.

11. Boynton, G.M., Engel, S.A., Glover, G.H., and Heeger, D.J. Linear Systems Analysis of Functional magnetic Resonance Imaging in Human V1. J Neurosci 1996; 16: 4207.

12. Bullier, J. Integrated model of visual processing. Brain Res. Rev. 2001; 36: 96–107.

13. Buracas, G.T., and Boynton, G.M. The effect of spatial attention on contrast response functions in human visual cortex. J Neurosci. 2007 Jan 3; 27(1):93-7.

14. Buxton, R.B., and Frank, L.R. A model for the coupling Between Cerebral Blood Flow and Oxygen Metabolism During Neural Stimulation. Journal of Cerebral Blood Flow & Metabolism 1997; 17: 64-72.

15. Buxton, R.B., Uludag, K., Dubowitz, D.J., and Liu, T.T.. Modeling the hemodynamic response to brain activation. NeuroImage 2004; 23: S220-S233.

16. Buxton, R.B., Wong, E.C., and Frank, L.R. Dynamics of Blood Flow and Oxygenation Changes During Brain Activation: The Balloon Model. MRM 1998; 39: 855-864.

17. Chow, L.S., Cook, G.G., Whitby, E. and Paley, M.N. Investigation of MR signal modulation due to magnetic fields from neuronal currents in the adult human optic nerve and visual cortex. Magn Reson Imaging. 2006 Jul; 24(6): 681-91.

18. Chu, R., de Zwart, J.A., van Gelderen, P., Fukunaga, M., Kellman, P., Holroyd, T. and Duyn, J.H. Hunting for neuronal currents: absence of rapid MRI signal changes during visual-evoked response. NeuroImage. 2004; 23(3):1059-67.

19. Cohen, D. and Nemoto, I. Ferromagnetic particles in the lung. Part I. The magnetizing process. IEEE Trans. Biomed. Eng. 1984; BME-31: 261–273.

20. Crick, F. and Koch, C. Are we aware of neural activity in primary visual cortex? Nature 1995; 375: 121–123.

21. Duysens, J., Schaafsma, S.J. and Orban, G.A. Cortical Off Response Tuning for Stimulus Duration. Vision Res. 1996; Vol. 36. No. 20. pp.3243-3251.

22. Engel, S.A. et al. fMRI of human visual cortex. Nature 1994; 369: 525.

23. Engel, S.A., Glover, G.H. and Wandell, B.A. Retinotopic Organization in Human Visual Cortex and the spetial Precision of Functional MRI. Cerebral Cortex Mar 1997; 7:181-192.

24. Fox M.D. and Raichle M.E. Sponaneous fluctuations in brain activity observed with functional magnetic resonance imaging. Nature Reviews Neuroscience, 2007; 8: 700-711.

25. Fox, M.D., Snyder, A.Z., Zacks, J.M. and Raichle, M.E. Coherent spontaneous activity accounts for trial-totrial variability in human evoked brain responses. Nature Neurosci. 2006; 9: 23–25.

26. Fox, P.T., Raichle, M.E., Mintun, M.A. and Dence, C. Nonoxidative glucose consumption during focal physiologic neural activity. Science 1988; 241: 462–464.

27. Friston, K.J., et al. Statistical parametric maps in functional imaging: a general linear approach. Human Brain Mapping 1995; 2:189-210.

28. Friston, K.J., Jezzard, P. and Turner, R. Analysis of functional MRI time-series. Hum Brain Map 1994; 1:153–171.

29. Friston, K.J., Mechelli, A., Turner, R., and Price, C.J. Nonlinear Responses in fMRI: The Balloon Model, Volterra Kernels, and Other Hemodynamics. NeuroImage 2000; 12: 466-477.

30. Goebel, R., Muckli, L., Zanella, F. E., Singer, W. and Stoerig, P. Sustained extrastriate cortical activation without visual awareness revealed by fMRI studies of hemianopic patients. Vision Res. 2001; 41: 1459–1474

31. Golay, X., Silvennoinen, M.J., Zhou, J., Clingman, C.S., Kauppinen, R.A., Pekar, J.J. and van Zijl, P.C.M. Measurement of Tissue Oxygen Extraction Ratios From Venous Blood T2: Increased Precision and Validation of Principle. Magnetic Resonance in Medicine. 2001; 46:282–291.

32. Grubb, R.L., Raichle, M.E., Eichling, J.Q., and Ter-Pogossian, M.M. The Effects of Changes in PaCO2 on Cerebral Blood Volume, Blood Flow, and Vascular Mean Transit Time. Stroke 1974; 5: 630-639.

33. Haacke,E.M., Lai, S., Reichenbach, J.R., Kuppusamy, K., Hoogenraad, F.G.C., Takeichi, H. and Lin W. In Vivo Measurement of Blood Oxygen Saturation Using Magnetic Resonance Imaging: A Direct Validation of the Blood Oxygen Level-Dependent Concept in Functional Brain Imaging. Human Brain Mapping. 1997; 5:341–346.

34. Hebden, J.C. and Delpy, D.T. Diagnostic imaging with light. Brit. J. Radiol. 1997; 70: 206–214.

35. Heeger, D.J. and Ress, D. What does fMRI tell us about Neuronal activity? Nature Reviews Neuroscience 2002; 3: 142-151.

36. Henson, R.N.A., Price, C.J., Rugg, M.D., Turner, R., and Friston, K.J. Detecting Latency Differences in Event-Related BOLD Responses: Application to Words versus Nonwords and Initial versus Repeated Face Presentations. NeuroImage 2002; 15: 83–97.

37. Hobbie, R. (1997) Intermediate physics for medicine and biology. New York: Springer-Verlag. P 136-227.

38. Horovitz, S.G., Rossion, B., Skudlarski, P. and Gore, J.C. Parametric design and correlational analyses help integrating fMRI and electrophysiological data during face processing. NeuroImage 2004; 22:1587-1595.

39. Horovitz, S.G., Skudlarski, P. and Gore, J.C. Correlations and dissociations between BOLD signal and P300 amplitude in an auditory oddball task: a parametric approach to combining fMRI and ERP. Magnetic Resonance Imaging 2002; 20(4):319-325.

40. Hyder, F. Neuroimaging With Calibrated fMRI. Stroke 2004; 35[suppl I]: 2635-2541.

41. Kennan, R.P., Horovitz, S.G., Maki, A., Yamashita, Y., Koizumi, H., and Gore, J.C. Simultaneous Recording of Event-Related Auditory Oddball Response Using Transcranial Near infrared Optical Topography and Surface EEG. NeuroImage 2002; 16: 587-592.

42. Kennan, R.P., Scanley, B.E., Innis, R.B. and Gore, J.C. Physiological Basis for BOLD MR Signal Changes Due to Neuronal Stimulation: Separation of Blood Volume and Magnetic Susceptibility Effects. Magnetic Resonance in Medicine. 1998; 40: 840-846.

43. Konn, D., Gowland, P. and Bowtell, R. MRI Detection of Weak Magnetic Fields Due to an Extended Current Dipole in a Conducting Sphere: A model for Direct Detection of Neuronal Currents in the Brain. Magnetic Resonance in Medicine 2003; 50:40–49.

44. Lamme, V.A. and Roelfsema, P.R. The distinct modes of vision offered by feedforward and recurrent processing. Trends Neurosci. 2000; 23: 571–579.

45. Lennie, P. The cost of cortical computation. Curr. Biol. 2003; 13: 493–497.

46. Liao, C.H., Worsley, K.J., Poline, J.B., Aston, J.A.D., Duncan, G.H., and Evans, A.C. Estimating the Delay of the fMRI Response. NeuroImage 2002; 16: 593–606.

47. Liu, H.L. and Gao, J.H. An investigation of the impulse functions for the nonlinear BOLD response in functional MRI. Magnetic Resonance Imaging 2000; 18: 931–938.

48. Logothetis, N.K., Pauls, J., Augath, M., Trinath, T. and Oeltermann, A. Neurophysiological investigation of the basis of the fMRI signal. Nature 2001; 412(6843):150-7.

49. Mayhew, J., Johnston, D., Martindale, J., Jones, M., Berwick, J., and Zheng, Y. Increased oxygen consumption following activation of brain: Theoretical footnotes using spectroscopic data from barrel cortex. NeuroImage 2001; 13: 973–985.

50. Merabet, L.B., Swisher, J.D., McMains, S.A., Halko, M.A., Amedi, A., Pascual-Leone, A. and Somers, D.C. Combined Combined activation and deactivation of visual cortex during tactile sensory processing. J Neurophysiol. 2007 Feb; 97(2):1633-41. Epub 2006 Nov 29.

51. Miller, K.L., Luh, W.M., Liu, T.T., Martinez, A., Obata, T., Wong, E.C., Frank, L.R. and Buxton, R.B. Nonlinear Temporal Dynamics of the Cerebral Blood Flow Response. Human Brain Mapping 2001; 13:1–12.

52. Milliken, G. A. A simple photoelectric colorimeter. J. Physiol. 1933; 79: 152.

53. Mitra, S. and Foste, T.H. Carbogen breathing significantly enhances the penetration of red light in murine tumours in vivo. Phys. Med. Biol. 2004; 49: 1891–1904.

54. Mulert, C., Jager, L., Schmitt, R., Bussfeld, P., Pogarell, O., Moller, H.J., Juckel, G. and Hegerl, U. Integration of fMRI and simultaneous EEG: towards a comprehensive understanding of localization and time-course of brain activity in target detection. Neuroimage. 2004; 22(1):83-94.

55. Muller, J.R., Metha, A.B., Krauskopf, J. and Lennie, P., 1999. Rapid adaptation in visual cortex to the structure of images. Science 285 (5432), 1405-1408.

56. Nir, Y., Hasson, U., Levy, I., Yeshurun, Y. and Malach, R. Widespread functional connectivity and fMRI fluctuations in human visual cortex in the absence of visual stimulation. Neuroimage 2006; 30: 1313–1324.

57. Nunez, P.L., Wingeler, B.M. and Silberstein, R.B. Spatial-temporal structures of human alpha rhythm: theory, microcurrent sources, multiscale measurements, and global binding of local networks. Hum Brain Map 2001; 13: 125-164.

58. Obata, T., Liu, T.T., Miller, K.L., Luh, W.M., Wong, E.C., Frank, L.R., and Buxton, R.B. Discrepancies between BOLD and flow dynamics in primary and supplementary motor areas: application of the balloon model to the interpretation of BOLD transients. NeuroImage 2004; 21 (1): 144– 153

59. Ogawa, S., Lee, T.M., Kay, A.R. and Tank, D.W. Brain magnetic resonance imaging with contrast dependent on blood oxygenation. Proc Natl Acad Sci USA 1990; 87:9868–9872.

60. Ogawa, S., Menon, R.S., Tank, D.W., Kim, S.G., Merkle, H., Ellerman, J.M., and Ugurbil, K. Functional Brain Mapping by Blood Oxygenation Level-Dependent Contrast Magnetic Resonance Imaging: A Comparison of Signal Characteristics with A Biophysical Model. Biophys. J. 1993; 64: 803-812.

61. Park, T.S., Lee, S.Y. and Park, J.H. Effect of nerve cell currents on MRI images in snall ganglia. Neuroreport 2004; 15:2783-2786.

62. Parkes, L.M., de Lange, F.P., Fries, P., Toni, I. and Norris, D.G. Inability to directly detect magnetic field changes associated with neuronal activity. Magn Reson Med. 2007; 57(2):411-6.

63. Petridou, N., Plenz, D., Silva, A.C., Loew, M., Bodurka, J. and Bandettini, P.A. Direct magnetic resonance detection of neuronal electrical activity. Proc Natl Acad Sci U S A. 2006; 103(43):16015-20.

64. Pollen, D.A. On the neural correlates of visual perception. Cereb. Cortex 1999; 9: 4–19.

65. Raichle, M.E. and Mintun, M.A. Brain work and brain imaging. Annu. Rev. Neurosci. 2006; 29: 449–476.

66. Rees, G., Kreiman, G. and Koch, C. Neural correlates of consciousness in humans. Nature Rev. Neurosci. 2002; 3: 261–270.

67. Robson, M.D., Dorosz, J.L., and Gore, J.C. Measurements of the Temporal fMRI Response of the Human Auditory Cortex to Trains of Tones. NeuroImage 1998; 7: 185-198.

68. Roe, A. W. (2003) in The Primate Visual System, eds. Collins, C. & Kaas, J. (CRC, New York), pp. 109–138.

69. Shulman, R.G., Rothman, D.L., Behar, K.L. and Hyder, F. Energetic basis of brain activity: implications for neuroimaging. Trends Neurosci. 2004; 27: 489–495.

70. Song, A.W. and Takahashi, A. Lorentz effect imaging. Magnetic Resonance Imaging 2001; 19:763-767.

71. Spees, W.M., Yablonskiy, D.A., Oswood, M.C. and Ackerman J.J.H. Water Proton MR Properties of Human Blood at 1.5 Tesla: Magnetic Susceptibility, T1, T2, T*2 , and Non-Lorentzian Signal Behavior. Magnetic Resonance in Medicine. 2001; 45:533–542.

72. Strangman, G., Culver, J.P., Thompson, J.H. and Boas, D.A. ‘‘A quantitative comparison of simultaneous BOLD fMRI and NIRS recordings during function brain activation,’’ Neuroimage 2002; 17: 719–731.

73. Tarkka, I.M. and Stokic, D.S. Source localization of P300 from oddball, single stimulus, and omitted-stimulus paradigms. Brain Topogr. 1998; 11(2):141-5.

74. Tarkka, I.M., Stokic, D.S., Basile, L.F. and Papanicolaou, A.C. Electric source localization of the auditory P300 agrees with magnetic source localization. Electroencephalogr Clin Neurophysiol. 1995; 96(6):538-45.

75. Tong, F. Primary visual cortex and visual awareness. Nature Reviews Neuroscience, 2003; 4: 219-229.

76. Truong, T.K. and Song, A.W. Finding neuroelectric activity under magnetic-field oscillations (NAMO) with magnetic resonance imaging in vivo. Proc Natl Acad Sci U S A. 2006; 103(33):12598-601.

77. Weisskoff, R.M. and Kiihne, S. MRI Susceptometry: Image-Based Measurement of Absolute Susceptibility of MR Contrast Agents and Human Blood. Magnetic Resonance in Medicine. 1992; 24: 375-383.

78. Villringer, A., Minoshima, S., Hock, C., Obrig, H., Ziegler, S., Dirnagl, U., Schwaiger, M. and Villringer, A. Assessment of local brain activation. A simultaneous PET and near-infrared spectroscopy study. Adv. Exp. Med. Biol. 1997; 413: 149–153.

79. Xiong, J., Fox, P.T. and Gao, J.H. Directly Mapping Magnetic Field Effects of Neuronal Activity by Magnetic Resonance Imaging. Human Brain Mapping 2003; 20:41-49.

80. Zhong, J., Kennan, R.P., Fulbright, R.K. and Gore, J.C. Quantification of Intravascular and Extravascular Contributions to BOLD Effects Induced by Alteration in Oxygenation or Intravascular Contrast Agents. Magnetic Resonance in Medicine. 1998; 40: 526-536.